İZMİR KÂTİP ÇELEBİ ÜNİVERSİTESİ 2010
GRADUATE SCHOOL OF NATURAL AND APPLIED SCIENCES

Nonlinear Viscoelastic Properties of Nano and Micro Sized Clay Suspensions

Submitted to the Graduate School of Natural and Applied Sciences
in partial fulfillment of the requirements for the degree of

Master of Science

in Nanoscience and Nanotechnology Engineering

by

Ceylan Ülker

ORCID 0000-0003-0793-7069

February, 2022

This is to certify that we have read the thesis **Nonlinear Viscoelastic Properties of Nano and Micro Sized Clay Suspensions** submitted by **Ceylan ÜLKER**, and it has been judged to be successful, in scope and in quality, at the defense exam and accepted by our jury as a MASTER'S THESIS.

APPROVED BY:

Advisor: **Asst. Prof. Dr. Ali ETTEHADİ**
İzmir Kâtip Çelebi University

Committee Members:

Asst. Prof. Dr. Ali ETTEHADİ
İzmir Kâtip Çelebi University

Assoc. Prof. Dr. Gürşat ALTUN
İstanbul Technical University

Assoc. Prof. Dr. Mustafa Hakan ÖZYURTKAN
İstanbul Technical University

Date of Defense: February 1, 2022

Declaration of Authorship

I, **Ceylan ÜLKER**, declare that this thesis titled **Title of the Thesis in English** and the work presented in it are my own. I confirm that:

- This work was done wholly or mainly while in candidature for the Master's / Doctoral degree at this university.
- Where any part of this thesis has previously been submitted for a degree or any other qualification at this university or any other institution, this has been clearly stated.
- Where I have consulted the published work of others, this is always clearly attributed.
- Where I have quoted from the work of others, the source is always given. This thesis is entirely my own work, with the exception of such quotations.
- I have acknowledged all major sources of assistance.
- Where the thesis is based on work done by myself jointly with others, I have made clear exactly what was done by others and what I have contributed myself.

Date: 01.02.2022

Nonlinear Viscoelastic Properties of Nano and Micro Sized Clay Suspensions

Abstract

Clay colloids and suspensions are distinguished from other colloidal minerals by wide ranges of application area. Clay-based colloidal systems are frequently used in various industries, including cosmetics, oil industry, medicine, pharmacy, catalysis, textiles, remediation, and food packaging. Mechanical and thermo-structural properties of these systems provide valuable information in terms of some important criteria such as shelf life, gelation process, and degradation time. The foucus point of this study is to consider the application of water-clay suspensions in drilling fluid more than aforementioned industries.

It is aimed to characterize the nonlinear viscoelastic properties of five different water-clay suspensions under Large Amplitude Oscillatory Shear (LAOS) based on the stress decomposition approach. Four type of sepiolite clay sample collected directly from specific beds near Eskisehir in Turkey and a commercial bentonite clay (Wyoming bentonite) as the API reference clay was considered to prepare fresh water-clay suspensions. Sepiolite clay rocks were subjected to some physical treatments to obtain nano- and micro-sized particle distribution.

Prepared water-clay suspensions were firstly subjected to LAOS test using Discovery Hybrid Rheometer (DHR-II) at 25°C. Furthermore, experimentally verified sepiolite sample (Türk Tajiri Bej, TTB) with nano-and micro- particle size distributions was

selected for further LAOS analysis at elevated temperatures. The material stress response was decomposed through Fourier transform (odd-integer harmonic decomposition) into elastic and viscous stress components. Lissajous-Bowditch loops (Lissajous curves) plotted in Pipkin space were assessed as rheological fingerprints to detect the initiation of nonlinear region and the nature of nonlinearity. Oscillation sweep tests were conducted to deliver viscoelastic nonlinearities of fluid systems as a function of strain and strain rate at four temperatures (25, 50, 100, 150° C) and frequencies (0.25, 0.5, 0.75, 1 Hz).

Lissajous-Bowditch curves analysis revealed that Bentonite suspension system provided stronger structural stability compared to other sepiolite suspension samples at 25° C. Even though nano-sized TTB sepiolite suspension demonstrated lower gel strength than micro-sized TTB at low temperatures, it providred almost the same gel strength with micro-sized TTB sepiolite suspension at 100°C and 150°C. The elastic nonlinear response was determined to be strain softening for the both fluid systems (Micro-and Nano-Sized) at all states since elastic parameters ($\boldsymbol{G'_L}$ **and** $\boldsymbol{G'_M}$) decrease. The viscous nonlinear response for both fluid systems was shear rate thinning at large strain rates since the dynamic viscosity parameters ($\boldsymbol{\eta'_M}$ **and** $\boldsymbol{\eta'_L}$) decrease. However, at low to moderate strain rates, the nano-sized TTB sepiolite suspension systems demonstrated more shear rate thickening than micro-sized TTB suspension behavior by the analysis of viscous parameters altogether.

Keywords: Nano-sized sepiolite, viscoelasticity, LAOS, clay suspensions, shear thickening

Nano ve Mikro Boyutlu Kil Süspansiyonlarının Doğrusal Olmayan Viskoelastik Özellikleri

Öz

Kil kolloidleri ve süspansiyonları, geniş uygulama alanları olması sebebiyle diğer kolloidal minerallerden ayrılmaktadır. Kil bazlı kolloidal sistemler kozmetik, petrol endüstrisi, tıp, eczacılık, kataliz, tekstil, iyileştirme ve gıda paketleme gibi çeşitli endüstrilerde sıklıkla kullanılmaktadır. Bu sistemlerin mekanik ve termo-yapısal özellikleri, raf ömrü, jelleşme süreci ve bozunma süresi gibi bazı önemli kriterler açısından önemli bilgiler sağlar Bu çalışmanın odak noktası, yukarıda belirtilen diğer endüstrilerden ziyade petrol endüstrisinde su-kil süspansiyonlarının sondaj sıvısında uygulanmasının ele alınmasıdır.

Bu çalışmada, Büyük Genlikli Salınımlı Kesme (LAOS) altında beş farklı su-kil süspansiyonunun doğrusal olmayan viskoelastik özelliklerinin karakterize edilmesi amaçlanmıştır. Türkiye'de Eskişehir yakınlarındaki belirli yataklardan doğrudan toplanan dört tip sepiolit kil numunesi ve API referans kili olarak ticari bir bentonit kili (Wyoming bentonit) saf su-kil süspansiyonları hazırlamak için kullanılmıştır. Sepiyolit kil kayaçları, nano ve mikro boyutlu parçacık dağılımı elde etmek için bazı fiziksel işlemlere tabi tutulmuştur. Hazırlanan su-kil süspansiyonları ilk olarak Discovery Hybrid Rheometer (DHR-II) kullanılarak 25° C'de LAOS testine tabi tutulmuştur. Ayrıca, nano ve mikro parçacık boyutu dağılımlarına sahip sepiyolit

numunesi (Türk Tajiri Bej, TTB), yüksek sıcaklıklarda daha fazla LAOS analizi için seçilmiştir. Malzeme stres tepkisi (material stress response), Fourier dönüşümü (tek tamsayılı harmonik ayrışma) yoluyla elastik ve viskoz stres bileşenlerine ayrıştırıldı. Pipkin uzayında çizilen Lissajous-Bowditch döngüleri (Lissajous eğrileri), doğrusal olmayan bölgenin başlangıcını saptamak için reolojik olarak değerlendirilmiştir. Osilasyonlu tarama testleri, dört sıcaklıkta (25, 50, 100, 150° C) ve frekanslarda (0.25, 0.5, 0.75, 1 Hz) gerinim (strain) ve gerinim hızının (strain rate) bir fonksiyonu olarak akışkan sistemlerinin viskoelastik doğrusal olup olmadıklarını saptamak için uygulanmıştır.

Lissajous eğrilerinin analizi, bentonit süspansiyon sisteminin 25° C' de diğer sepiolit süspansiyon örneklerine kıyasla daha fazla yapısal kararlılığa sahip olduğunu ortaya koymuştur. Düşük sıcaklıklarda mikro boyutlu TTB den daha düşük jel kuvveti özelliği gösteren Nano boyutlu TTB sepiolit süspansiyonu, 100°C ve 150°C'de mikro boyutlu TTB sepiolit süspansiyonu ile hemen hemen benzer jel kuvveti sağladığı görülmüştür. Elastik doğrusal olmayan tepki, elastik parametreler $\boldsymbol{(G'_L \text{ and } G'_M)}$ azaldığından, her iki akışkan sistemi için tüm durumlarda gerinim yumuşaması (strain softening) olarak belirlendi. Her iki akışkan sistemi için de viskoz doğrusal olmayan tepki, dinamik viskozite parametreleri ($\boldsymbol{\eta'_M \text{ and } \eta'_L}$) azaldığından, büyük gerinim hızlarında kesme hızında incelme olmuştur. Bununla birlikte, düşük ila orta gerilim oranlarında, nano boyutlu TTB sepiolit süspansiyon sistemleri, viskoz parametrelerin tamamı analizi ile mikro boyutlu TTB süspansiyon davranışından daha fazla kesme kalınlaşması (shear thickening) göstermiştir.

Anahtar Kelimeler: Nano boyutlu sepiyolit, LAOS, viskoelastisite, kil süspansiyonları, kesme kalınlaşması

To my dear family…

Acknowledgment

To begin with, I would like to thank Asst. Prof. Dr. Ali ETTEHADİ, a valuable consultant who has answered all the questions I have always asked and he helped me to complete the project with more qualified resources with the resources he provides. I would also like to express my sincere thanks to Assoc. Prof. Dr. Gürşat ALTUN of Istanbul Technical University's Petroleum and Natural Gas Engineering Department for sharing his valuable knowledge and for supporting us during this work. Last but not least, I'd like to express my gratitude to my dear mother and father, who have always been supportive of me in all aspects of my life.

Izmir Kâtip Celebi University's Coordination Office of Scientific Research Projects (IKCU-NP-MUM-0001) and Turkey's Scientific and Technological Research Council funded this thesis (TUBITAK-217M723 & TUBITAK-119M084).

Ceylan ÜLKER

Table of Contents

List of Figures

Liste of Table

List of Abbreviations

API	American Petroleum Institute
DR	Dissipation ratio
DHR-II	Discovery Hybrid Rheometer
LAOS	Large Amplitude Oscillatory Shear
L-B	Lissajous Bowditch
VE	Viscoelasticity
HDPE	High Density Polyethylene
LDPE	Low Density Polyethylene
PS	Polystyrene
FT	Fourier Transform
NTTB (NS)	Nano sized TTB sepiolite

Liste of Symbols

G'_L	Large strain modulus
G'_M	Minimum strain modulus
G’	Storage modulus
G’’	Loss modulus
S	Stiffening ratio
T	Thickening ratio
σ/σ_{max}	Normalized total stress responses
σ'/σ'_{max}	Normalized elastic component
σ''/σ''_{max}	Normalized viscous component
$\dot{\gamma}/\dot{\gamma}_{max}$	Strain rate
η'_L	Large strain-rate dynamic viscosity
η'_M	Minimum strain-rate dynamic viscosity
v_3/v_1	Viscous chebyshev coefficient
e_3/e_1	Elastic chebyshev coefficient
γ_0	Strain amplitude
σ_{max}	Maximum stress
$(E_d)_{pp}$	Pure plastic dissipation energy
E_d	Dissipation energy
ϕ	Dissipation ratio

Chapter 1

Introduction

Clays are utilized as natural resources in a variety of industries, including ceramics, paper, paint, petroleum, effluent clarity, catalysis[1]. Their structure, composition, and physical qualities are the main factors affected their usage area [2]. Clay suspensions as the colloidal minerals can be used for a variety of purposes such as cosmetics, the oil industry, medicine, pharmacy, catalysis, textiles, cleanup, and food packaging.

Bentonite and sepiolite, predominantly constituted of the mineral montmorillonite, are two of the most well-known and commonly used clays distributed in water in various industries. Bentonite minerals are used in a variety of sectors, including ceramics, cement, paints, food, drilling fluids, pharmacy, and paper manufacturing [3], [4]. Sepiolite is used to absorb agricultural chemicals, water, and oil, as well as as a suspension in a variety of applications like saline drilling fluids, dyes, and pharmaceuticals, as well as catalytic applications in the fiber reinforced cement industry, rubber industry, bioreactors, industrial waste water treatment, and flue gas waste removal [5].

Understanding the science behind the different shear mechanisms of various Clays in water suspensions can lead to characterize thier mechanical and thermostructural properties. All of these provide useful information about some critical features of clay colloidal systems such as shelf life, gelation process, and degradation time.

Most advanced technologies including quality control, design and process assessment, and commercial product formulation require an understanding of rheological behavior of materials. The nature of mineral clays and their mechanical characteristics in different suspension systems necessitate an evaluation of the rheological properties of these systems. Various methodologies, equipment, and rheological approaches have already been identified and contributed to the literature to explore the rheological behavior of these aqueous suspensions. The rheological properties of suspensions, colloids, and dispersions are often analyzed under elastic, viscous, and viscoelastic deformations [6]. The rheological properties of sepiolite base drilling fluid under viscous deformations have been described in a number of research [7]–[11]. Furthermore, different experimental approaches were used to evaluate the rheological properties of bentonite suspensions [12]–[14]. Some studies have been conducted on how the rheological characteristics of clays will alter when they are reduced to nano size. In some recent studies nano-sized clay suspensions have been investigated for different industrial applications. Mohammadi et al., (2015) investigated the usage of nanoclay from the Kheirabad mine as a drilling fluid additive, and compared the findings to the bentonite based drilling fluid widely used in drilling operations [15]. Nano clays are ideal for packaging applications because of their excellent barrier characteristics and transparency. According to Patel et al. (2005) nanoclay is utilized as a rheological modifier in paints, inks, greases, and cosmetics, as well as as a drug carrier in medicinal applications and for the treatment of industrial waste water [16].

The Large Amplitude Oscillatory Shear (LAOS) Test can be used to investigate complex fluids' nonlinear viscoelastic behavior. The parametric responses of stress vs. strain or strain-rate curves are used to conduct the LAOS method. The LAOS method was developed to explore the rheological properties of some industrial liquids like polymer solutions and melts [17], colloidal dispersions [18], food products [19] and hair or skin gels [20]. Currently, there is a lot of interest in applying the LAOS test to evaluate nonlinear behavior of materials [21]-[22],[17],[23]-[24]. The linear and non-linear viscoelastic rheological properties of water-clay suspensions should be considered since they exhibit both viscous and elastic features when subjected to shear deformation.

This study attempted to characterize the nonlinear viscoelastic properties of bentonite, and four type of sepiolite suspensions including one nano sized sepiolite clay suspensions under Large Amplitude Oscillatory Shear (LAOS) based on stress decomposition approach. In the present study the LAOS rheological procedure is applied for the first time in the case of nano-sized TTB sepiolite clay suspensions. The aim of this study is to comprehensively investigate and simulate the LAOS behavior of nano-and micro-sized TTB sepiolite clay suspensions. The rheological behavior of these aqueous suspensions was reported as a function of frequency and strain. The evolution of plotted normalized intra-cycle stress-strain behavior was evaluated regarding both strain and frequency. In addition, all LAOS parameters were analyzed and reported along with previously unreported shear mechanisim (strain thickening and strain hardening behaviors) as a function of both applied strain and frequency.

Chapter 2

Literature Review

In this section, recent studies are given for diffrent industrial usage of nano-sized clay suspensions. Additionally, literature is presented for LAOS studies, viscoelasticity of drilling fluids and sepiolite clays.

2.1 Applications of Nano-sized Clays

Nanoscale particles provide numerous benefits in a variety of fields due to their unique properties. When reduced to nano size, clay is one of the materials that has a wide range of applications in a variety of industries. Clays are materials with a wide range of applications that occur naturally in nature and are thus inexpensive. The surface areas of the clays increase dramatically as they are reduced to the nanoscale. Nano clays are used in a variety of fields, including medicine, cosmetics, paint, drilling fluid, packaging, and water treatment, due to this and other important properties.

The effect of nanoclay on the rheology of drilling fluids is studied. This study found that at optimal clay concentrations, Kheirabad modified clay behaves well for drilling [15]. Shakip et al. investigated that nano-clay outperformed nano titanium, copper nanooxide, nano alumina, nano clay, and CMC in the rotational viscometer. This material also performed well in the filtration test, and nano-clay performed better than others in controlling filtration. This is due to the fact that a 6 percent concentration of nanoclay increases the viscosity of the drilling fluid[25].

Cheraghian (2017) revealed that the addition of nanoparticles to drilling fluid raises the viscosity of the fluid. The rheological properties of the fluid, such as apparent viscosity (AV), plastic viscosity (PV), yielding point (YP), mud cake thickness, and fluid loss (FL), were studied before and after the addition of different concentrations of nanoclay. Clay nanoparticles have been used in this study to improve the rheological properties of drilling fluids. The results demonstrated that nanoclay controls fluid loss and is resistant to both high temperatures and fluid loss [26].

2.2 Large amplitude oscillatory shear (LAOS) studies

Early studies from 1960 to 1975 considered nonlinear properties of several viscoelastic materials based on oscillatory shear and introduced stress waveform analysis with Fourier transform approach [17], [27]–[34]. These studies defined the concept of Large Amplitude Oscillatory Shear (LAOS); however, its application could not be developed further due to some technical problems stemmed from lack of hardware and computational methods. The LAOS test protocols introduced by Giacomin and Dealy [35], and Dealy and Wissbrun [36] extended the knowledge and provided more information about the experimental process and analysis of data. However, a substantial progress in LAOS test interpretation has been achieved in a comprehensive study by Ewoldt [37]. They established new measures to evaluate viscoelastic nonlinearity in Large Amplitude Oscillatory Shear (LAOS). A rheological framework was introduced by Ewoldt et al. 2008 based on total stress decomposition into elastic and viscous stress characters using Fourier transform approach. They signified both elastic and viscous component of total stress by Chebyshev polynomials and derived nonlinear viscoelastic parameters to quantify nonlinearity based on LAOS protocol. Ewoldt et al. (2008) expressed that parametric plots involving closed Lissajous-Bowditch curves were able to visualize nonlinear viscoelastic characters of materials by depicting trajectories of oscillation stress σ(t) as a function of strain γ or strain rate $\dot{\gamma}$.

Numerous studies have recently considered LAOS protocols to evaluate nonlinear viscoelastic properties of some materials and expanded the usage of LAOS test in various industries [6], [17], [19], [20], [23], [37]–[42]. By the best knowledge of the authors, no study was found about nonlinear viscoelastic characteristics of nano-sized TTB sepiolite suspensions.

2.3 Sepiolite based colloidals

Recently, nano-sized sepiolite clay is used in various applications especially in drilling fluids. Abdo et. al, (2016) investigated the effect of nano-sized sepiolite clay in rheological properties of drilling fluids. According to the study nano-sized sepiolite clay improved the gel strength and fluid loss of drilling fluids at high pressure and high temperature conditions [43]

As a fibrous clay mineral, sepiolite is a naturally occurred hydrous magnesium silicate [44] . Numerous studies were reported about mineralogical properties of sepiolite that makes it valuable for a wide range of applications. However, limited studies considered the sepiolite clay as a main constituent in designing water-based drilling fluids. The usage of sepiolite drilling fluid (drilling mud) in hostile conditions such as high temperature, high pressure, and excessive salinity has been investigated in some relevant studies [7], [8], [45]–[49]. The common point in all of these studies is that the usage of several additives to control and improve the filtration properties of proposed sepiolite muds is necessary. Although providing appropriate rheological properties at extreme temperatures (>150^{o} C), filtration control ability of sepiolite muds has been failed and reported to be unacceptable [7], [9], [48]. Further studies revealed that the filtration properties of sepiolite muds could economically be controlled by the usage of recently available commercial additives [10], [11]. None of these studies considers the nonlinear viscoelastic properties of sepiolite suspensions in rheological characterization.

Chapter 3

Method and Materials

3.1 Materials

Four sepiolite clays commertially named as TTB, YD-K, Kurtşeyh, and S were used to prepare clay-water suspension systems investigated in this study. Raw sepiolite clay samples were collected directly from beds near Sivrihisar-Eskişehir district of Turkey and subjected to some physical treatments to obtain fine scaled sepiolite sapmles. Large crushers were used to reduce the particles of sepiolite clays to a smaller size. Clay powders with nano-scale particle sizes were created using a high-speed dynamic air classifier following rotary grinding and vibratory disc mill in department of mineral processing engineering at Istanbul Technical University. In addition, commercial Wyoming bentonite clay (QUIK-GEL) provided by Baroid Company was used as a major additive for bentonite-water suspension. Particle size distribution results of Nano–sized TTB (NTTB) sepiolite clay that is measured by Nano-ZS90 zetasizer is given in Figure 3.1. Nano-ZS90 zetasizer is showed in Figure 3.2.

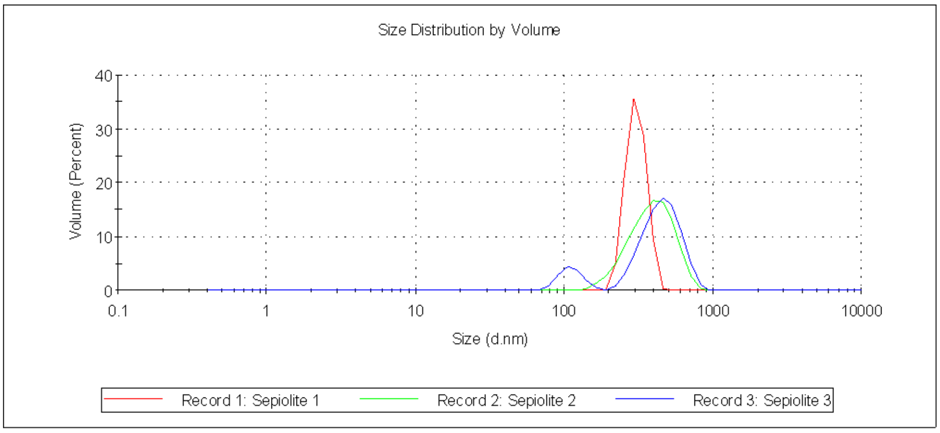

Figure 3.1: Zetasizer analysis results of Nano-sized TTB sepiolite clay.

Figure 3.2: Size of Nano-sized TTB sepiolite clay is measured by Nano-ZS90 zetasizer.

It is known that the prefix "nano" denotes one billionth, or 10^{-9}, in the International System of Units; hence, one nanometer is one billionth of a meter. Figure 3.3 also shows the particle size of nano-sized TTB sepiolite with respect to cumulative volume percent. Particle size distribution curves for other clay samples are also presented in Appendix A. Table 1 lists the d(0.1), d(0.5), and d(0.9) values obtained from particle size distribution analysis for all used samples. The percentages 10%, 50%, and 90% of particles under the reported particle size are represented by the particle size distributions d(0.1), d(0.5), and d(0.9) [50].

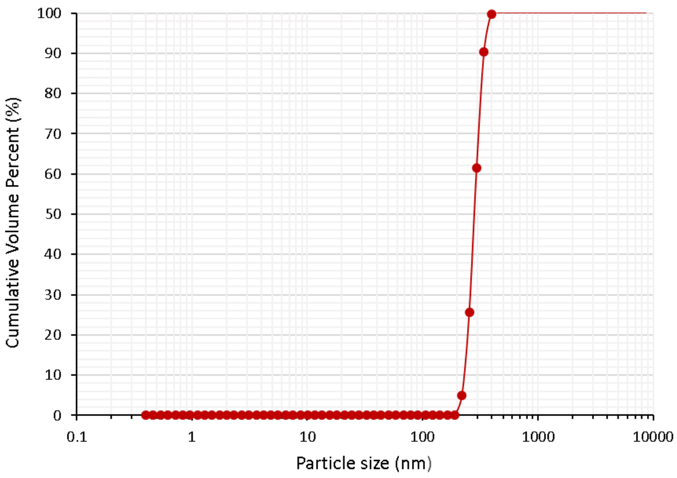

Figure 3.3: Cumulative volume percent versus to particle size for Nano-sized TTB sepiolite clay.

Tablo3.1: d(0.1), d(0.5), and d(0.9) values for all sepiolite clay samples.

Type of clay	d (0.1)	d (0.5)	d (0.9)	Unit
TTB	8.7	30.2	69.2	µm
Kurtşeyh	7.59	30.2	79.4	µm
YDK	8.71	34.67	69.2	µm
S	3.8	22.91	52.48	µm
NTTB	220	295	342	nm

3.1.1 Sample Preparation Protocol

API RP-13B Standard was employed in preparing the clay-water suspensions. All samples were based on the formulation of 350 ml of water phase (distilled water) containing sepiolite, bentonite clays. All clay suspensions are mixed with multimixer during 20 minutes. The amount of clay content in both bentonite suspension and sepiolite suspensions were determined as 13 and 17.5 gr, respectively.

Figure 3.4: Clay suspensions is mixed by using Multimixer.

3.2 Methods

3.2.1 Experimental setup and adjusted parameters

An advanced stress-controlled rheometer (DHR-2 rheometer, TA Instruments, USA) was used to test rheological properties of samples under LAOS. In addition, stress-controlled measurements for colloidal dispersion complex fluid systems (i.e., drilling fluids) is more convenient as they are yield stress fluids. Oscillatory shear deformation of clay suspensions was conducted based on frequency sweep and strain sweep protocols. Complete contact between the sample and two plates was established by setting gap between the upper plate (rotating plate) and Peltier plate (static plate) to be 1.0 mm. It provides the area of contact that is equal to or smaller than the overlapping area of two plates. For the tests at 25° C and 50° C, a cross-hatched solvent trap plate geometry with a diameter of 60 mm and serration on every millimeter were used to avoid occurrence of apparent wall slip. In addition, solvent trap cover was used to provide thermally stable (uniform temperature) vapor barrier environment even at 25° C to prevent evaporation and/or drying of tested sample. The fluid samples were pre-shared at a shear rate of 5 sec^{-1} for 30 second to erase any shear history already created. High sensitivity pressure cell unit of DHR-II with a concentric cylinder geometry (cup and rotor) was used to characterize rheological properties at pressurized environment and elevated temperatures (100 and 150° C). All samples were conditioned by pre-shearing at the rate of 400 sec^{-1} for 120 second prior to test using the pressure cell unit. The strain sweep protocol was carried out at an angular velocity of 10 rad/sec at strain amplitudes from 0.001% to 1000% using parallel plate with crosshatched surface (Ø60 mm) at 25° C. Nonlinear rheological behavior and transition from linear (SAOS) to nonlinear (LAOS) region were determined based on strain sweep protocol. This test was performed at same amount of angular velocity and stress interval using the pressure cell unit at 150° C to avoid evaporation. Oscillatory stress sweep at four frequencies (0.25, 0.50, 0.75, 1 Hz) was also applied to provide deep insight on frequency effect. The range of appropriate frequencies was achieved after testing in too low and too high frequencies by considering sample evolution and instrument inertia effect. Fingerprints of inertia effect was observed for the tested samples at 1 Hz; consequently, testing frequency was limited to maximum of 1 Hz.

The nonlinear data analysis is performed based on Fourier transformation from time domain to frequency spectrum using Fourier Transform (FT) rheology embedded on TRIOS software provided by TA Instrument. It follows by extraction of harmonics, recasting of harmonics, and reconstruction of sinusoidal waves; and consequently, LAOS parameters (non-linear rheological parameters) are calculated. Transient mode was selected during data analysis. Adjusted parameters as conditioning time and sampling time were set to be 1 cycle and 20 sec. In other words, for each stress amplitude and frequency 5, 10, 15 and 20 cycles of LAOS were conducted at 0.25, 0.5, 0.75, and 1 Hz.

3.2.2 Oscillation Amplitude Sweep Tests

The first stage in characterization of viscoelastic behavior is to perform amplitude sweep test and determine the change in the storage and loss moduli (G', G") with increasing strain amplitude at constant frequency. Viscoelastic behavior is observed under small strains up to a critical strain where the initial structural network of material begins to deform. Distortion in material structure increase with increasing strain applied and the deformation response changes from linear to nonlinear viscoelasticity. The amplitude sweep is used to determine the Linear Visco-Elastic region (LVE) of the sample and identify structural stability and dynamic yield point. The amplitude sweep test was carried out at an angular velocity of 10 rad/s at strains from 0.001% to 1000% using parallel plate with crosshatched surface (Ø60 mm) at 25°C. Pressure cell unit was used to apply this test at high temperatures

3.2.3 LAOS protocol procedure

The Large Amplitude Oscillatory Shear (LAOS) measurements were performed to qualify and quantify the nonlinear rheological behavior of fluid samples for strain amplitude varying from 0.01 to 1000 % at 0.25 Hz of frequency. The amount of 0.25 Hz was selected as a tested frequency after some pre-testing regarding instrument inertia effect. The impact of inertia come into play at high frequencies, even if the inertia calibration of the instrument was carried out. In addition, the concerns regarding inertia and lost continuum were removed as the fluid inertia correction from the instrument options was activated. For each stress parameters (amplitude, frequency) a sufficient number of LAOS cycles ranging from 5 to 20 were run to guarantee steady state measurements. The LAOS protocol procedure was explained in details by Ewoldt et al., [37] and they stated that LAOS is the most convenient way to analyze nonlinear viscoelasticity of samples compared to other tests. The Fourier-Transform (FT) software application inserted in the TA DHR-2 rheometer was used to analyze the nonlinear data. The FT-rheology follows by extraction of harmonics, recasting of harmonics, and reconstruction of sinusoidal waves; and subsequently, LAOS parameters were calculated. The Lissajous-Bowdtich curves and the nonlinear viscoelastic parameters such as maximum/minimum strain dynamic moduli, stiffening ratio, elastic/viscous Chebyshev coefficients, maximum/minimum rate dynamic viscosities, and thickening ratio were obtained by FT-rheology application known as TRIOS. More detailed information about Chebyshev equations and interpretations of LAOS parameters were given in recent studies [37]- [6]. Nonlinear parameters and their indications (shear mechanism) have been illustrated schematically by Ettehadi et al., 2021 to make the procedure easy to follow and use [51].

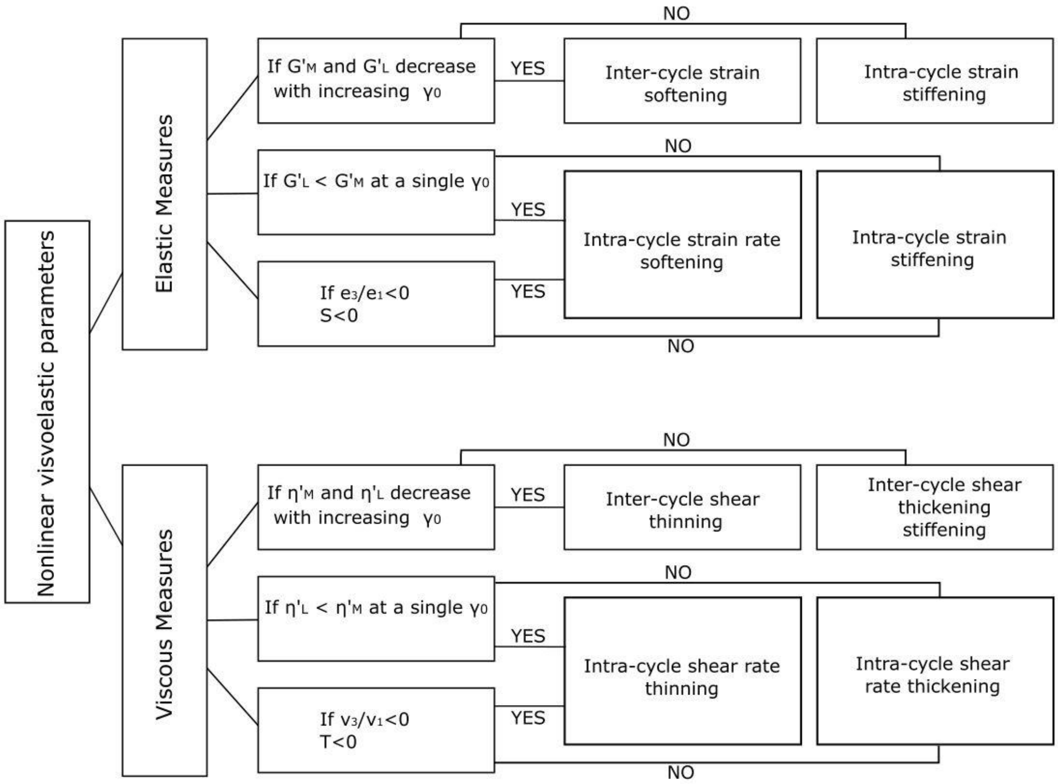

Figure 3.5: Nonlinear viscoelastic parameters obtained under LAOS and their indications [51].

Dissipation ratio was also used as another parameter to evaluate viscoelasticity in suspension samples. Even though, Lissajous-Bowditch curves provide qualitatively nonlinear behavior of clay suspension samples, dissipation ratio enable to summarize information of Lissajous curves [52]. Enclosed area of Lissajous curves indicated dissipated energy of sample during oscillatory strain. In a one cycle, a perfect plastic material dissipates a certain amount of energy that is equal to;

$$(\boldsymbol{E_d})_{pp} = \boldsymbol{4\gamma_0\sigma_{max}} \tag{3.1}$$

Where $\boldsymbol{\gamma_0}$ is strain amplitude, $(\boldsymbol{E_d})_{pp}$ is pure plastic dissipation energy and $\boldsymbol{\sigma_{max}}$ is maximum stress. Generally, actual dissipated energy of a cycle by a strain-controlled LAOS response is only a function of the first-order viscous Fourier coefficient and is calculated by

$$\boldsymbol{E_d = \oint \sigma d\gamma = \pi G_1'' \gamma_0^2} \tag{3. 2}$$

Ewoldt et. al. (2010) intelligently offered that the ratio of actual dissipated energy to perfect plastic dissipation energy gives dissipation ratio as indicated below [52] :

$$\boldsymbol{\phi = E_d/(E_d)_{pp} = {}^{\pi G_1''\gamma_0}\!/_{4\sigma_{max}}} \tag{3.3}$$

Energy dissipation ratio (Ø) could be an effective indictor to quantify dissipation and nonlinearity. Figure 3.5 summarizes that If ϕ = 0, no energy is dissipated, thus the material behaves purely elastic. When ϕ = 1, the entire energy of material was dissipated and the response is perfect plastic. In the case of ϕ = π/4, the behavior of samples will be Newtonian [37].

The ratio of actual dissipated energy to perfect plastic dissipation energy gives dissipation ratio as indicated below:

$$\boldsymbol{\phi = E_d/(E_d)_{pp} = {}^{\pi G_1''\gamma_0}\!/_{4\sigma_{max}}} \begin{cases} 1 & \text{Perfect Plastic} \\ \pi/4 = 0.785 & \text{Newtonian} \\ 0 & \text{Purely Elastic} \end{cases} \tag{3.4}$$

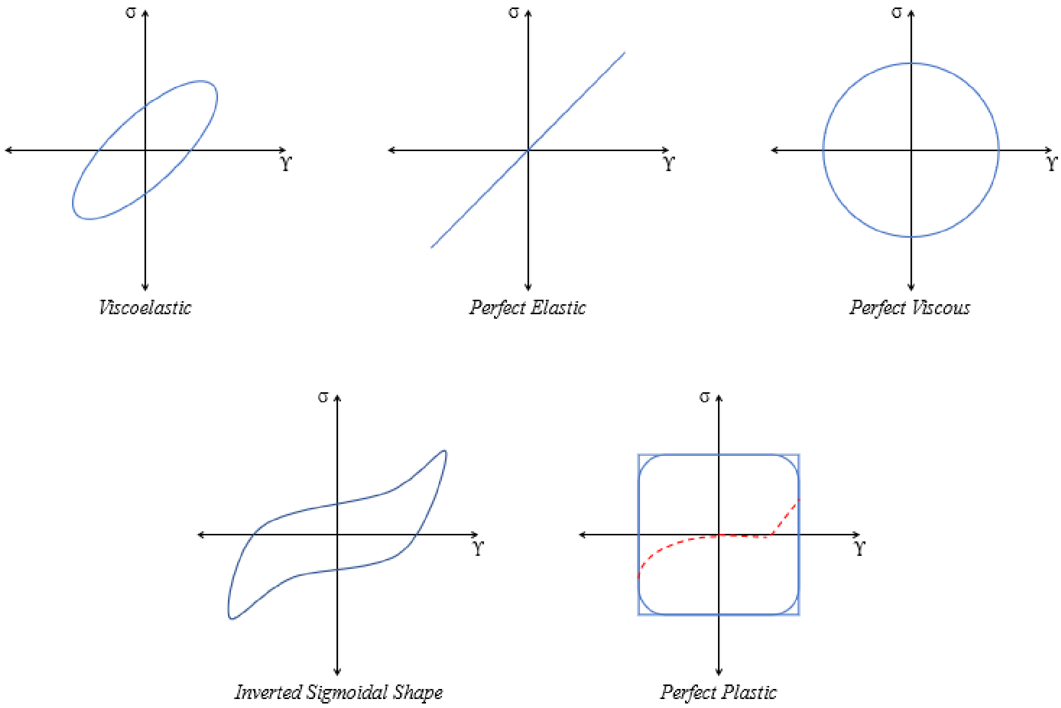

Figure 3.6**:** Stress-strain Lissajous curve of linear viscoelastic, perfect elastic, perfect viscous, inverted sigmoidal shape and perfect plastic behavior [52].

Chapter 4

Result and Discussion

4.1. Amplitude Sweep Test

Strain sweep experiments were used to investigate LAOS behaviors of suspensions at frequencies of 0.25, 0.5, 0.75, and 1 Hz. Figure 4.1 obviously depicts the transition between linear and nonlinear regimes. The storage and loss modulus (G' and G") of a nano-sized sepiolite suspension as a function of strain amplitude, γ_o at 0.25 Hz and 25° C are shown in this figure. At low-stress amplitudes, the moduli show a plateau (linear viscoelastic (LVE) regime limit), followed by a large drop in G' and a modest reduction in G". G' starts to decrease at 1.27 % (percent) oscillation strain while G" remains constant until 8.3 % oscillation strain, at which point G" decreases at a slower rate than G'. Strain (output signal) and stress (input signal) are sinusoidal inside the LVE regime (plateau). Furthermore, strain is identified as the output signal by a constant amplitude and phase lag over cycling. This means that the material's microstructure remains stable during the cycling process. Moving forward, the output signal begins to deviate from a sinusoidal shape for stress amplitudes matching to the decline of the moduli. Furthermore, as the strain amplitude increases for a fixed stress amplitude, the strain amplitude and phase lag change slightly over time. This shows that applied shear stress is breaking the material microstructure's stability.

When a significant deviation from a sinusoidal shape is observed in the output strain signal far from the linear VE regime, higher non-linearities come into the picture. The amplitude and phase lag progress significantly over a cycle, the microstructure is almost completely damaged, and the non-linear flow pattern is mostly considered.

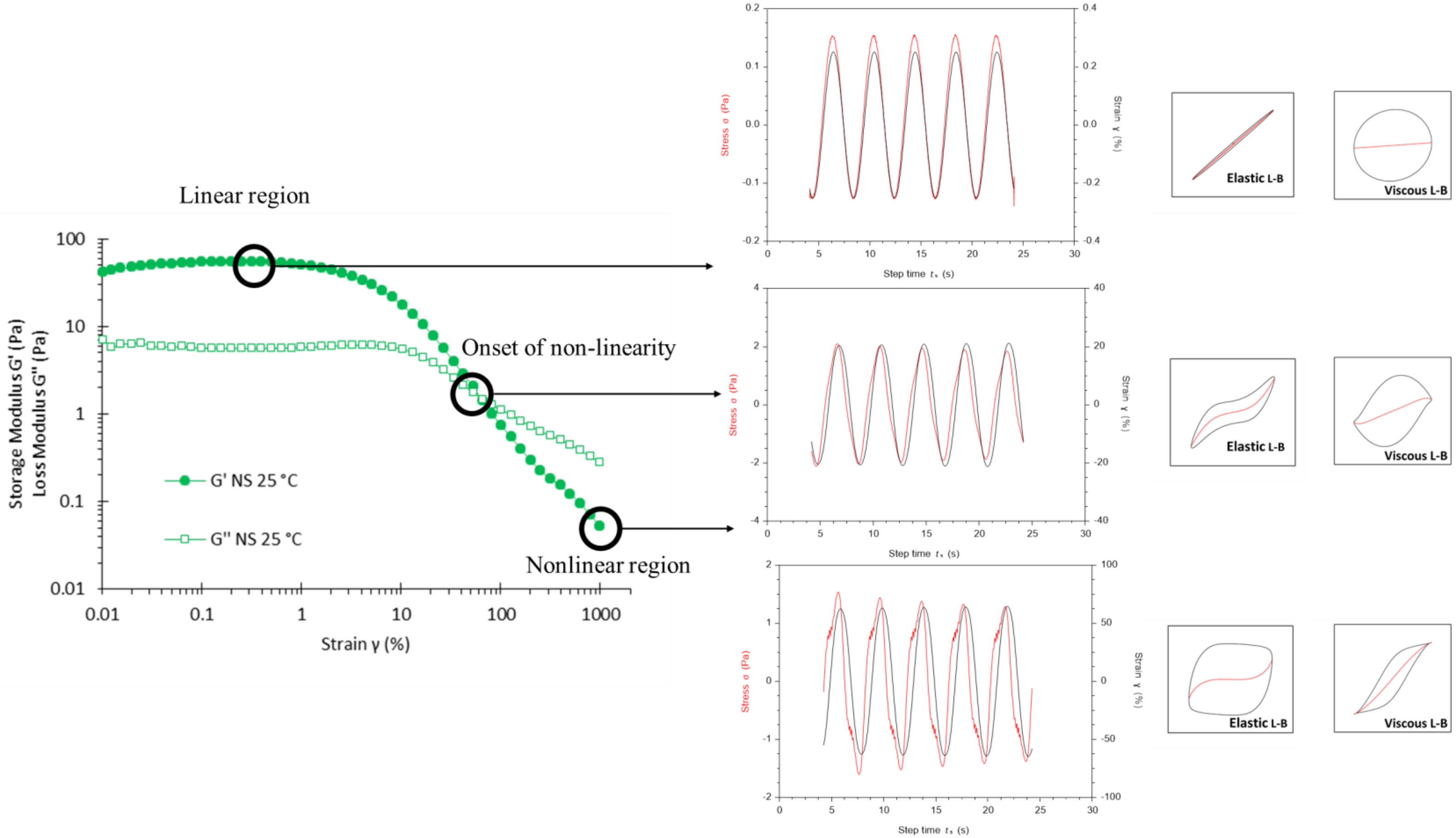

Figure 4.1: Strain Sweep of nano-sized sepiolite suspension with dynamic modulus G' and G''

Figure 4.1 also includes Lissajous curves representing stress vs. strain and strain rate at three strain amplitudes ranging from linear to non-linear. The measured stress wave in linear region is sinusoidal, and the stress vs. strain and strain rate describe an ellipsoid shape. Instead that, the material behaves nonlinearly, and the stress-strain representation's ellipsoid shape transforms into a much more geometrically complex shape. Elastic and viscous stresses are the components of non-linear response that are in phase with the strain and in phase with the strain rate [53]. These are distinct functions that represent straight lines in the linear region through the origins of Lissajous curves. The ellipsoid shapes, on the other hand, tilt with increasing strain. Although these components (elastic and viscous stresses) continue to be distinct functions, they can no longer be represented by a straight line. As a result, higher order Fourier coefficients are required to describe viscous and elastic stresses.

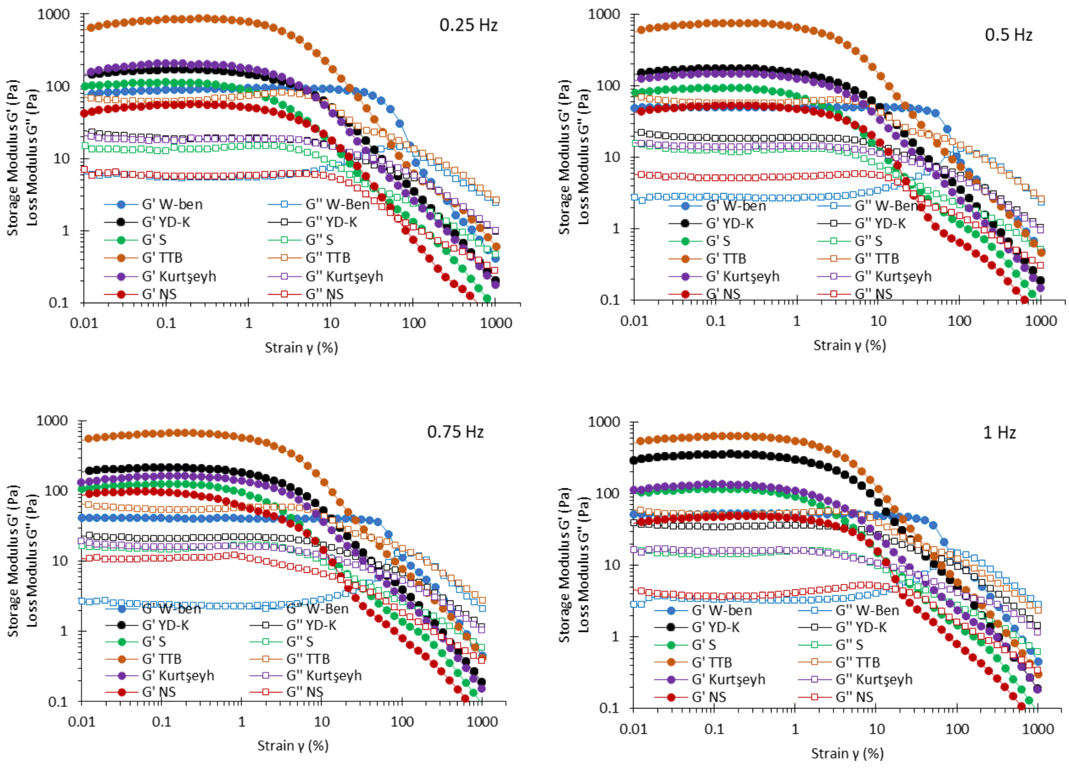

Figure 4.2**:** Storage modulus (**G'**) and loss modulus (**G"**) as a function of strain amplitude for bentonite, YD-K, S, TTB, Kurtşeyh and nano-sized sepiolite suspensions at four different temperatures.

Figure 4.2 depicts strain sweeps for six suspensions at four different frequencies. In this figure, the limit of linear VE and the onset of non-linear regions are clearly visible.

The type of clay and increasing frequency have a minor effect on the transition from linear to nonlinear flow. The quantitative and qualitative differences in G' and G'' behaviors were not changed considerably by LAOS response for different frequencies. This finding is in accordance with the colloidal system literature [23]. The onset of non-linear behavior took place at 0.25 Hz for TTB, Nano sepiolite, YD-K, and Kurtseyh sepiolite clay suspensions with a strain of 1% and remained essentially unchanged at the other higher frequencies studied. When compared to the other sepiolite clay suspensions, the onset of non-linearity occurred at lower strain (0.4 percent) for the S type sepiolite suspension at all of the studied frequencies. For almost all frequencies, strain sweeps revealed that the start of nonlinearity for the Wyoming bentonite suspension occurred at 20% strain. The longer linear viscoelastic region of Wyoming bentonite corresponds to a more stable and flexible structural network formed by the van der Waals attractive forces between clay particles in water. This outcome is to be anticipated because bentonite suspensions prepared with fresh water perform well at low to moderate temperatures.

For all frequencies in the linear VE region, however, all of the sepiolite clay suspensions had a higher storage modulus (G') than the bentonite suspension. Measured data in the linear VE region showed that TTB sepiolite suspension has much more elastic fraction compared to the other sepiolite and bentonite clays. The nano sepiolite-based suspension, on the other hand, has the least elasticity when compared to other sepiolite clay suspensions. Maximum *G'* values in the linear VE region were in the range of 6.29×10^2 to 8.51×10^2 Pa for TTB sepiolite suspension at all the frequencies. The nano sepiolite-based suspension, on the other hand, has the least elasticity when compared to other sepiolite clay suspensions. Maximum *G'* values in the linear VE region were in the range of 4.59×10^1 to 5.48×10^1 Pa for nano sepiolite suspension at all the frequencies. Maximum G' values in the linear VE region for Wyoming bentonite, YD-K, S, and Kurtseyh suspensions, on the other hand, have ranged from 0.4110^2 to $0.93\ 10^2$ Pa, $3.5\ 10^2$ to $1.7\ 10^2$ Pa, $0.93\ 10^2$ to $1.3\ 10^2$ Pa, and $1.3\ 10^2$ to $2.1\ 10^2$ Pa, respectively. The stiffness of the sample or the gel strength is represented by G' values in the LVE region. It is concluded that the nano sepiolite suspension and bentonite suspension yielded a lower gel strength compare to that of the other clay suspensions. On the other hand TTB sepiolite suspension yielded a higher gel strength compare to that of the other clay suspensions. All of the clay suspensions exhibited shear thinning behavior, regardless of frequency because of the fact G’ and G’’ decreasing with increasing strain. For all sepiolite suspensions, a significant decrease in the storage modulus (G') and the loss modulus (G") was observed at the entrance of the LAOS region. After an almost constant value in the LVE region, the G" curve for bentonite suspension rapidly increases to a distinct peak (maximum). The curve then decreases significantly again. Loss modulus (G") values characterize the fraction of deformation energy lost due to internal friction while shear stress is applied. The material begins to flow before the structural breakdown as it approaches the flow point where the first few individual bonds in the network of forces decay. The material's entire microstructure, however, remains firmly held together. This means that G' continues to outperform G" in the sample throughout the testing period.

At the highest frequency applied, crossover in G' and G" values was observed for bentonite and TTB suspensions up to 52.5 % and 42.33 %, respectively (1 Hz). However, at around 21 % strain, a crossover stress modulus was observed for nano sepiolite and S sepiolite suspension, indicating an early structural decay caused by an increase in fluidity with increasing strain. Based on linear viscoelastic parameters, the TTB sepiolite and Wyoming bentonite suspensions had higher gel strength, a more stable network, and a more elastic character.

It is obvious that storage modulus of nano-sized sepiolite suspension is less according to the other suspensions except 0.75 Hz. However, lineer VE range of bentonite suspension is higher than other five suspensions at four frequencies. Diversely, micro-sized sepiolite suspension has more storage modulus than the all of suspensions. Whereas, storage modulus of micro-sized TTB sepiolite suspension is 845.92 Pa, storage modulus of nano-sized sepiolite suspension is 55.54 Pa demonstrating that more power is required to pump TTB sepiolite suspension in shallow wells. Taking all of the mentioned above consideration, nano-sized sepiolite suspension is more preferable than the micro-sized TTB sepiolite suspensions at drilling operations under low temperatures.

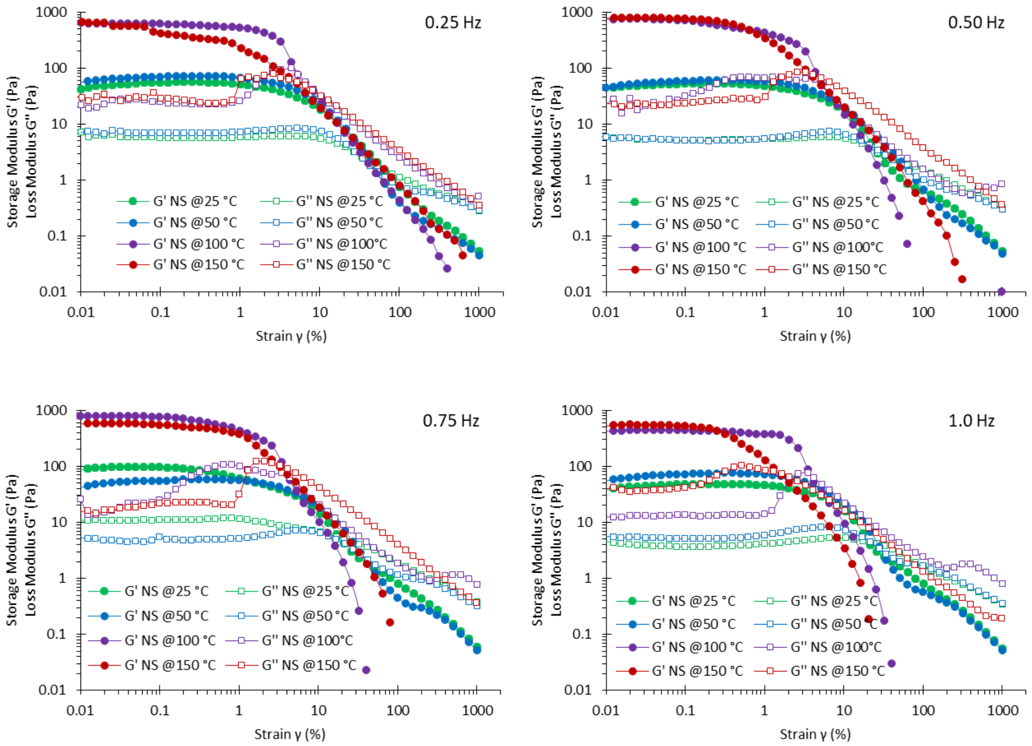

Figure 4.3: Storage modulus (**G'**) and loss modulus (**G"**) as a function of strain amplitude for nano-sized sepiolite suspensions at four different temperatures.

Figure 4.3 present the results of amplitude sweep tests on nano-sized sepiolite suspensions at four different temperatures and frequencies. For 0.25 Hz frequency, the G' value of nano sepiolite suspensions was reported to be 53.26 Pa, 71.33 Pa, 559.61 Pa, and 552.84 Pa for 25° C, 50° C, 100° C, and 150° C temperatures, respectively. Additionaly at 150° C temperature onset of nonlinearity of nano sepiolite is lower than the other three temperatures indicate that increasing temperature give rise to weak structural stability at small strains. At other increasing frequencies (0.50, 0.75 1.0 Hz), the situation did not change considerably.

Based on linear viscoelastic parameters, the nano sepiolite suspensions had lower gel strength, and a less elastic character at low temperatures (25° C, 50° C). On the other hand at high temperatures gel strength and elastic character are much higher impliying more pump power requirement at drilling operations. It could be resulted that nano sepiyolit suspension is preferable at low temperatures since at low tempratures less pump power is required. It is also observable that, at high temperatures (100, 150° C), there was a clear overshoot in loss modulus at intermediate amplitudes, particularly in micro-sized and nano-sized sepiolite suspensions. This finding is consistent with Hyun et al's Type III response [54] (weak strain overshoot) for some complex fluids, in which the loss modulus increases at intermediate stresses before decreasing at larger strain amplitudes. The loss modulus overshoot is a notable marker of the transition from largely solid (viscoelastic equilibrium in linear region) to primarily fluid (plastic flow) [55].

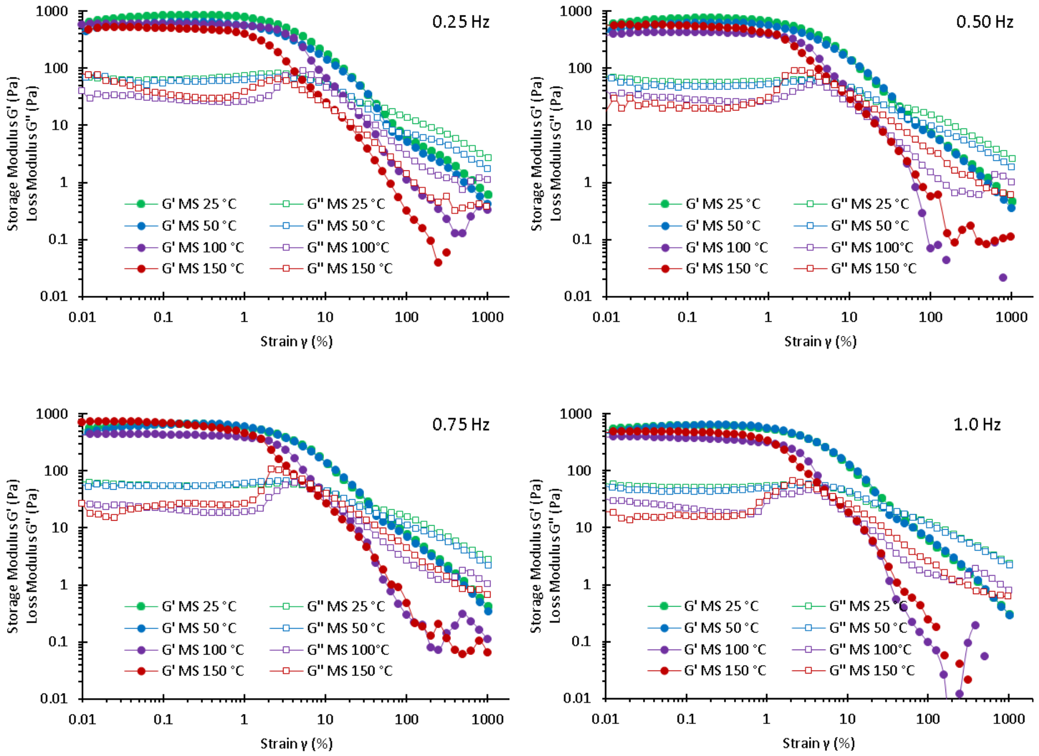

Figure 4.4: Storage modulus (**G'**) and loss modulus (**G"**) as a function of strain amplitude for micro-sized sepiolite suspensions at four different temperatures.

As can be seen in Figure 4.4, there is no significant difference between the G' values at all four temperatures and frequencies. The storage modules at 25° C, 50° C, 100° C, and 150° C were reported to be 592.11 Pa, 636.81 Pa, 502.81 Pa, and 511.95 Pa, respectively, for 0.25 Hz frequency. It is clearly seen that the TTB sepiolite suspension shows similar gel strength and elasticity at low and high temperatures at four different frequencies. Accordingly, although the elasticity and gel strength of the micro-sized TTB sepiolite do not change visibly depending on the temperature, the properties such as the elasticity and gel strength of the nano-sized sepiolite suspension significantly change depending on the temperature. Furthermore, as shown in Figure 4.4, the lineer

VE range of the TTB sepiolite suspension is nearly same at all four temperatures indicating structural stability does not effect by increasing temperature.

4.2 Rheological behavior in non-linear (LAOS) region

Comprehensive assessment of the nonlinear viscoelastic character of six water clay suspensions was qualified based on Lissajous-Bowditch curves and quantified by nonlinear parameters. The nonlinear oscillatory responses of fluid samples at a fixed frequency (0.25 Hz) were visually evaluated using normalized Lissajous- Bowditch curves at 25° C, 50° C, 100° C and 150° C. Lissajous- Bowditch curves were normalized in terms of the maximum stresses (σ/σ_{max}, σ'/σ'_{max},σ''/σ''_{max})and maximum strain and shear rate amplitude (γ/γ_{max} and $\dot{\gamma}/\dot{\gamma}_{max}$). Pipkin diagrams involved Lissajous-Bowditch curved under 0.063, 0.63, 6.31, 63, 125, 268, 812, and 1015% strain deformations were created to evaluate nonlinearities. The Lissajous- Bowditch curves were evaluated along with the energy dissipation ratio to obtain a better insight into viscoelastic responses. Normalized Lissajous-Bowditch curves were generated and given through from Figures 4.5 through 4.8. Elastic and viscous projections of Lissajous curves provide in-dividual plots of normalized total stress (black lines) and normalized elastic component in stress versus strain plane and the viscous component of stress in stress versus strain rate plane (red lines). Lissajous curves provided a more sensitive indicator of nonlinearity since the appearance of higher harmonics in FT Rheology is the reason for changes in the Lissjous curves' shape.

4.2.1 Evaluation of normalized elastic projection of Lissajous curves

Figure 4.5 shows elastic Lissajous–Bowditch curves as a function of frequency for all clay suspensions. Ewoldt et al. [39]-[18] revealed circular trajectories in elastic Lissajous curves are presented as response of viscous dominated materials. Elastic dominated behavior was characterized by narrow elliptical trajectories, while viscoelastic behavior was characterized by elliptical trajectories with finite major to minor axes. Figure 4.5 demonstrates that as the strain was increased, the elliptical shape of the stress response became wider and more distorted, indicating increased non-linearity, suspended structural decay, and viscous behavior. As a result, the elastic

Lissajous–Bowditch loops' circular shape and larger size would be obvious evidence of the transition from elastic dominant behavior to more liquid-like viscous behaviour [37]- [42]. While non-linearity (change from a narrow ellipse) starts after 0.63% for all sepiolite suspensions, the Lissajous curves of Wyoming bentonite suspensions showed that the transition from linear to non-linearity began after 6.31% strain. In other words, in sepiolite suspensions, nonlinearity and structural deformation start earlier than in Wyoming bentonite suspensions. Furthermore, when compared to all sepiolite suspensions, Wyoming bentonite suspension exhibited more elastically dominated behavior. The trajectories of all sepiolite suspensions were increasing wider and faster than those of Wyoming bentonite suspension, as seen in the elastic Lissajous–Bowditch curves in Figure 4.5.

The elastic component (σ') of stress, illustrated by the red lines in Figure 4.5 elastic Lissajous curves, can also help in understanding the material's viscous and elastic properties, as well as its non-linearity. In the linear region, this component seems to be a straight line passing through the origin. As the non-linearity begins, distortion in the material structure is induced, the deviation will be seen. The more structural deformation occurs as the shape of elastic component lines deviates from rectilinear, indicating softer and fluid-like behavior. A quick glance on Figure 4.5 reveals that beyond lineer VE range, the deviation of elastic component (σ') projections (red lines) are visible for all the studied clay suspensions imply that deformation in the material structure is observed.

Energy dissipation ratio (ϕ) defined by Ewoldt, 2008 could be an effective indictor to quantify dissipation and nonlinearity[37]. Figure 4.6 shows the changes in energy dissipation ratio concerning strain amplitude for all clay suspensions at 0.25 Hz, 0.50 Hz, 0.75 Hz and 1.0 Hz frequency. Following observation can be made by evaluating dissipation ratio as a function of strain amplitude for six clay suspensions examined at 25° C in this study. As can be seen in Figure 4.6, the energy dissipation ratio (ϕ) shows 0 up to 1% in all clay suspensions except bentonite clay suspension. This explains that suspensions show excellent elastic properties up to 1%. On the other hand, it is seen that the bentonite suspension maintains its structural stability up to 10% strain deformation. As a result the energy dissipation ratio is almost zero for all six clay suspensions at low strain amplitudes indicating a perfect elastic response. The dissipation ratio is increased with increasing strain and finally, a maximum ratio of about 0.87 was recorded which is a clear sign of viscous behavior.

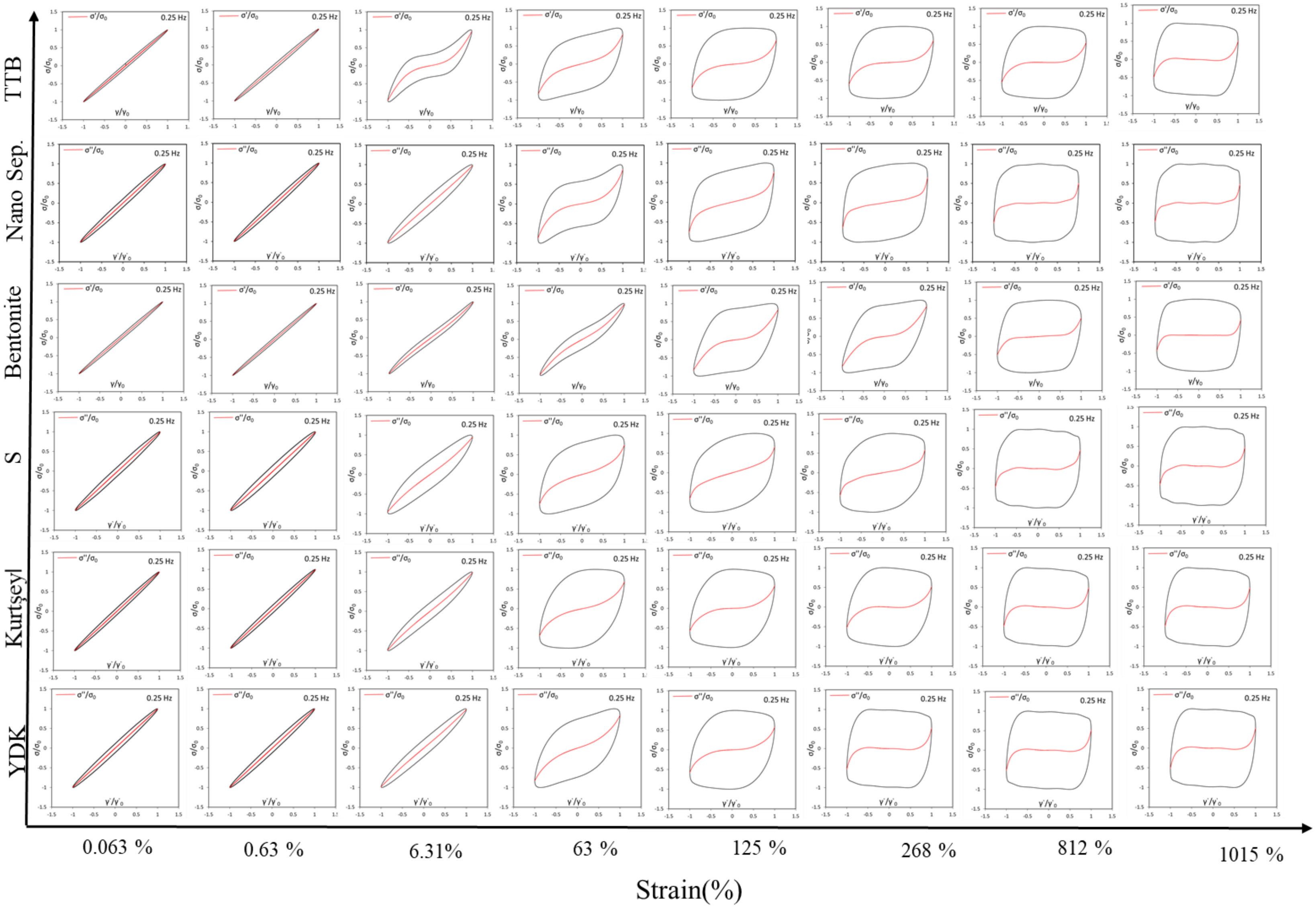

Figure 4.5: Lissajous-Bowditch curves for the elastic component of six water-clay suspensions at 0.25 Hz frequency.

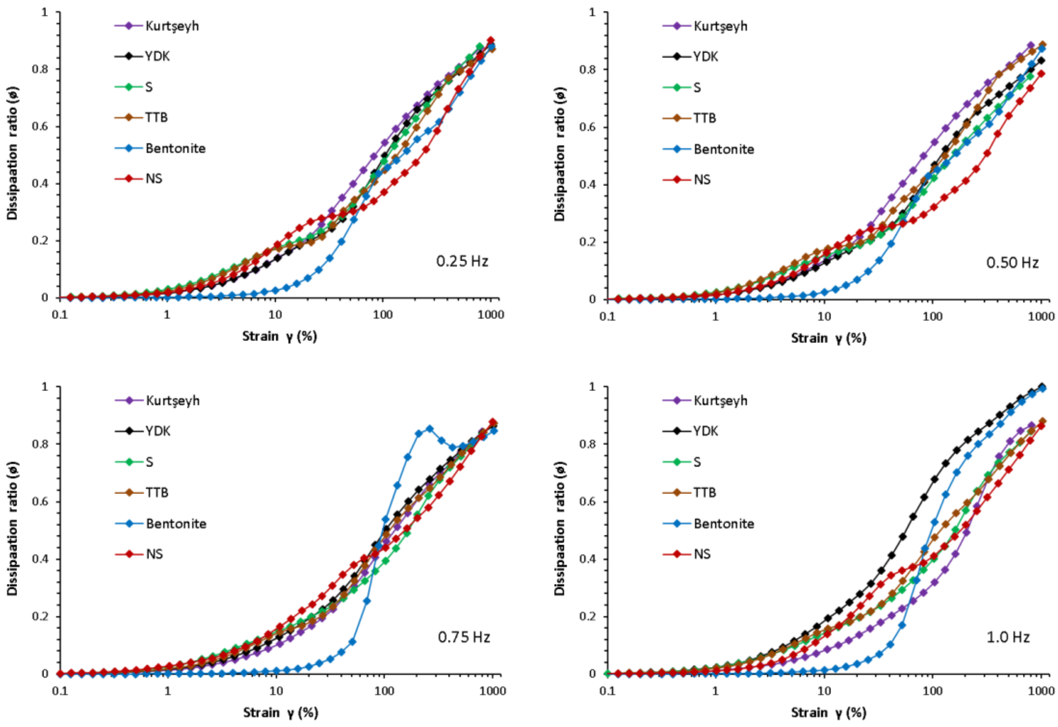

Figure 4.6**:** Dissipation ratio for six suspensions at 25° C and four different frequencies.

Figures 4.8 and 4.9 show Lissajous curves for nano and TTB sepiolite suspensions respectively at four different temperatures (25° C, 50° C, 100° C, 150° C) and a constant frequency of 0.25 Hz, respectively. Transition from linear to non-linear flow suggesting structural breakdown, can be identified from deformation in the shape of Lissajous curves. Under all of four temperatures (25° C, 50° C, 100° C, 150° C) deviation in shape of Lissajous curves was observed with increasing strain amplitude for nano and TTB sepiolite suspensions which exhibits viscous behavior even at small strains. Figure 4.8 shows how, at low strain values, increasing temperature causes Lissajous curves to narrow. At higher temperatures, the elastic property and gel strength increase. These findings are also in agreement with those of the amplitude sweep test. In addition, with the onset of nonlinearity, Lissajous curves appear to be wider at high temperatures. This indicates that the nano sepiolite suspension dissipates more energy at higher temperatures. However, there was no noticeable difference in the elasticity of TTB sepiolite suspension with increasing temperature. Based on this analysis, it can be concluded that TTB sepiolite suspension has more thermal stability than nano sepiolite suspension. Figure 4.7 indicates the dissipation ratio of nano and TTB sepiolite suspensions under four temperatures and at two frequencies (0.25 Hz, 1.0 Hz). Following observation can be made by evaluating dissipation ratio as a function of strain amplitude for two sepiolite clay suspensions examined in this study;

- At low temperatures, the energy dissipation ratio (DR) is almost zero for two sepiolite suspensions (nano-micro sized TTB) at low strain amplitudes indicating a perfect elastic response. The dissipation ratio is increased with increasing strain and finally, a maximum ratio of about 0.89 was recorded which is a clear sign of viscous behavior. However, as temperature increased, DR value in the nano suspension decreased more than in the TTB suspension.

- The dissipation ratio value in both suspensions increased dramatically at 0.25 Hz frequency as the excellent elasticity started to deteriorate at high temperatures.

- Compared with TTB sepiolite suspension the dissipation ratio for nano sepiolite suspension is higher at low strain amplitudes and lower at high strain amplitude with increasing temperature to 150° C. This implies more elastic behavior in low strains for TTB sepiolite suspension and more viscous behavior at high strains compare to nano sepiolite suspension. TTB sepiolite suspension has a larger dissipation ratio indicating more energy dissipation and viscous behavior than nano sepiolite suspension under large strains.

- At 1.0 Hz and 150° C, the dissipation ratio for nano sepiolite suspension is much lower than others indicating a stronger elastic response compare to other sepiolite suspension. This could be a sign of flocculation for nano sepiolite suspension at high temperatures.

Another important aspect impacting the material's elastic and viscous properties during oscillatory flow is frequency. Higher strain rates and greater energy spent for oscillatory flow resulted from higher frequencies combined with increased strain [38]. Because the area covered by the loops is proportional to the energy used during oscillatory flow, as the frequency increases, the trajectories become wider and more deviated, indicating softer and more liquid-like viscous dominating behavior. This detection can be seen in the elastic Lissajous–Bowditch curves of all clay suspensions.

This can be better identified in the TTB clay more than the others. By increasing frequency from 0.25 to 1 Hz, the Lissajous curves became wider and thicker indicating less elasticity and dominant viscous character for the TTB suspension at 1 Hz.

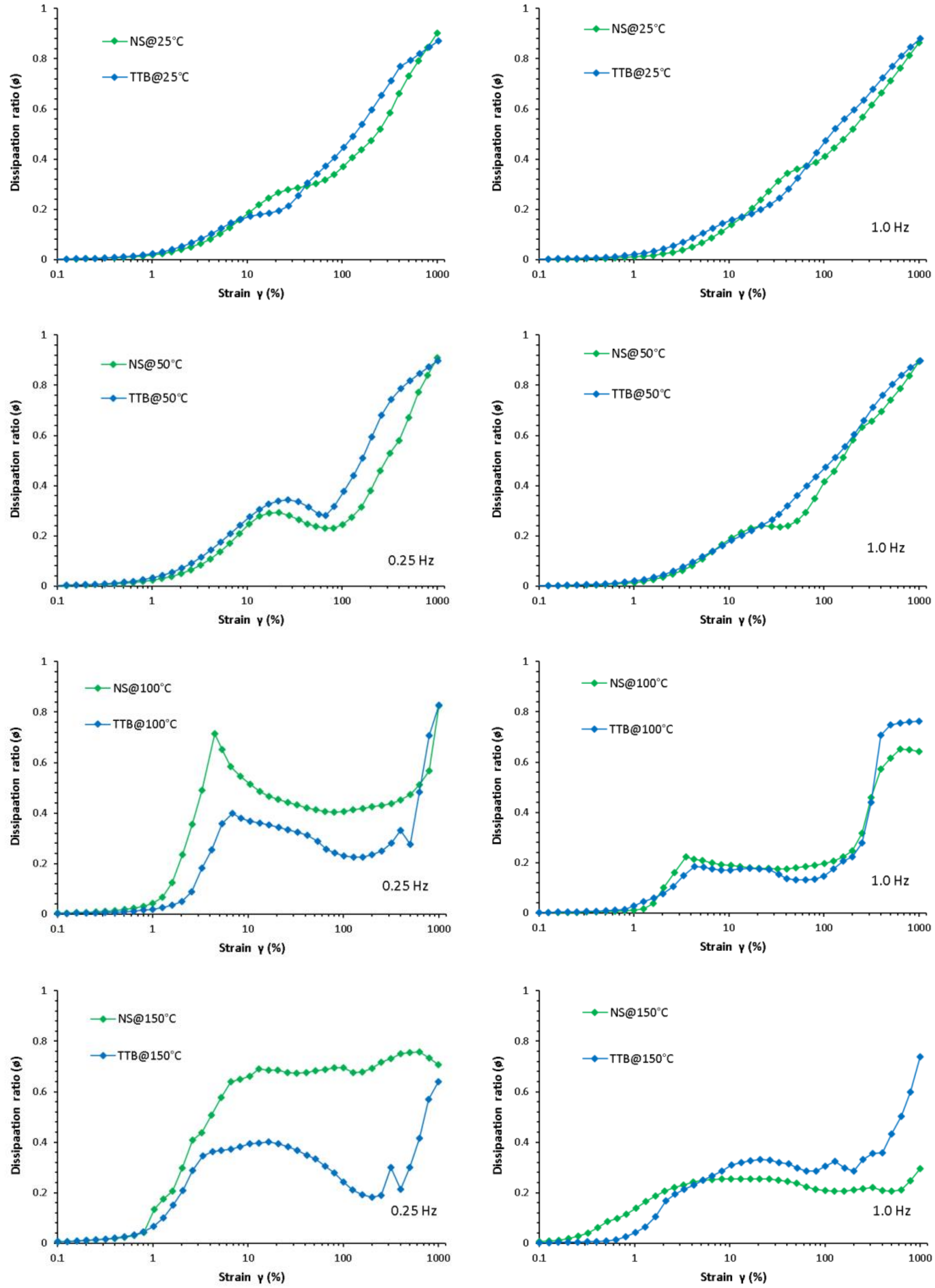

Figure 4.7: Dissipation ratio of nano-sized and micro-sized sepiolite samples at 0.25 Hz and 1.0 Hz.

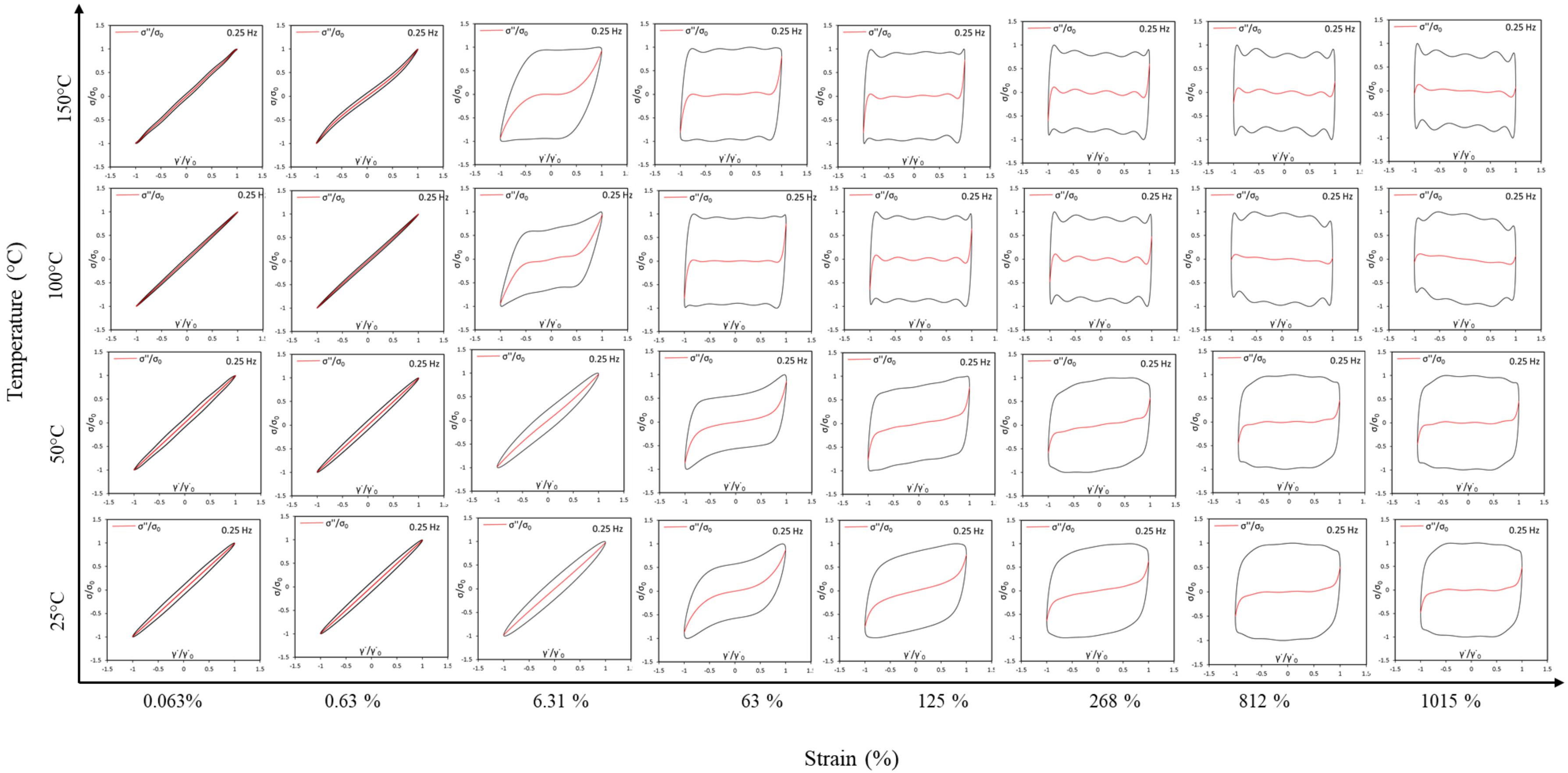

Figure 4.8: Lissajous-Bowditch curves for the elastic component of nano sepiolite clay suspensions at 0.25 Hz frequency for four different temperatures (25° C, 50° C, 100° C, 150° C).

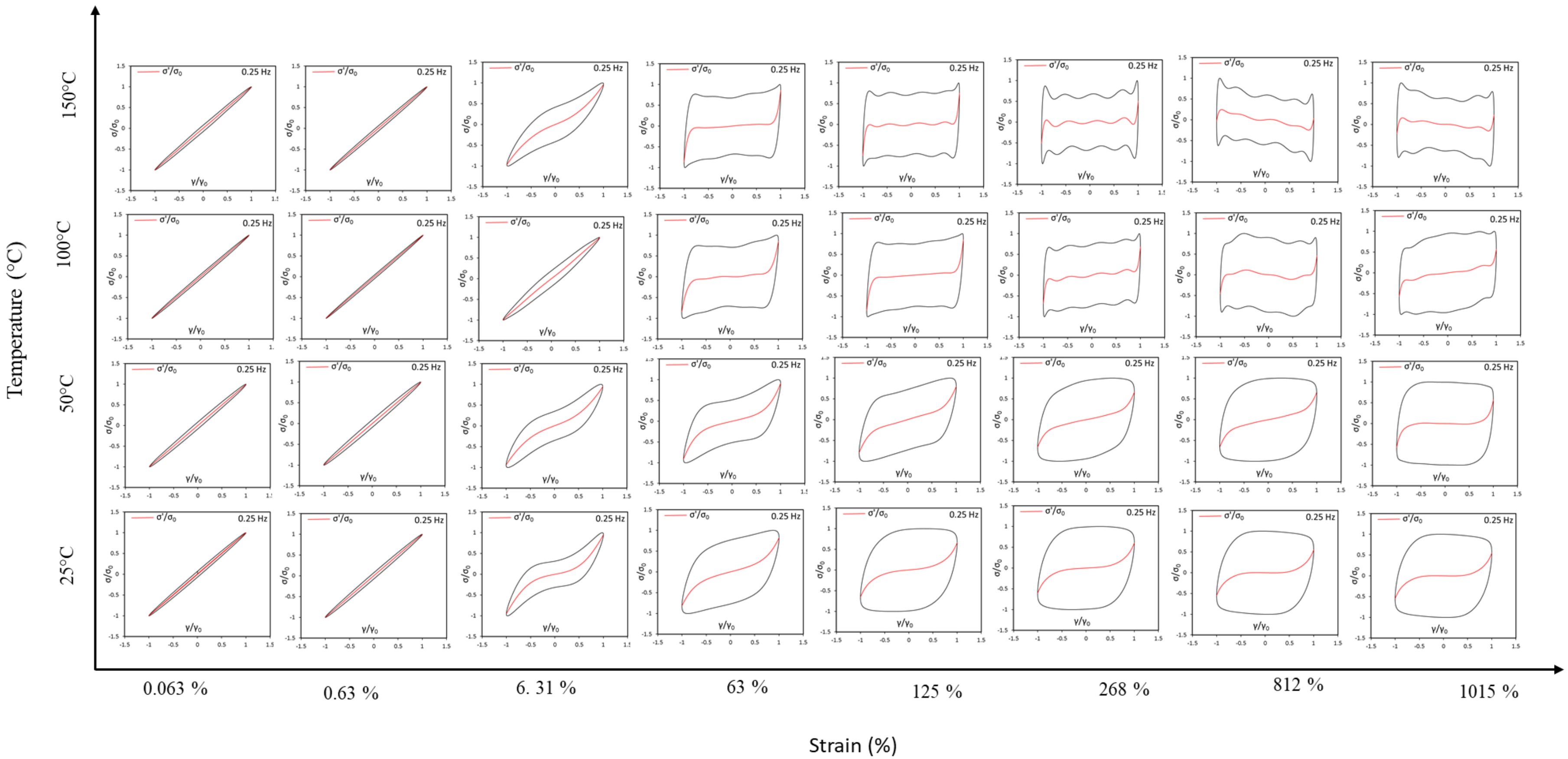

Figure 4.9: Lissajous-Bowditch curves for the elastic component of TTB sepiolite clay suspensions at 0.25 Hz frequency for four different temperatures (25° C, 50° C, 100° C, 150° C.

4.2.2 Evaluation of normalized viscous projection of Lissajous curves

In order to qualitative evaluation of viscous projection for each sample, Lissajous-Bowditch curves are plotted as normalized total stress responses $\boldsymbol{\sigma/\sigma_{max}}$, (black lines) and normalized viscous component $\boldsymbol{\sigma''/\sigma''_{max}}$ (red lines) as a function of normalized strain rate $\boldsymbol{\dot{\gamma}/\dot{\gamma}_{max}}$. Normalized viscous Lissajous-Bowditch curves for six clay suspensions at 25° C are depicted in Figure 4.10. In Figures 4.11 and 4.12, the L-B curves of nano and TTB sepiolite suspensions at four different temperatures, respectively, are given at a constant frequency of 0.25 Hz. As the ellipses become wider, the viscoelastic behavior will take precedence over the linear viscous behavior.

From a viscous viewpoint, the circular shape of stress responses disappeared and was replaced by an elliptic shape as strain increased from 0.0063 to 1015 percent (Figure 4.10). With increasing strain rate amplitude in the nonlinear region, the Lissajous curves become tighter and narrow representing more viscous dissipation. The Lissajous curves changed to a sigmoidal curve (S shape) at relatively high strain rate values designating a strong shear thinning properties in viscous response of total stress for six clay suspensions. The stress response for the bentonite clay suspensions was represented by a larger ellipse than the other clay suspensions, as shown in Figure 4.10. The circularity in the shape of trajectories was greater in the other suspensions (up to 63 percent strain). This indicates that the bentonite clay suspensions have a more stable and elastic dominant suspension than the others. In the non-linear region, the elliptical shape of the stress response for nano and S sepiolite suspension was smaller and narrower than that of the others, indicating more fluid-like and viscous behavior. The elliptic shape of stress response trajectories became wider as the frequency was reduced from 1 to 0.25 Hz, and the distance of ellipses from circle trajectories decreased, confirming the stiffer and elastic behavior of suspensions (Appendix A-B). All of the clay suspensions exhibited this characteristic.

In Figure 4.11 and 4.12 similar to the elastic L-B curves, deformation in the shape of viscous Lissajous curves implies that evolution from linear to non-linear flow was observed with increasing strain amplitude for two clay suspensions. Unlike elastic stress components, an increase in the slope of the viscous stress component (red line) is identified as the signature of gradual transition from elasticity to the plasticity. The transition from elastic behavior to viscous behavior was more pronounced in both of nano and TTB sepiolite suspensions at 150° C as a rapid increase in the slope of the viscous stress component and an abrupt shape deformation was observed in their L-B curves. A secondary loop identified as self-intersection in viscous L-B curves was observed for both sepiolite suspensions at high strain amplitude and 150° C. The formation of secondary loops in the stress-strain rate plot has been previously re-ported for some materials under the LAOS test.

It means that at this particular point the elastic stress is zero and stress response is not dependent on strain amplitude. Secondary loops in the stress-strain rate plot are an indication of viscoelastic overshoot which can be identified by negative slopes of minimum strain modulus (G'_M) in the stress-strain plane. This phenomenon in viscoelastic behavior is reported to be similar to the shear stress overshoot at the intercept of steady shear flow[56]. The secondary loops are expected when the broken microstructure of the sample network is reversibly recovered. Therefore, these loops appear in L-B curves when the time for recovering microstructure is lower than the oscillatory deformation time which is strong evidence of thixotropic recovery in nano and TTB sepiolite suspensions. Lissajous curves are only convenient for a qualitative evaluation of viscoelastic nonlinearity. Quantitative evaluation of nonlinear viscoelasticity should be performed using nonlinear elastic and viscous LAOS parameters.

All of these observations were confirmed and concluded from the interpretation of elastic Lissajous-Bowditch curves. The Lissajous-Bowditch curves are inconvenient for assessing non-linearity quantitatively. They can be a valuable way to visually in qualitative investigation. To quantify non-linearity under LAOS, the other LAOS factors should be evaluated. ($\boldsymbol{G'_L}$, $\boldsymbol{G'_M}$, $\boldsymbol{\eta'_L}$, $\boldsymbol{\eta'_M}$, $\boldsymbol{e_3/e_1}$, $\boldsymbol{v_3/v_1}$, $\boldsymbol{S}$, $\boldsymbol{T}$).

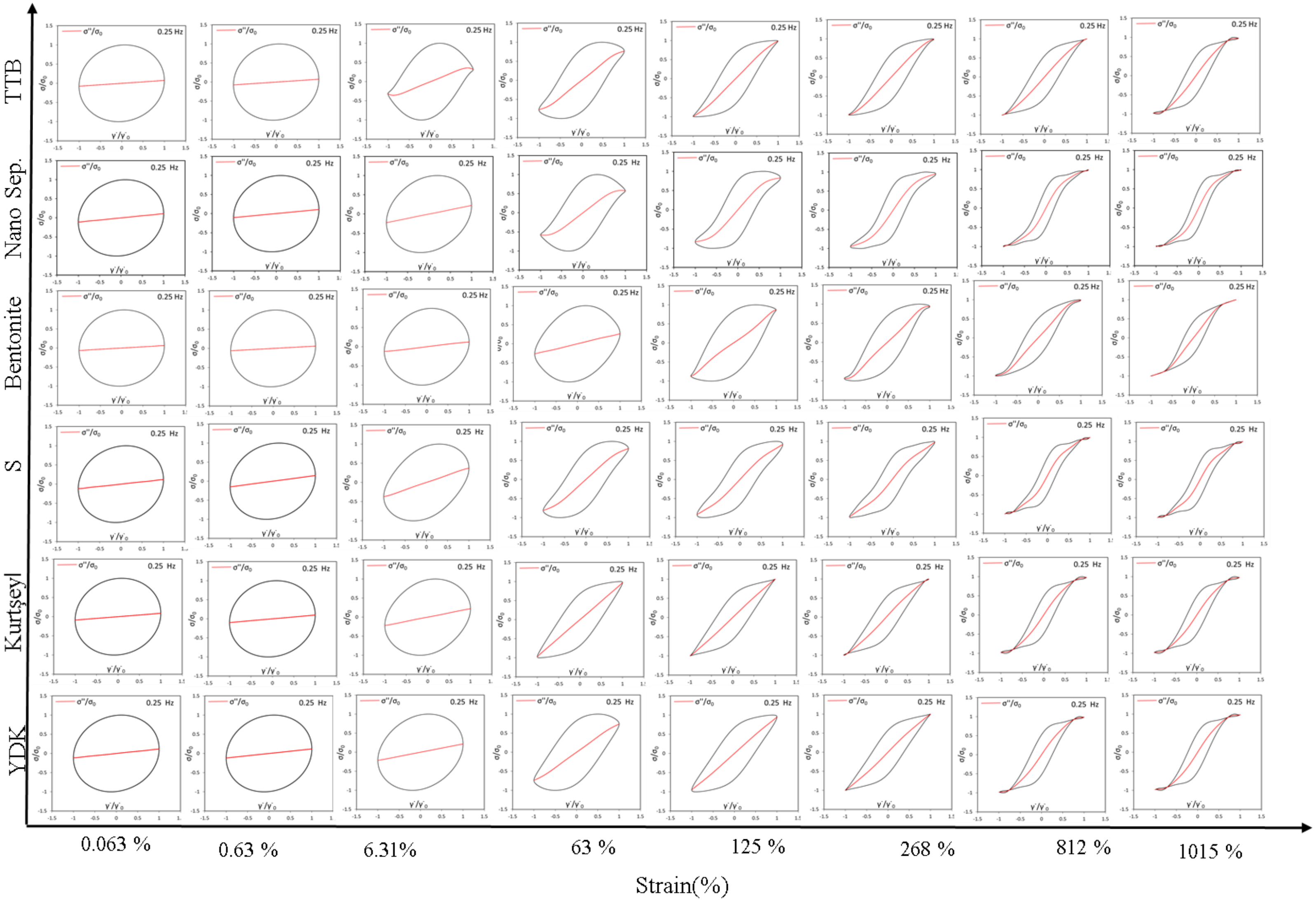

Figure 4.10: Lissajous-Bowditch curves for the viscous component of six water-clay suspensions at 0.25 Hz frequency.

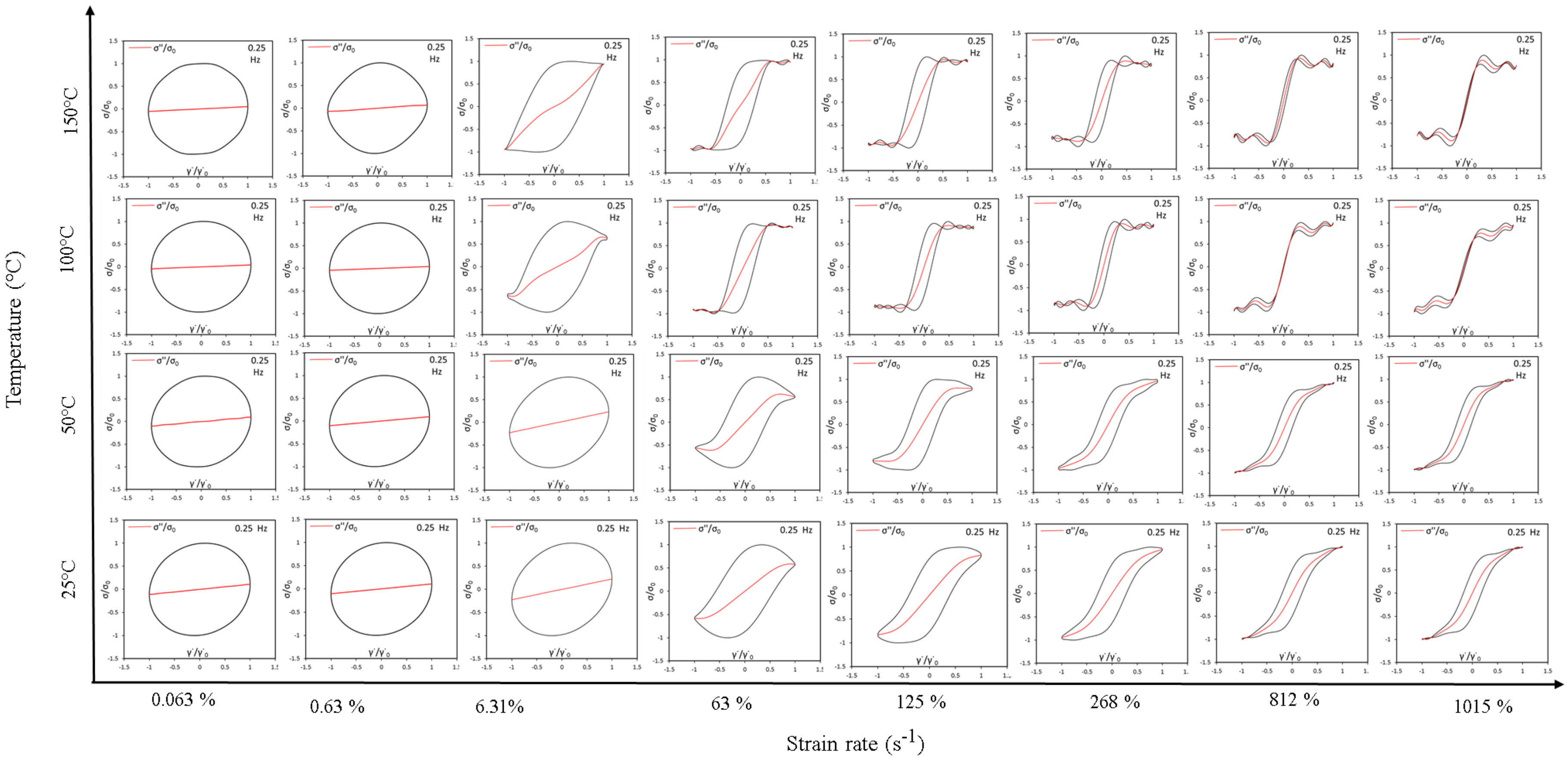

Figure 4.11: Lissajous-Bowditch curves for the viscous component of nano sepiolite clay suspensions at 0.25 Hz frequency for four different temperatures (25° C, 50° C, 100° C, 150° C).

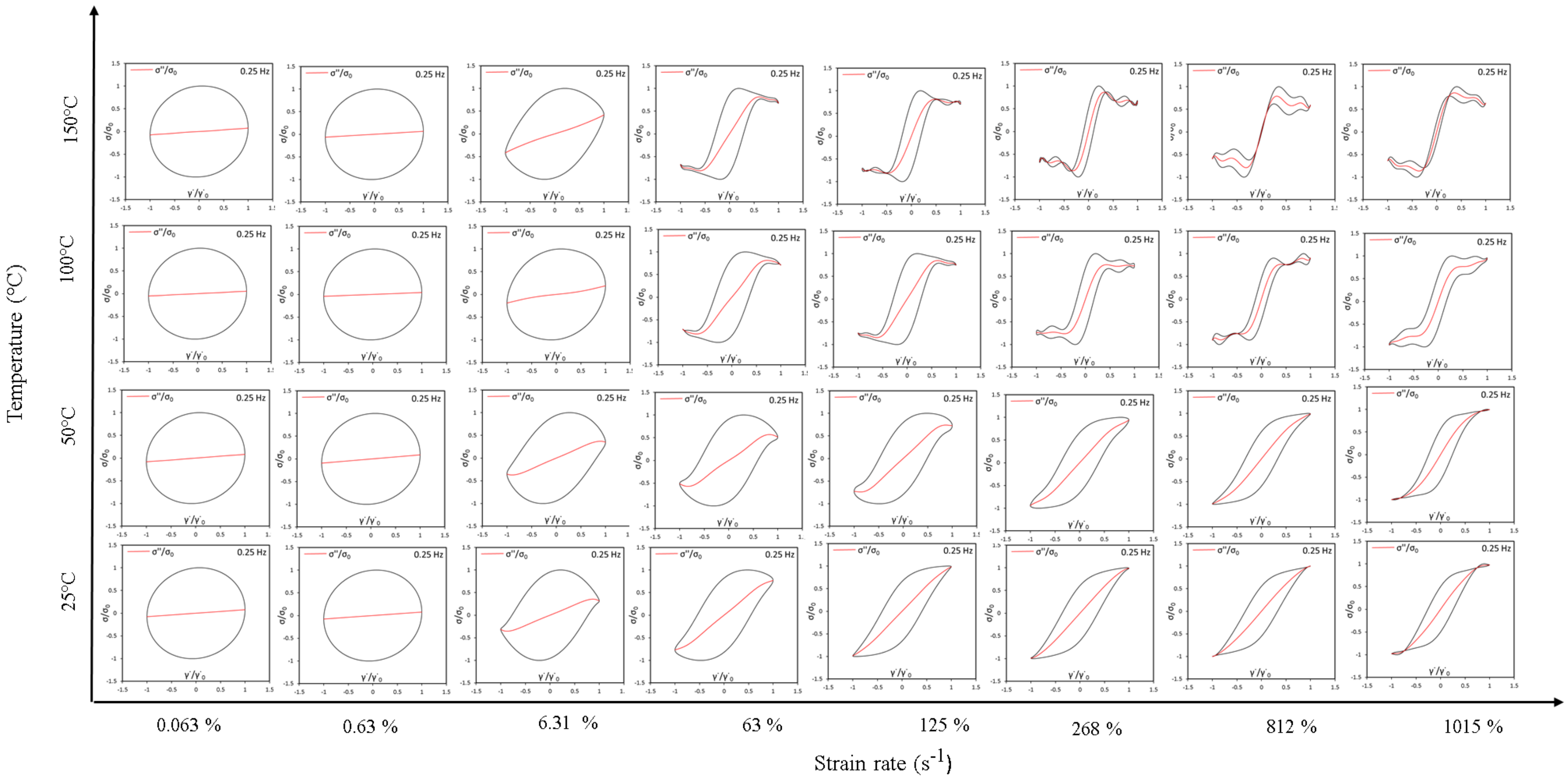

Figure 4.12: Lissajous-Bowditch curves for the viscous component of TTB sepiolite clay suspensions at 0.25 Hz frequency for four different temperatures (25° C, 50° C, 100° C, 150° C).

4.3 Nonlinear Elastic Parameters of Clay Suspensions

Nonlinear elastic parameters ($\boldsymbol{G'_L}, \boldsymbol{G'_M}, \boldsymbol{e_3/e_1}, \boldsymbol{S}$) were considered to quantify the nonlinear elastic response of clay suspensions. The change in large strain moduli ($\boldsymbol{G'_L}$) with applied strain amplitudes for nano, TTB, S, YDK, Kurtşeyh sepiolite and bentonite clay suspensions at 25° C under four frequencies (0.25, 0.50, 0.75, 1.0 Hz) are illustrated in Figures 4.13. In order to present a more detailed and clear observation, the change in large and minimum strain moduli ($\boldsymbol{G'_L}$, $\boldsymbol{G'_M}$) values of each clays are presented in Figure 4.14 under the frequencies of 0.25 to 1.0 Hz and at 25° C.

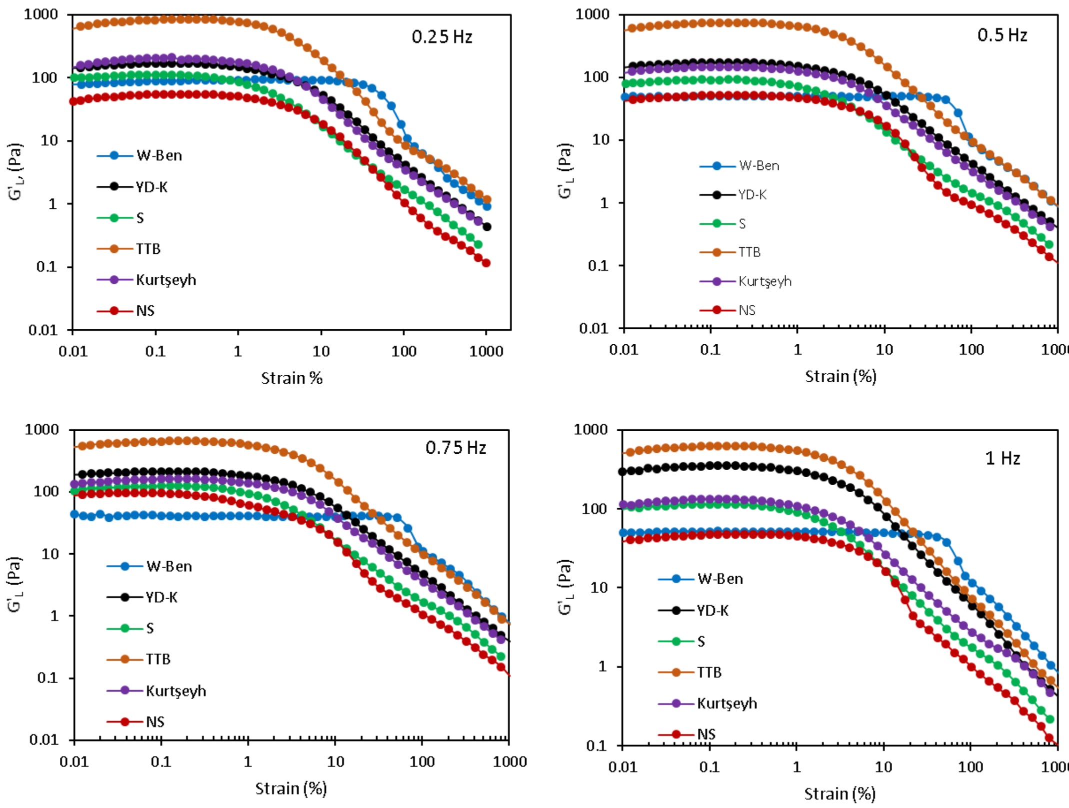

Figure 4.13: Large strain modulus (G'$_L$) values for water-clay suspensions at 25° C and four different frequencies.

Nano sepiolite and Bentonite clay suspension are the two suspensions with the lowest (G'_L) value among the six clay suspensions for all frequencies. Therefore, its elastic properties are less dominant than other clay suspensions. On the other hand, at low strain in the linear area, TTB clay suspension has the highest large strain modulus (G'_L) values in all frequencies. However, it is lower than the large strain modulus (G'_L)

obtained for Wyoming bentonite suspension at high strain (over 10%), despite the fact that its G'_L values are already the highest among sepiolite clay suspensions. Longer linearity is observed in Wyoming bentonite suspension, with the lowest and highest large strain modulus (G'_L) values in the linear and nonlinear regions, respectively. Except YDK clay suspension, increasing frequency leads to decreasing of the amount of large strain modulus (G'_L) for all suspensions(Figure 4.13). This contradiction should be interpreted in light of the morphological structures of clay minerals and the interaction of YD-K clay particles with the aqueous phase, which is not the topic of this study. Test results revealed that nano clay suspension has the lowest amount of large strain modulus (G'_L) in nonlinear region, although except 0.25 Hz frequency its large strain modulus (G'_L) values is higher than or equal to bentonite clay suspensions at linear region. Except for nano sepiolite, all sepiolite clay suspensions have a larger large strain modulus (G'_L) in the linear region than bentonite suspensions. This means that nano sepiolite has a lower gel strength at low temperatures than other suspensions. Therefore, less power is used to pump the nano sepiolite suspension at low temperatures during drilling operations.

Figure 4.14 represents the variation of large and minimum strain modulus $\boldsymbol{G'_L}$ **and** $\boldsymbol{G'_M}$ as a function of strain amplitude at 0.25 and 1 Hz to make a detailed comparison. As a common observation for all suspensions both large and minimum strain moduli ($\boldsymbol{G'_L}$, $\boldsymbol{G'_M}$) were reduced to the first harmonic storage modulus (G') in linear region indicating little nonlinearity. In addition, both $\boldsymbol{G'_L}$ **and** $\boldsymbol{G'_M}$ were dramatically decreased by increasing strain amplitude indicating strong inter cycle strain softening behavior for all suspensions at 25° C temperature. However decrement in the minimum strain modulus $\boldsymbol{G'_M}$ was much more than the large strain modulus $\boldsymbol{G'_L}$ as strain amplitude was increased and all suspensions were subjected to nonlinearities ($\boldsymbol{G'_M}$) was decreased more quickly than ($\boldsymbol{G'_L}$). For instance, the large strain modulus ($\boldsymbol{G'_L}$) was decreased from 50.46 Pa t.o 0.79 Pa for the nano suspensions while the minimum strain modulus ($\boldsymbol{G'_M}$) decrease from 48.7Pa to 0.27 Pa with the increasing strain amplitude from 1% to 127%. This indicates that the strain-rate softening of the elastic modulus dominated the elastic nonlinearity of all drilling mud samples. In the nonlinear region, the difference between minimum strain modulus ($\boldsymbol{G'_M}$) and large strain modulus ($\boldsymbol{G'_L}$) decreases with increasing frequency. TTB clay suspension has a greater difference between $\boldsymbol{G'_L}$ **and** $\boldsymbol{G'_M}$ at all frequencies, indicating a more stable gel structure than the others. It is also obvious that at 25° C all clay suspensions exhibits strain softening behavior at high stains under both frequencies (0.25 and 1.0 Hz).

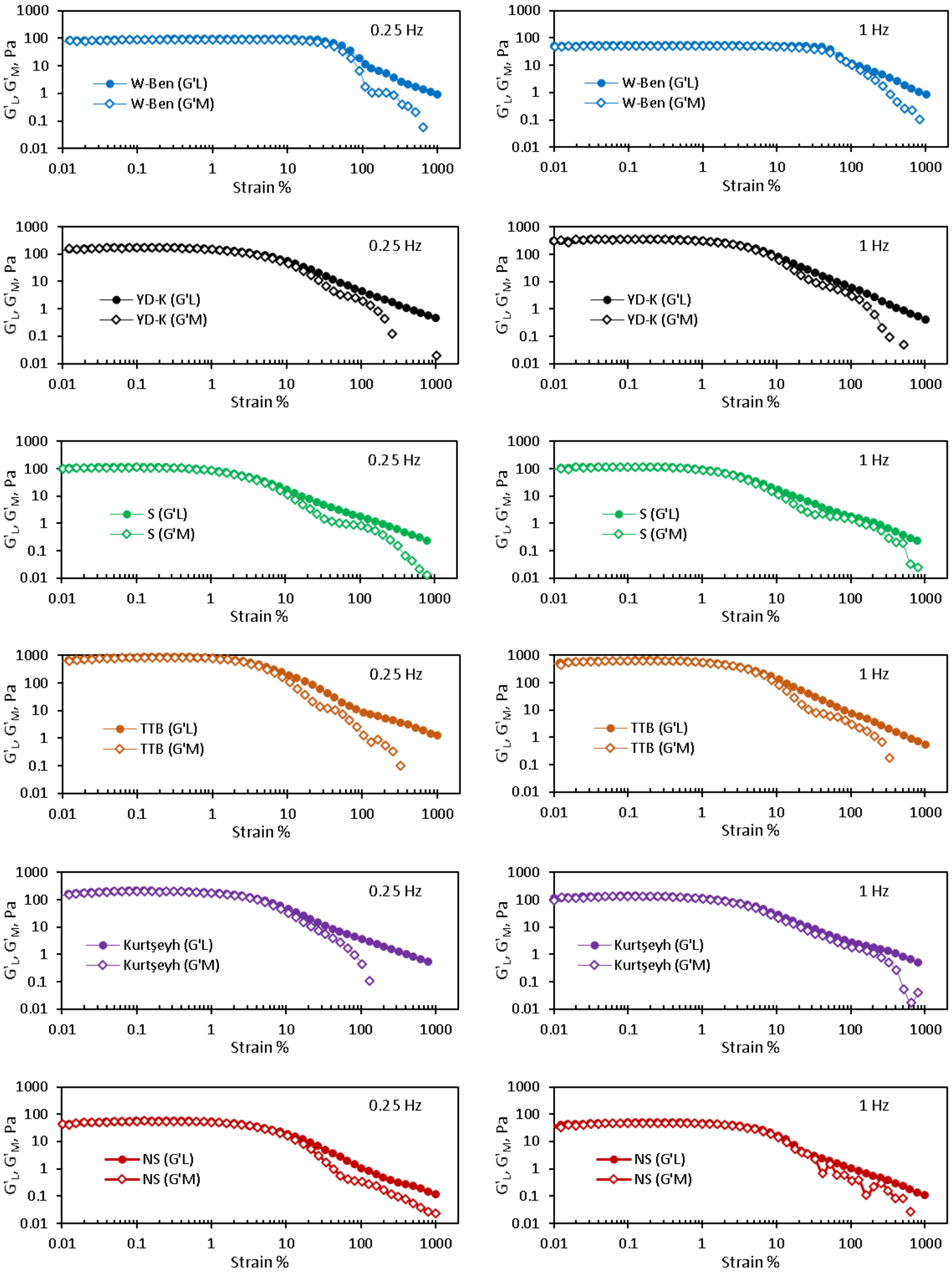

Figure 4.14: Large and minimum strain modulus ($G'L$,$G'M$) as a function of the strain amplitude at 0.25 and 1 Hz.

Figures 4.15 and 4.16 depict how G'_L **and** G'_M change with increasing temperature for nano and TTB sepiolite suspensions at the constant frequencies of 0.25 and 1 Hz, respectively. While the G'_L values for nano and TTB suspensions at 25° C were 41.7 Pa and 640 Pa, respectively, it was 490.67 Pa for both suspensions at 150° C. With the increase in temperature, the G'_L value of the nano suspension significantly increased, while the G'_L value of the TTB sepiolite suspension slightly decreased.

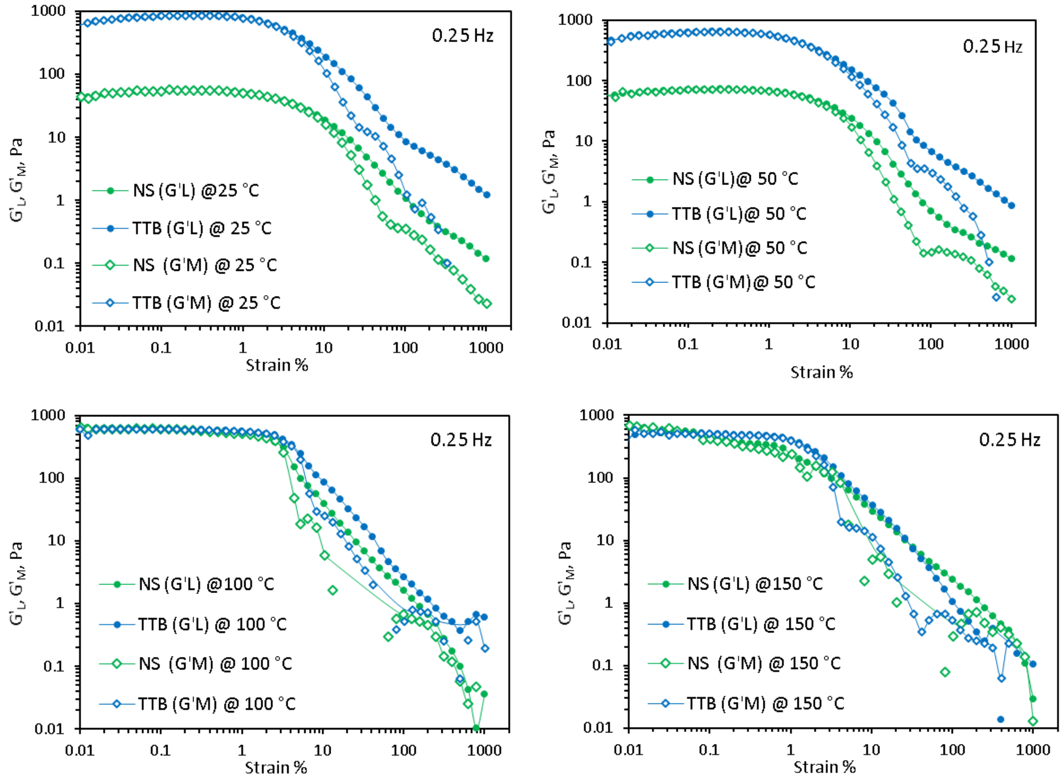

Figure 4.15: Large strain modulus (G'$_L$) and minimum strain modulus (G'$_M$) values for water-clay suspensions at 0.25 Hz frequency and four different temperatures.

It means that with the increase in temperature, the gel strength and elasticity property of the nano suspension increased substantially, while the TTB suspension decreased slightly. In addition, G'_L and G'_M values of nano and TTB suspensions decreased with the increase of strain value at all four temperatures implying inter-cycle strain softening behavior. On the other hand, it was seen that there was no obvious change in G'_L and G'_M values of nano and TTB sepiolite clay suspensions at increasing frequency in Figure 4.16. The change in large and minimum strain moduli G'_L and G'_M with applied strain amplitude was plotted for both suspensions systems in Figure 4.17 and at 0.25 and 1 Hz with respect to four temperatures (25, 50, 100, 150° C).

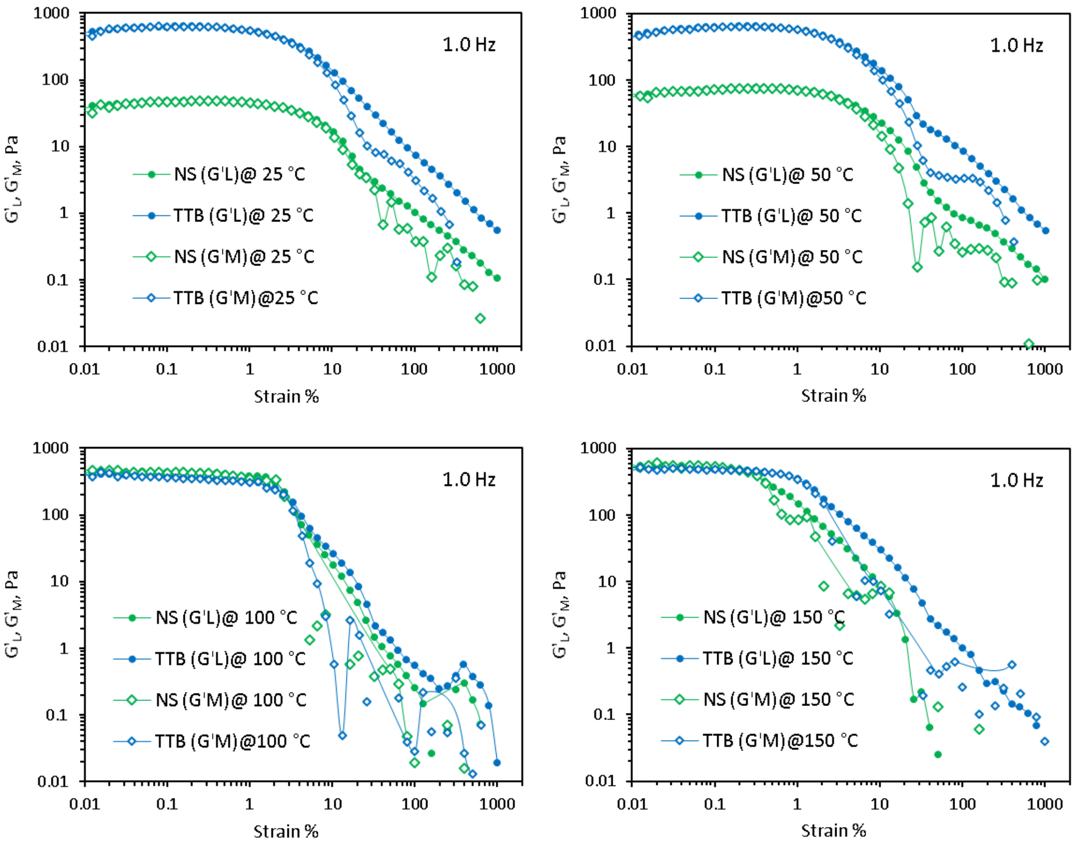

Figure 4.16: Large strain modulus (G'L) and minimum strain modulus (G'M) values for water-clay suspensions at 1.0 Hz frequency and four different temperatures.

Both $\boldsymbol{G'_L}$ **and** $\boldsymbol{G'_M}$ were equalized to the first harmonic storage modulus (G') in the linear region for two sepiolite clay suspensions. Softening behavior was observed in both suspensions as $\boldsymbol{G'_L}$ **and** $\boldsymbol{G'_M}$ decrease with increasing strain amplitude at 0.25 and 1 Hz and all temperatures tested (25, 50, 100, 150° C). The general insight about the large and minimum strain moduli pronounced strain softening behavior for all cay suspensions as the overall elastic nonlinear response.

As the elastic nonlinear parameters, stiffening ratio (S) and elastic Chebyshev coefficient (e3/e1) are also utilized to determine intra-cycle strain stiffening or softening nonlinearities. Figure 4.18 demonstrated the change of stiffening ratio (S) and elastic Chebyshev coefficient (e3/e1) with strain amplitude increasing for all clay suspensions at 25° C. These two parameters are zero in the linear viscoelastic region, however, with increasing strain and frequency (from 0.25 to 1.0 Hz) both parameters take positive values for all suspensions at 25° C.

Therefore, by considering only the sign of S and e3/e1 in the nonlinear region, the strain stiffening behavior should be observed in all clay suspensions at 25° C. The same evaluation in terms of these two elastic parameters is valid for nano and TTB clay suspensions at 50° C in Figüre 4.18. As seen in Figure 4.18, two parameters (e3/e1), (S) show positive values for both nano and TTB clay suspensions at all strain values from 25° C to 100° C implying strain stiffening behavior. It is followed by a negative value for S parameter at larger strains indicating a transition from strain-stiffening to strain softening behavior at 150° C.

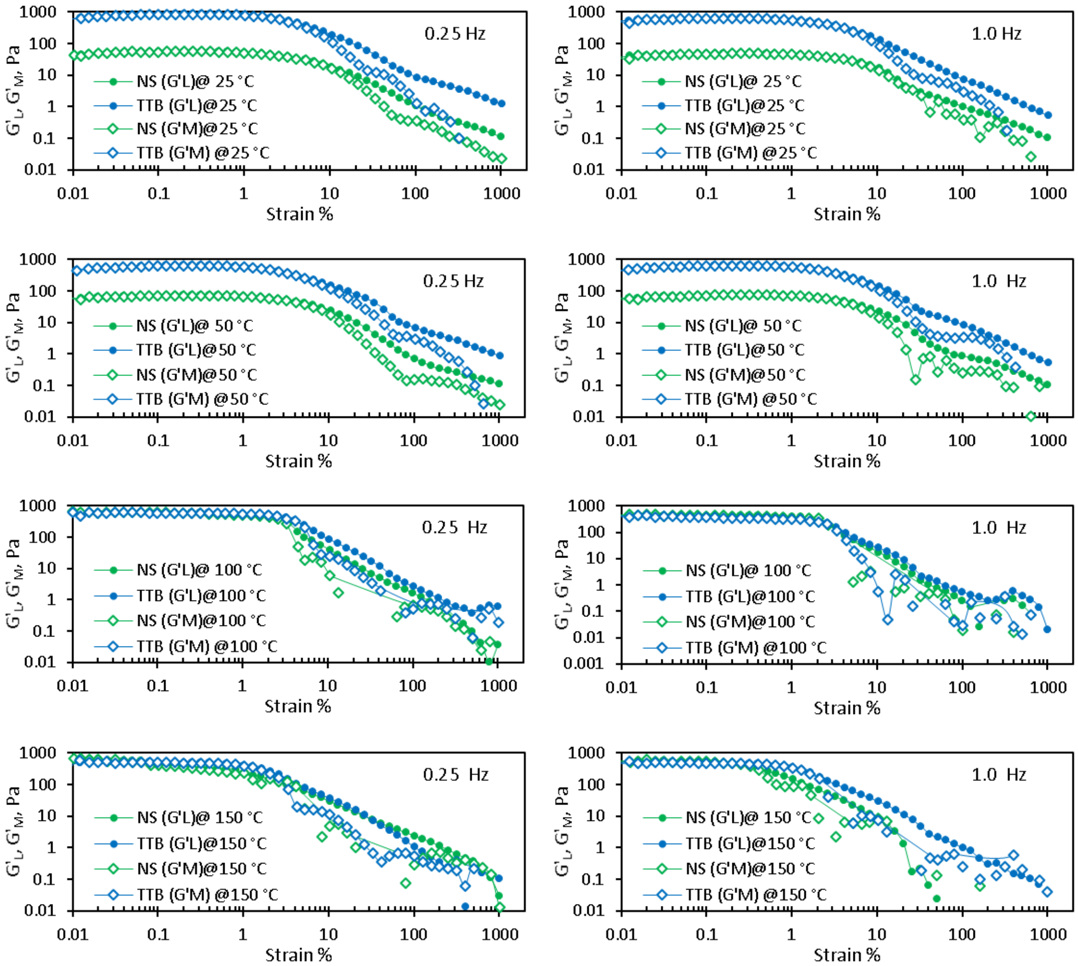

Figure 4.17: Large and minimum strain modulus ($G'L$,$G'M$) as a function of the strain amplitude at 0.25 and 1 Hz.

Therefore, the interpretation of nonlinear viscoelastic behavior based on stiffening ratio (S) and elastic Chebyshev coefficient (e3/e1) resulted in intra-cycle stiffening behavior dominantly for two clay suspensions. However, the overall response of all mud samples are strain softening (based on $\boldsymbol{G'_L}$ **and** $\boldsymbol{G'_M}$) and should not be confused with this intra-cycle stiffening behavior. This contrast results from the definition of stiffening ratio (S). The nonlinear response of a material is said to be strain stiffening if the large strain modulus $\boldsymbol{G'_L}$ is greater than the minimum strain modulus and based on the definition of stiffening ratio; S>0= ($\boldsymbol{G'_L}$- $\boldsymbol{G'_M}$)/ $\boldsymbol{G'_L}$ [37]. On the other hand, S will be greater than zero if $\boldsymbol{G'_M}$ decrease faster than $\boldsymbol{G'_L}$or $\boldsymbol{G'_L}$increases faster than $\boldsymbol{G'_M}$. Therefore, positive stiffening ratio can be realized as either the strain stiffening or the strain rate softening of the material [23].

When an elastic response dominates, the stiffening ratio might hide the accurate interpretation of nonlinearities. Hence, the cause of action in $\boldsymbol{G'_L}$ **and** $\boldsymbol{G'_M}$ should be initially considered to understand the elastic response of material. The applicable interpretation of the elastic nonlinearities for tested clay suspensions is strain-rate softening. The strong increase and decrease in S and e3/e1 values at high strains are most likely due to the rheometer inertia effect.

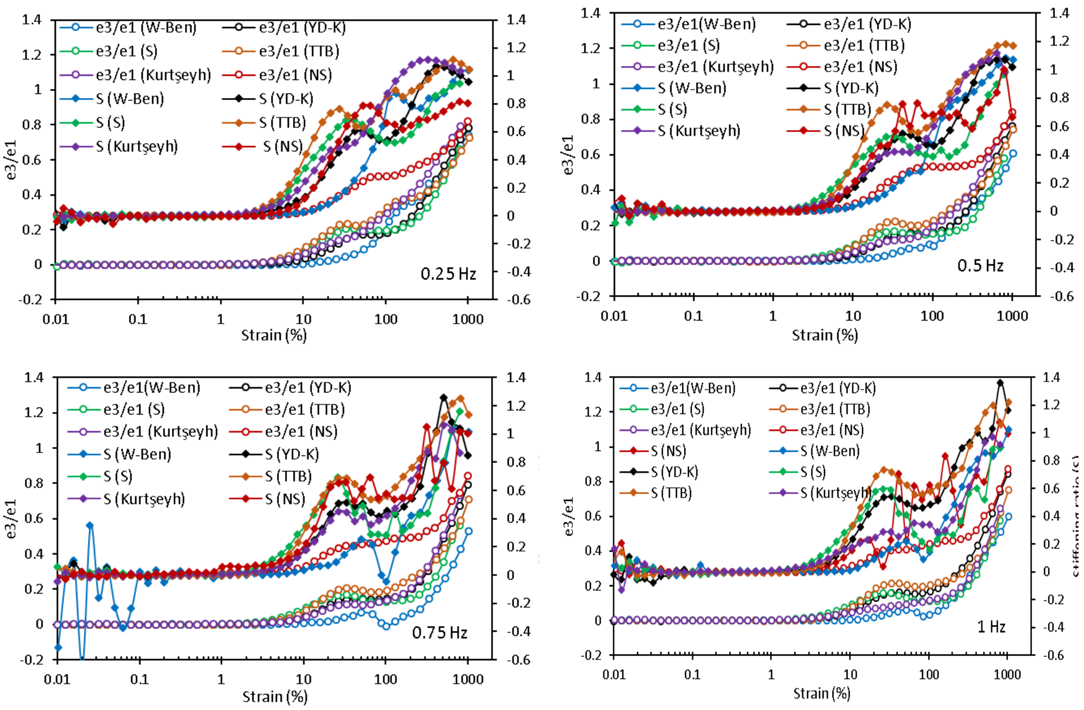

Figure 4.18: e $_3$/e $_1$ and S values for water-clay suspensions at four different frequencies.

When an elastic response dominates, the stiffening ratio might hide the accurate interpretation of nonlinearities. Hence, the cause of action in $\boldsymbol{G'_L}$ **and** $\boldsymbol{G'_M}$ should be initially considered to understand the elastic response of material. The applicable

interpretation of the elastic nonlinearities for tested clay suspensions is strain-rate softening. The strong increase and decrease in S and e3/e1 values at high strains are most likely due to the rheometer inertia effect.

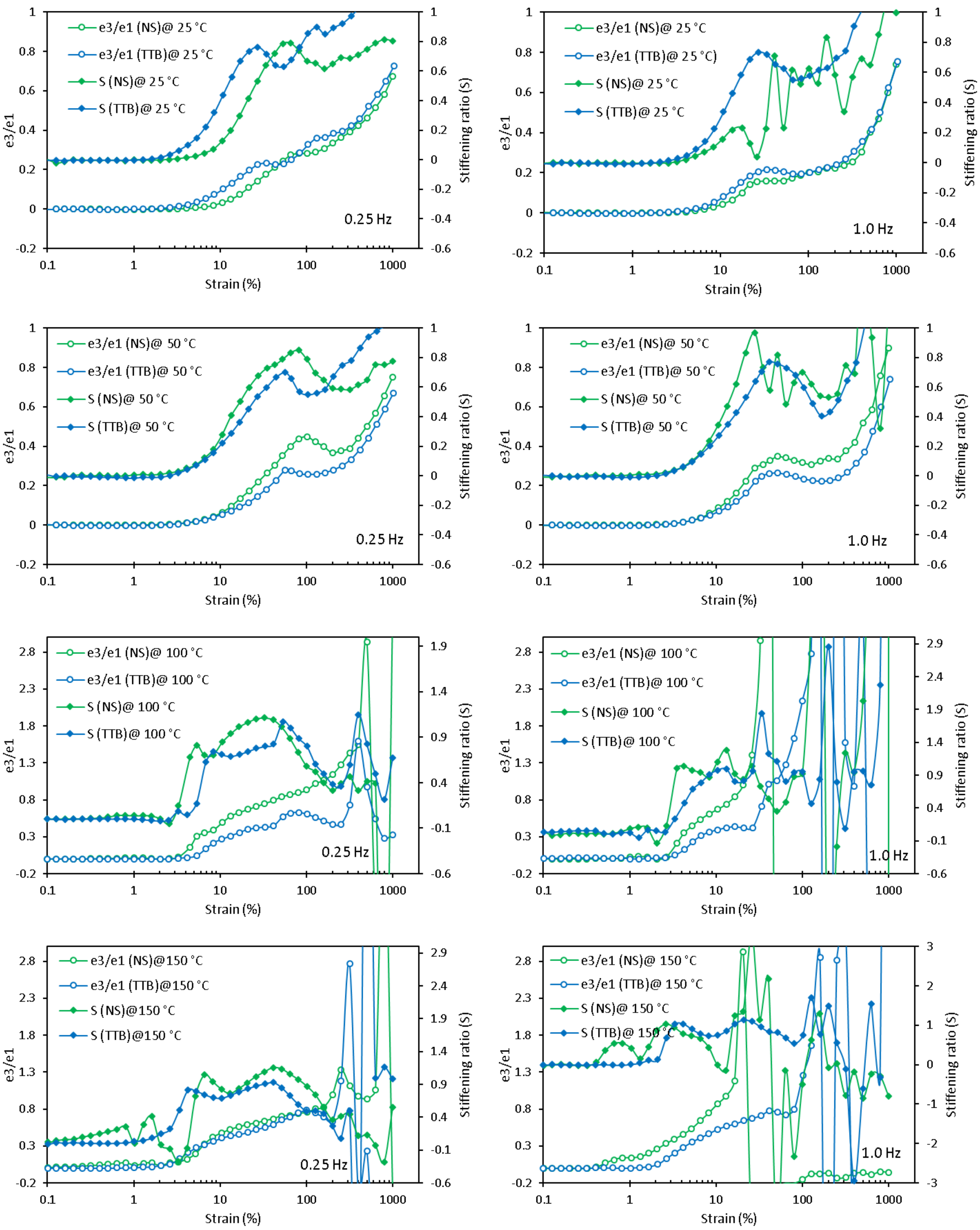

Figure 4.19: e $_3$/e $_1$ and S values for nano-sized and micro-sized sepiolite suspensions at 0.25 Hz and 1.0 Hz frequencies

4.4 Nonlinear Viscous Parameters of Clay Suspensions

The nonlinear viscous parameters $(\eta'_L, \eta'_M, v_3/v_1, T)$ were considered for quantitative interpretation of the nonlinear viscous response of all of six clay suspensions at 25° C. Figure 4.20 illustrates the large strain- rate dynamic viscosity (η'_L) and the minimum strain-rate dynamic viscosity (η'_M) values with respect to strain rate for all clay suspensions at four different frequencies. To digging deep, the changes in the large strain-rate dynamic viscosity (η'_L) and minimum strain-rate dynamic viscosity (η'_M) values for all water-clay suspensions individually at 0.25 and 1 Hz of frequencies were displayed in Figure 4.21.

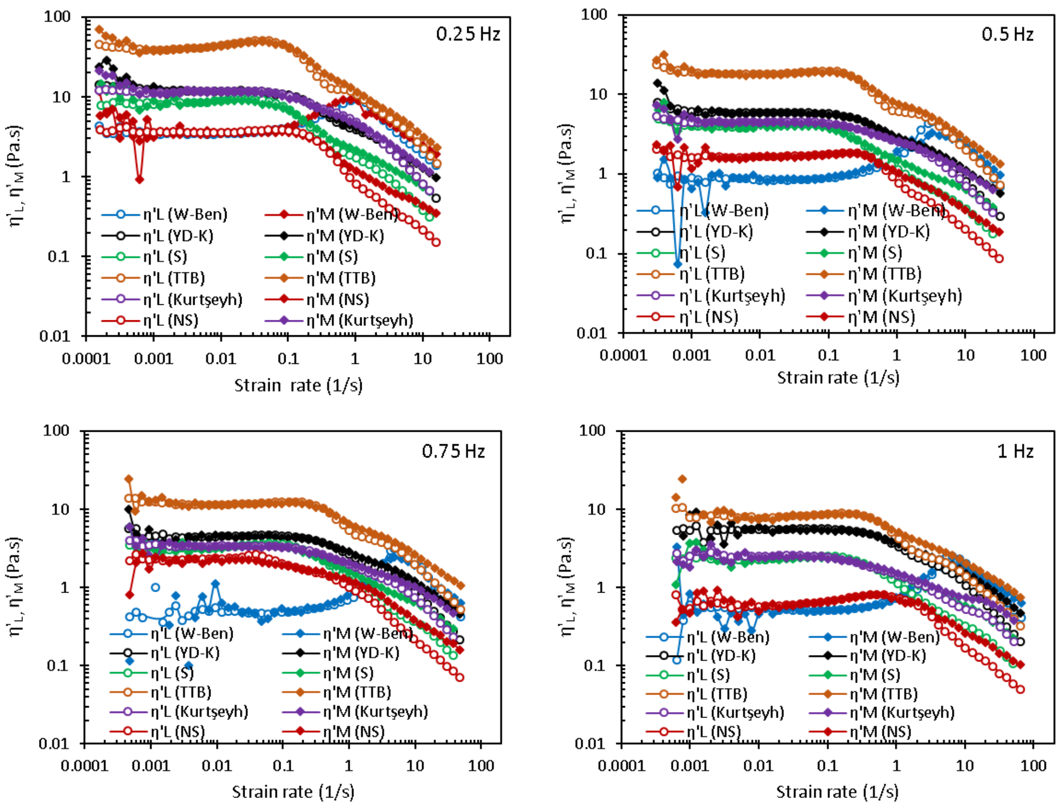

Figure 4.20: Large $(\eta'L)$ and minimum strain rate viscosity $(\eta'M)$ change vs. strain rate values for water-clay suspensions at four different frequencies.

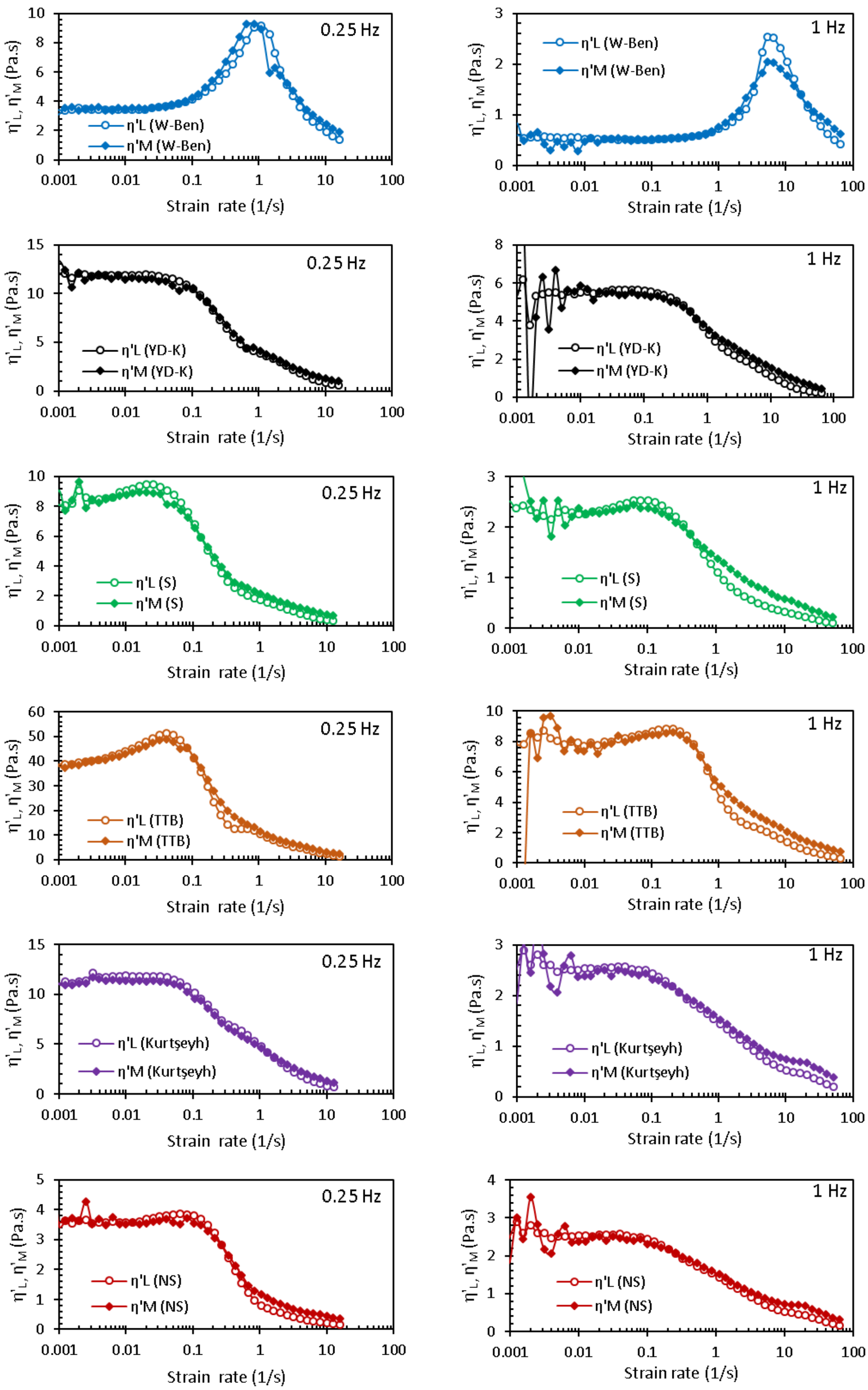

Figure 4.21: Changes in large strain-rate dynamic viscosity ($\eta' L$) and minimum strain-rate dynamic viscosity ($\eta' M$) values for all water-clay suspensions at 25° C, 0.25 Hz and 1 Hz of frequency.

In Figure 4.21 it is clear that for the TTB, nano TTB, Kurtşeyh, S and YDK sepiolite clay suspension sample, the nonlinearity of large strain-rate dynamic viscosity ($\boldsymbol{\eta'_L}$) at low and moderate strain amplitudes is greater than that of minimum strain-rate dynamic viscosity ($\boldsymbol{\eta'_M}$) impying shaer rate thickening behavior. On the other hand, for all clay suspension samples shear rate thinning ($\eta'_M > \eta'_L$) behavior is observed at large strain rates. In Figure from 4.22 up to 4.25 changes in large strain-rate dynamic viscosity ($\boldsymbol{\eta'_L}$) and minimum strain-rate dynamic viscosity ($\boldsymbol{\eta'_M}$) values for TTB and NTTB sepiolite suspensions are given at four temperatures (25° C, 50° C, 100° C, 150° C), respectively. As a first, large strain-rate dynamic viscosity ($\boldsymbol{\eta'_L}$) and minimum strain-rate dynamic viscosity ($\boldsymbol{\eta'_M}$) values for nano sepiolite suspensions is lower than TTB sepiolite suspensions.

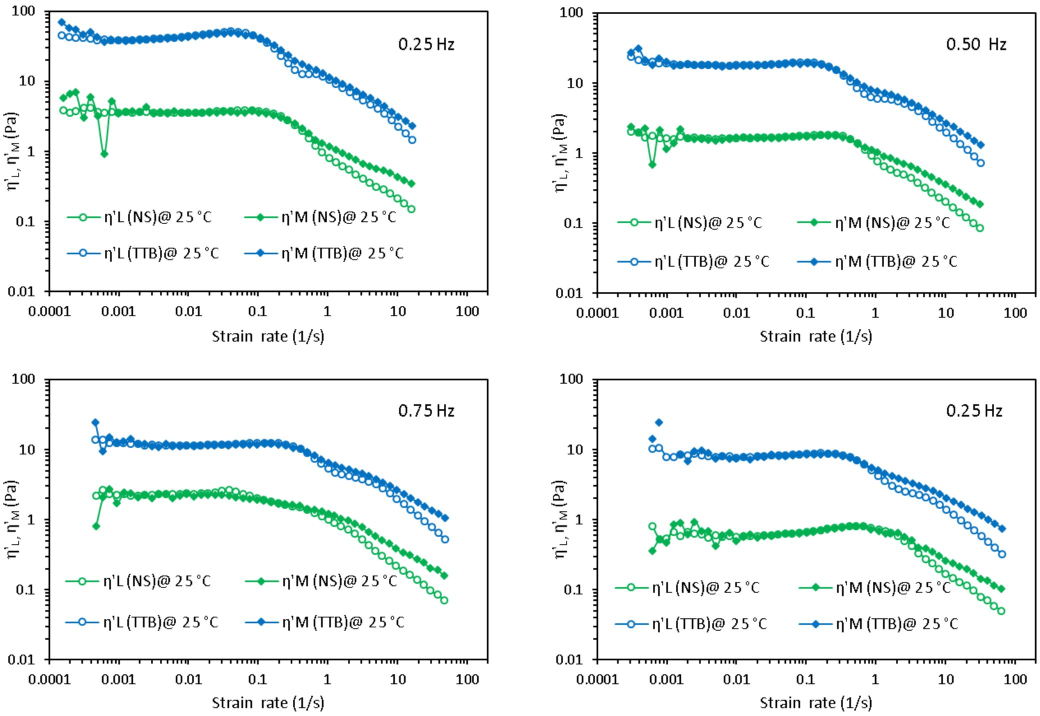

Figure 4.22: Changes in large strain-rate dynamic viscosity ($\eta'L$) and minimum strain-rate dynamic viscosity ($\eta'M$) values for nano and micro sized suspensions at 25° C and four different frequencies.

As seen in Figures 4.22 and 4.23, at moderate and high strain rates nano and TTB sepiolite clay suspensions showed shear rate thinning behavior under low temperatures for different four frequencies. It can be observed that for both low temperatures, at 0.75 Hz frequency, at low strain value, ($\boldsymbol{\eta'_L}$) is greater than ($\boldsymbol{\eta'_M}$) implying shear rate thickening. Meanwhile, it was observed that large strain-rate dynamic viscosity ($\boldsymbol{\eta'_L}$)

and minimum strain-rate dynamic viscosity ($\boldsymbol{\eta'_M}$) values for TTB and nano TTB sepiolite suspension samples decreased significantly as the frequency value increased (Figure 4.22 and Figure 4.23).

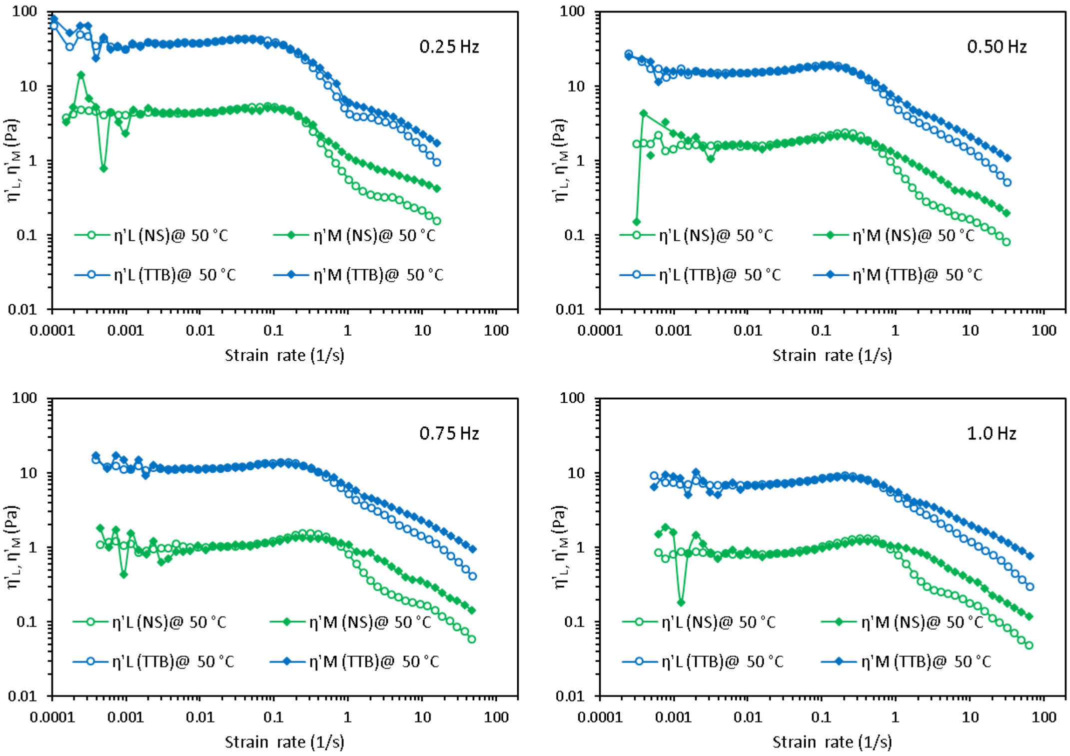

Figure 4.23: Changes in large strain-rate dynamic viscosity ($\eta' L$) and minimum strain-rate dynamic viscosity ($\eta' M$) values for nano and micro sized suspensions at 50° C and four different frequencies.

In Figure 4.24 and Figure 4.25 for high temperatures (100° C, 150° C) the results of micro TTB and nano TTB suspensions differ considerably from low temperatures. Unlike at low temperatures, there is no significant difference between large strain-rate dynamic viscosity ($\eta' L$) and minimum strain-rate dynamic viscosity ($\eta' M$) values for both suspensions at high temperatures. However, as the frequency increases, the $\eta' L$ and $\eta' M$ values of both suspensions decrease slightly. As it is seen in Figure 4.24 and Figure 4.25 for nano TTB and TTB suspensions, the $\eta' L$ value is greater than $\eta' M$ at low and medium strain rate values for all four frequencies demonstrating shear rate thickening behavior. Low frequencies represent times when the drilling fluid is stationary in the well. As a result, the higher thickening at high temperatures of nano TTB compared to TTB indicates that it has a high ability to suspend particles. Besides, both clay suspensions showed shear rate thinning behavior ($\eta' L < \eta' M$) at high strain rate values.

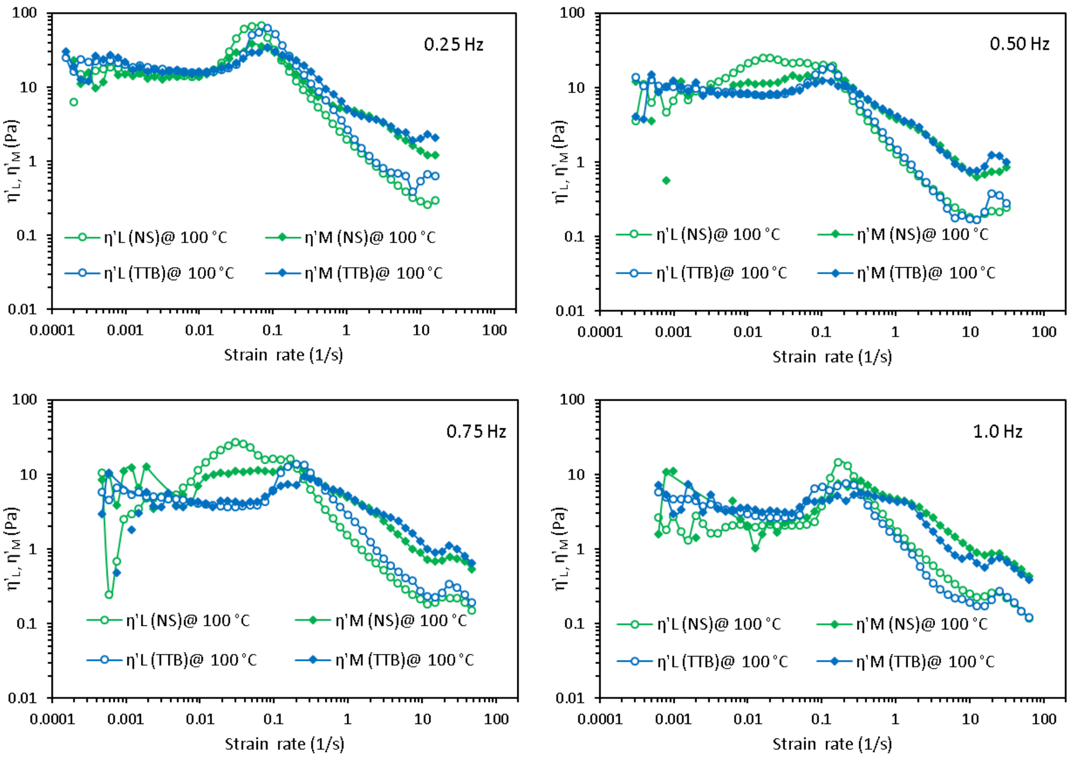

Figure 4.24: Changes in large strain-rate dynamic viscosity ($\eta' L$) and minimum strain-rate dynamic viscosity ($\eta' M$) values for nano and micro sized suspensions at 100° C and four different frequencies.

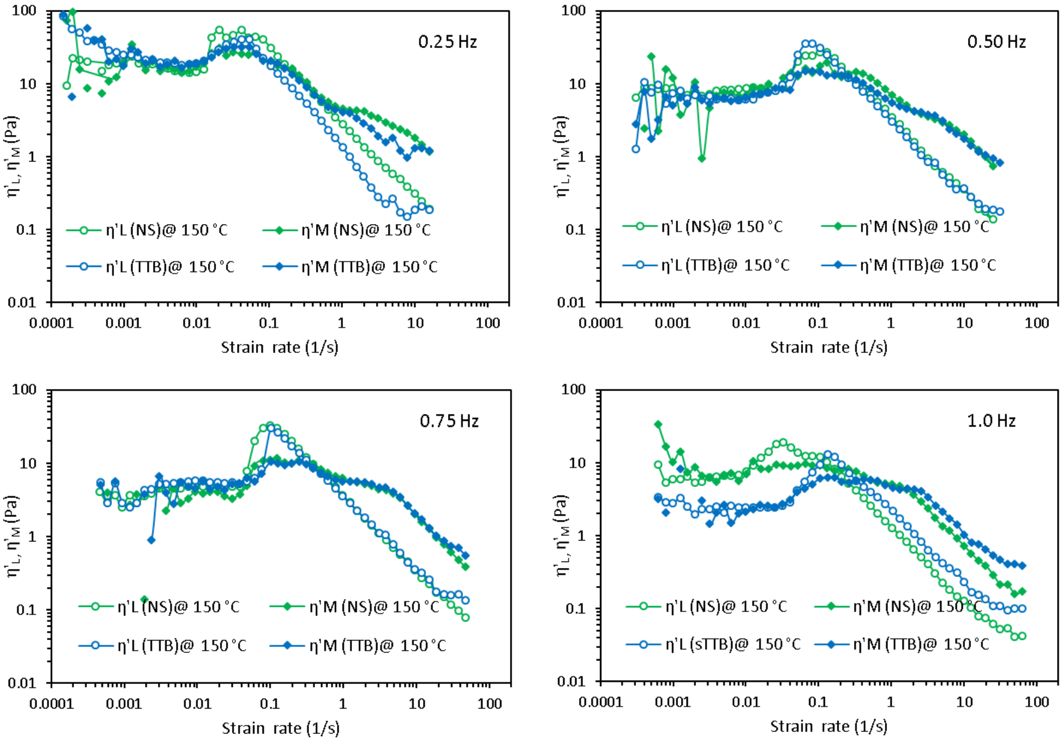

Figure 4.25: Changes in large strain-rate dynamic viscosity ($\eta'L$) and minimum strain-rate dynamic viscosity ($\eta'M$) values for nano and micro sized suspensions at 150° C and four different frequencies.

Viscous nonlinear character of both mud samples can also be identified with concern to shear thickening ratio (T) and third-order viscous Chebyshev coefficient (v_3/v_1). Figure 4.26 plots how these two parameters change with the increasing strain amplitude applied to all clay suspensions at 0.25 Hz, 0.50 Hz, 0.75 Hz and 1 Hz. The sign of the shear thickening ratio (T) shows whether the viscous nonlinearity of the material is thin (T<0) or thick (T>0). The thickening ratios of all clay suspensions indicate the same shear thickening and shear thinning behavior with increasing strain amplitude, as explained by changes in η'_M and η'_L (Figure 4.26).

Figure 4.27 shows the third-order viscous Chebyshev coefficient v_3/v_1 and thickening ratio (T) values of Nano TTB and TTB clay suspensions for four temperatures at 0.25 and 1.0 Hz frequency. It is clear that as it is mentioned in η'_M and η'_L plots, at high temperatures (100° C, 150° C) Nano TTB clay suspension sample demonstrate more shear rate thickening ($v_3/v_1>0$) behavior than TTB sepiolite suspension at low and moderate strain rates. It is implying that suspension ability of nano TTB sepiolite suspension is more than TTB sepiolite suspension at high temperatures. Therefore, nano TTB sepiolite suspension sample shows high performanse cutting transport and hole cleaning in drilling operations. To illustrate rheological behavior of all clay suspensions Table 4.1 is given below.

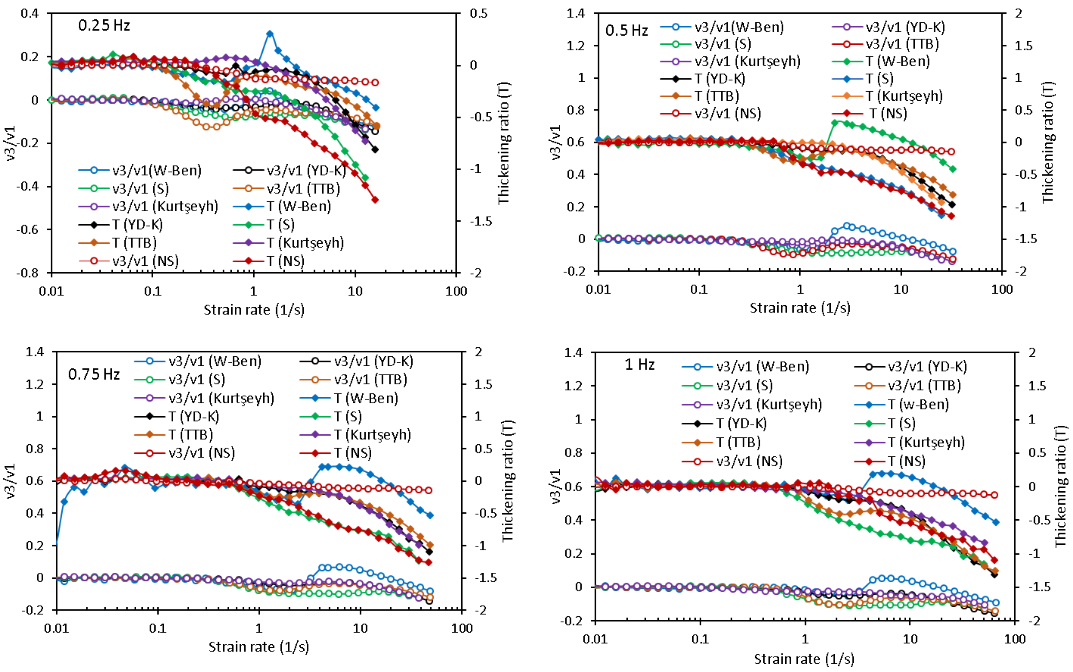

Figure 4.26: v₃/v ₁ and T values for water-clay suspensions at four different frequencies.

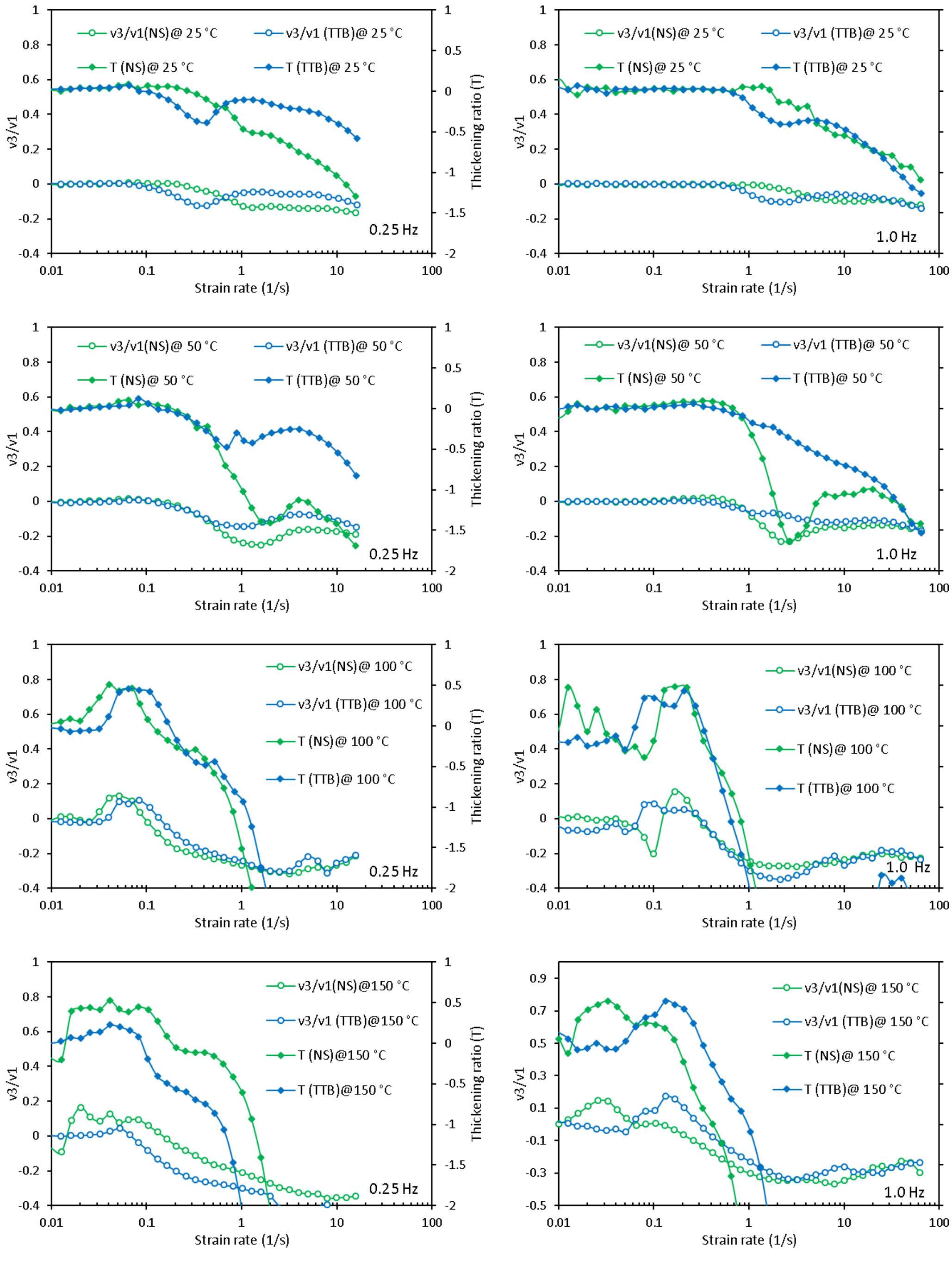

Figure 4.27: v ₃/v ₁ and T values for nano-sized and micro-sized sepiolite suspensions at four different temperatures and 0.25 Hz, 1.0 Hz frequencies.

Table 4.1: Nonlinear viscoelastic dominant behaviors for all clay suspensions.

Suspension	Elastic nonlinearity	Viscous nonlinearity	
	G'_L, and G'_M	η'_L, and η'_M	
	Moderate and large strain	Low /moderate strain	Large strain
Kurtşeyh@ 25°C	*strain rate softening*	shear rate thickening	*shear rate thinning*
S@ 25°C	*strain rate softening*	*shear rate thickening*	*shear rate thinning*
YDK@ 25°C	*strain rate softening*	*shear rate thickening*	*shear rate thinning*
Bentonite@ 25°C	*strain rate softening*	*shear rate thinning / shear thickening*	*shear rate thinning*
NS@ 25°C	strain softening	*shear rate thickening*	*shear rate thinning*
TTB@ 25°C	strain softening	*shear rate thickening*	*shear rate thinning*
NS@ 50°C	strain softening	*shear rate thickening*	*shear rate thinning*
TTB @50°C	strain softening	*shear rate thickening*	*shear rate thinning*
NS@ 100°C	strain softening and *strain stiffening*	*shear rate thickening*	*shear rate thinning*
TTB @ 100°C	strain softening and *strain stiffening*	*shear rate thickening*	*shear rate thinning*
NS@ 150°C	strain softening and *strain stiffening*	*shear rate thickening*	*shear rate thinning*
TTB @ 150°C	strain softening and *strain stiffening*	*shear rate thickening*	*shear rate thinning*

Chapter 5

Conclusions

- It is obvious that storage modulus of nano-sized sepiolite suspension is less compered to the other suspensions except 0.75 Hz. However, lineer VE range of bentonite suspension is higher than other five suspensions at all frequencies. Diversely, micro-sized sepiolite suspension has more storage modulus than the others. Whereas, storage modulus of micro-sized (TTB) sepiolite suspension is 845.922 Pa, storage modulus of nano-sized sepiolite suspension is 55.537 Pa demonstrating that more power is required to pump TTB sepiolite suspension in shallow wells. Taking all of the mentioned above consideration, nano-sized sepiolite suspension is more preferable than the micro-sized (TTB) sepiolite suspensions at drilling operations at low temperatures.
- Although the elasticity and gel strength of the micro-sized TTB sepiolite do not change visibly depending on the temperature, the elasticity and gel strength of the nano-sized sepiolite suspension significantly different depending on the temperature. The lineer VE range of the TTB sepiolite suspension is nearly same at all four temperatures indicating structural stability is not affected by increasing temperature.
- In Lissajous-Bowditch curves, the elastic property and gel strength increase under higher temperatures. These findings are also in agreement with those of the amplitude sweep test. In addition, with the onset of nonlinearity, Lissajous curves appear to be wider at high temperatures. This indicates that the nano sepiolite suspension dissipates more energy at higher temperatures. However, there was no noticeable difference in the elasticity of TTB sepiolite suspension with increasing temperature.

- At 1.0 Hz and 150° C, the dissipation ratio for nano sepiolite suspension is much lower than others indicating a stronger elastic response compare to other sepiolite suspension. This could be a sign of high suspension ability for nano sepiolite suspension at high temperatures.

- Secondary loops appear in viscous L-B curves when the time for recovering microstructure is lower than the oscillatory deformation time which is strong evidence of thixotropic recovery in nano and TTB sepiolite suspensions.

- TTB clay suspension has a greater difference between $\boldsymbol{G'_L}$ **and** $\boldsymbol{G'_M}$ at all frequencies, indicating a more stable gel structure than the others. It is also obvious that at 25° C all clay suspensions exhibits strain softening behavior at high strains under both of frequencies (0.25 and 1.0 Hz).
- Softening behavior was observed in both suspensions as $\boldsymbol{G'_L}$ **and** $\boldsymbol{G'_M}$ decrease with increasing strain amplitude at 0.25 and 1 Hz and all temperatures tested (25, 50, 100, 150 ◦C). The general insight about the large and minimum strain moduli pronounced strain softening behavior for all cay suspensions as the overall elastic nonlinear response.
- For nano TTB and micro TTB suspensions, the η'_L value is greater than η'_M at low and medium strain rate values for all four frequencies demonstrating shear rate thickening behavior. Low frequencies represent times when the drilling fluid is stationary in the well. As a result, the higher thickening at high temperatures of nano TTB compared to TTB indicates that it has a high ability to suspend particles. Besides, both clay suspensions showed shear rate thinning behavior ($\eta'_L < \eta'_M$) at high strain rate values.

- Nano TTB clay suspension sample demonstrate more shear rate thickening ($v_3/v_1>0$) behavior than micro TTB sepiolite suspension at low and moderate strain rates. It is implying that suspension ability of nano TTB sepiolite suspension is more than TTB sepiolite suspension at high temperatures. Therefore, nano TTB sepiolite suspension sample shows high performance cutting transport and hole cleaning in drilling operations.

Recommendations

In this experimental research, the nonlinear viscoelastic properties of nano-sized TTB sepiolite clay suspensions compared to micro-sized clay suspensions were examined using the LAOS test. In order for this study to make a better contribution to drilling operations, it is recommended that further studies on nano sized sepiolite clay suspensions should be carried out by the usage of commercial additives in the formulation of suspensions.

References

[1] L. L. Y. Chang, *Industrial mineralogy: materials, processes, and uses*. Prentice Hall, 2002.

[2] R. E. Grim, “Some applications of clay mineralogy,” *Am. Mineral. J. Earth Planet. Mater.*, vol. 45, no. 3–4, pp. 259–269, 1960.

[3] D. Wattanasiriwech, K. Srijan, and S. Wattanasiriwech, “Vitrification of illitic clay from Malaysia,” *Appl. Clay Sci.*, vol. 43, no. 1, pp. 57–62, 2009.

[4] E. Tombacz and M. Szekeres, “Colloidal behavior of aqueous montmorillonite suspensions: the specific role of pH in the presence of indifferent electrolytes,” *Appl. Clay Sci.*, vol. 27, no. 1–2, pp. 75–94, 2004.

[5] H. H. Murray, “Overview—clay mineral applications,” *Appl. Clay Sci.*, vol. 5, no. 5–6, pp. 379–395, 1991.

[6] A. Ettehadi, M. Tezcan, and G. Altun, “Rheological behavior of water-clay suspensions under large amplitude oscillatory shear,” *Rheol. Acta*, vol. 59, no. 9, pp. 665–683, 2020.

[7] L. L. Carney and R. L. Meyer, “A new approach to high temperature drilling fields,” 1976.

[8] U. Serpen, “Use of sepiolite clay and other minerals for developing geothermal drilling fluids,” *Appl. Mech. Eng.*, vol. 4, no. spec., pp. 309–313, 1999.

[9] G. Altun and U. Serpen, “Investigating improved rheological and fluid loss performance of sepiolite muds under elevated temperatures,” 2005.

[10] G. Altun, A. E. Osgouei, and U. Serpen, “Controlling rheological and fluid loss properties of sepiolite based muds under elevated temperatures,” in

Proceedings World Geothermal Congress, Bali, Indonesia, April, 2010, pp. 25–29.

[11] A. E. Osgouei, M. H. Ozyurtkan, and G. Altun, “Dynamic filtration properties of fresh water sepiolite-based muds,” *Energy Sources, Part A Recover. Util. Environ. Eff.*, 2014, doi: 10.1080/15567036.2011.563267.

[12] P. F. Luckham and S. Rossi, “The colloidal and rheological properties of bentonite suspensions,” *Adv. Colloid Interface Sci.*, vol. 82, no. 1–3, pp. 43–92, 1999.

[13] B. Abu-Jdayil, M. Ghannam, and M. S. Nasser, “The modification of rheological properties of bentonite-water dispersions with cationic and anionic surfactants,” *Int. J. Chem. Eng. Appl.*, vol. 7, no. 2, p. 75, 2016.

[14] A. Benchabane and K. Bekkour, “Effects of anionic additives on the rheological behavior of aqueous calcium montmorillonite suspensions,” *Rheol. acta*, vol. 45, no. 4, pp. 425–434, 2006.

[15] M. Mohammadi, M. Kouhi, A. Sarrafi, and M. Schaffie, “Studying rheological behavior of nanoclay as oil well drilling fluid,” *Res. Chem. Intermed.*, 2015, doi: 10.1007/s11164-013-1391-x.

[16] H. A. Patel, R. S. Somani, H. C. Bajaj, and R. V. Jasra, “Nanoclays for polymer nanocomposites, paints, inks, greases and cosmetics formulations, drug delivery vehicle and waste water treatment,” *Bull. Mater. Sci.*, 2006, doi: 10.1007/BF02704606.

[17] K. Hyun *et al.*, “A review of nonlinear oscillatory shear tests: Analysis and application of large amplitude oscillatory shear (LAOS),” *Prog. Polym. Sci.*, vol. 36, no. 12, pp. 1697–1753, 2011.

[18] R. H. Ewoldt, C. Clasen, A. E. Hosoi, and G. H. McKinley, “Rheological fingerprinting of gastropod pedal mucus and synthetic complex fluids for biomimicking adhesive locomotion,” *Soft Matter*, vol. 3, no. 5, pp. 634–643, 2007.

[19] P. Ptaszek, “A geometrical interpretation of large amplitude oscillatory shear (LAOS) in application to fresh food foams,” *J. Food Eng.*, vol. 146, pp. 53–61, 2015.

[20] S. Ozkan, T. W. Gillece, L. Senak, and D. J. Moore, “Characterization of yield stress and slip behaviour of skin/hair care gels using steady flow and LAOS measurements and their correlation with sensorial attributes,” *Int. J. Cosmet. Sci.*, vol. 34, no. 2, pp. 193–201, 2012.

[21] R. W. Chan, “Nonlinear viscoelastic characterization of human vocal fold tissues under large-amplitude oscillatory shear (LAOS),” *J. Rheol. (N. Y. N. Y).*, vol. 62, no. 3, pp. 695–712, 2018.

[22] T. J. Faber, L. C. A. Van Breemen, and G. H. McKinley, “From firm to fluid–Structure-texture relations of filled gels probed under Large Amplitude Oscillatory Shear,” *J. Food Eng.*, vol. 210, pp. 1–18, 2017.

[23] S. Khandavalli and J. P. Rothstein, “Large amplitude oscillatory shear rheology of three different shear-thickening particle dispersions,” *Rheol. Acta*, vol. 54, no. 7, pp. 601–618, 2015.

[24] C. Yildirim-Mavis, M. T. Yilmaz, E. Dertli, M. Arici, and D. Ozmen, “Non-linear rheological (LAOS) behavior of sourdough-based dough,” *Food Hydrocoll.*, vol. 96, pp. 481–492, 2019.

[25] J. T. Shakib, V. Kanani, and P. Pourafshary, “Nano-clays as additives for controlling filtration properties of water-bentonite suspensions,” *J. Pet. Sci. Eng.*, 2016, doi: 10.1016/j.petrol.2015.11.018.

[26] G. Cheraghian, “Application of Nano-Particles of Clay to Improve Drilling Fluid,” *Int. J. Nanosci. Nanotechnol.*, 2017.

[27] A. R. Payne, “The dynamic properties of carbon black-loaded natural rubber vulcanizates. Part I,” *J. Appl. Polym. Sci.*, vol. 6, no. 19, pp. 57–63, 1962.

[28] W. P. Fletcher and A. N. Gent, “Nonlinearity in the dynamic properties of vulcanized rubber compounds,” *Rubber Chem. Technol.*, vol. 27, no. 1, pp.

209–222, 1954.

[29] S. Onogi, T. Masuda, and T. Matsumoto, "Non-linear behavior of viscoelastic materials. I. disperse systems of polystyrene solution and carbon black," *Trans. Soc. Rheol.*, vol. 14, no. 2, pp. 275–294, 1970.

[30] J. S. Dodge and I. M. Krieger, "Oscillatory shear of nonlinear fluids I. Preliminary investigation," *Trans. Soc. Rheol.*, vol. 15, no. 4, pp. 589–601, 1971.

[31] T. Matsumoto, Y. Segawa, Y. Warashina, and S. Onogi, "Nonlinear behavior of viscoelastic materials. II. The method of analysis and temperature dependence of nonlinear viscoelastic functions," *Trans. Soc. Rheol.*, vol. 17, no. 1, pp. 47–62, 1973.

[32] H. Komatsu, T. Mitsui, and S. Onogi, "Nonlinear viscoelastic properties of semisolid emulsions," *Trans. Soc. Rheol.*, vol. 17, no. 2, pp. 351–364, 1973.

[33] T. Tee and J. M. Dealy, "Nonlinear viscoelasticity of polymer melts," *Trans. Soc. Rheol.*, vol. 19, no. 4, pp. 595–615, 1975.

[34] K. Walters and T. E. R. Jones, "Further studies on the usefulness of the Weissenberg rheogoniometer," in *Proceedings of the Fifth International Congress on Rheology*, 1970, vol. 4, pp. 337–350.

[35] A. J. Giacomin and J. M. Dealy, "Large-amplitude oscillatory shear," in *Techniques in rheological measurement*, Springer, 1993, pp. 99–121.

[36] J. M. Dealy and K. F. Wissbrun, *Melt rheology and its role in plastics processing: theory and applications*. Springer Science & Business Media, 2012.

[37] R. H. Ewoldt, A. E. Hosoi, and G. H. McKinley, "New measures for characterizing nonlinear viscoelasticity in large amplitude oscillatory shear," *J. Rheol. (N. Y. N. Y).*, vol. 52, no. 6, pp. 1427–1458, 2008.

[38] G. Yazar, O. Duvarci, S. Tavman, and J. L. Kokini, "Non-linear rheological behavior of gluten-free flour doughs and correlations of LAOS parameters with gluten-free bread properties," *J. Cereal Sci.*, vol. 74, pp. 28–36, 2017.

[39] R. H. Ewoldt, A. E. Hosoi, and G. H. McKinley, “Rheological fingerprinting of complex fluids using large amplitude oscillatory shear (LAOS) flow,” *Annu. Trans. Rheol. Soc.*, vol. 15, p. 3, 2007.

[40] G. Yazar, O. C. Duvarci, S. Tavman, and J. L. Kokini, “Effect of mixing on LAOS properties of hard wheat flour dough,” *J. Food Eng.*, vol. 190, pp. 195–204, 2016.

[41] G. Yazar, O. Duvarci, S. Tavman, and J. L. Kokini, “Non-linear rheological properties of soft wheat flour dough at different stages of farinograph mixing,” *Appl. Rheol.*, vol. 26, no. 5, pp. 1–11, 2016.

[42] G. Yazar, O. C. Duvarci, S. Tavman, and J. L. Kokini, “LAOS behavior of the two main gluten fractions: Gliadin and glutenin,” *J. Cereal Sci.*, vol. 77, pp. 201–210, 2017.

[43] J. Abdo, H. AL-Sharji, and E. Hassan, “Effects of nano-sepiolite on rheological properties and filtration loss of water-based drilling fluids,” 2016, doi: 10.1002/sia.5997.

[44] J. M. Huggett, *Clay minerals*. Elsevier, 2005.

[45] L. L. Carney and N. Guven, “Investigation of High-Temperature Fluid Loss Control Agents in Geothermal Drilling Fluids,” 1982.

[46] N. Guven, D. J. Panfil, and L. L. Carney, “Comparative rheology of water-based drilling fluids with various clays,” 1988.

[47] L. W. Hilscher and W. R. Clements, “High-temperature drilling fluid for geothermal and deep sensitive formations,” 1982.

[48] U. Serpen, M. Haciislamoglu, and O. Tuna, “Use of Sepiolite Resources of Turkey in geothermal Muds,” in *Proceedings, 9th International Petroleum Congress of Turkey, Ankara*, 1992, pp. 17–21.

[49] U. Serpen, “Investigation on Geothermal Drilling Muds with High Temperature Stability,” 2000.

[50] J. D. Muñoz Sierra, C. Lafita, C. Gabaldón, H. Spanjers, and J. B. van Lier, "Trace metals supplementation in anaerobic membrane bioreactors treating highly saline phenolic wastewater," *Bioresour. Technol.*, 2017, doi: 10.1016/j.biortech.2017.03.032.

[51] A. Ettehadi, C. Ülker, and G. Altun, "Nonlinear viscoelastic rheological behavior of bentonite and sepiolite drilling fluids under large amplitude oscillatory shear," *J. Pet. Sci. Eng.*, 2021, doi: 10.1016/j.petrol.2021.109210.

[52] F. K. G. Schreuders, L. M. C. Sagis, I. Bodnár, P. Erni, R. M. Boom, and A. J. van der Goot, "Small and large oscillatory shear properties of concentrated proteins," *Food Hydrocoll.*, 2021, doi: 10.1016/j.foodhyd.2020.106172.

[53] K. S. Cho, K. Hyun, K. H. Ahn, and S. J. Lee, "A geometrical interpretation of large amplitude oscillatory shear response," *J. Rheol. (N. Y. N. Y).*, 2005, doi: 10.1122/1.1895801.

[54] K. Hyun, S. H. Kim, K. H. Ahn, and S. J. Lee, "Large amplitude oscillatory shear as a way to classify the complex fluids," *J. Nonnewton. Fluid Mech.*, vol. 107, no. 1–3, pp. 51–65, 2002.

[55] G. J. Donley, P. K. Singh, A. Shetty, and S. A. Rogers, "Elucidating the G ″overshoot in soft materials with a yield transition via a time-resolved experimental strain decomposition," *Proc. Natl. Acad. Sci.*, vol. 117, no. 36, pp. 21945–21952, 2020.

[56] J. L. KOKINI and G. J. PLUTCHOK, "PREDICTING STEADY AND OSCILLATORY SHEAR RHEOLOGICAL PROPERTIES OF CMC/GUAR BLENDS USING THE BIRD-CARREAU CONSTITUTIVE MODEL," *J. Texture Stud.*, 1987, doi: 10.1111/j.1745-4603.1987.tb00568.x.

Appendices

APPENDIX A:

Particle Size of Sepiolite Clays

In this section cumulative volume percent (%) versus to particle size (μm) and volume percent (%) versus to particle size (μm) are given for S, YDK, Kurtşeyh and micro-sized TTB sepiolite clays respectively.

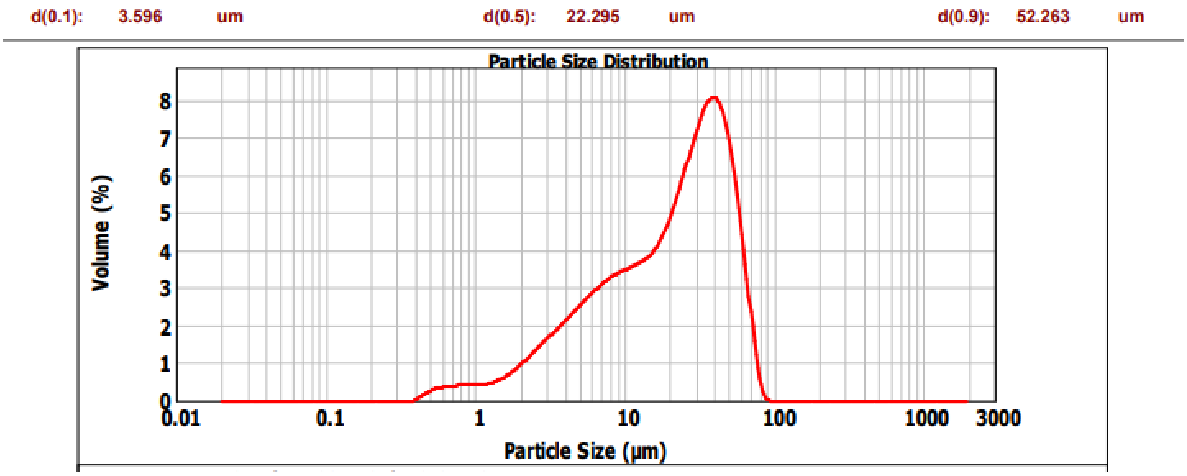

Figure A. 1: Volume percent versus to particle size for S sepiolite clay.

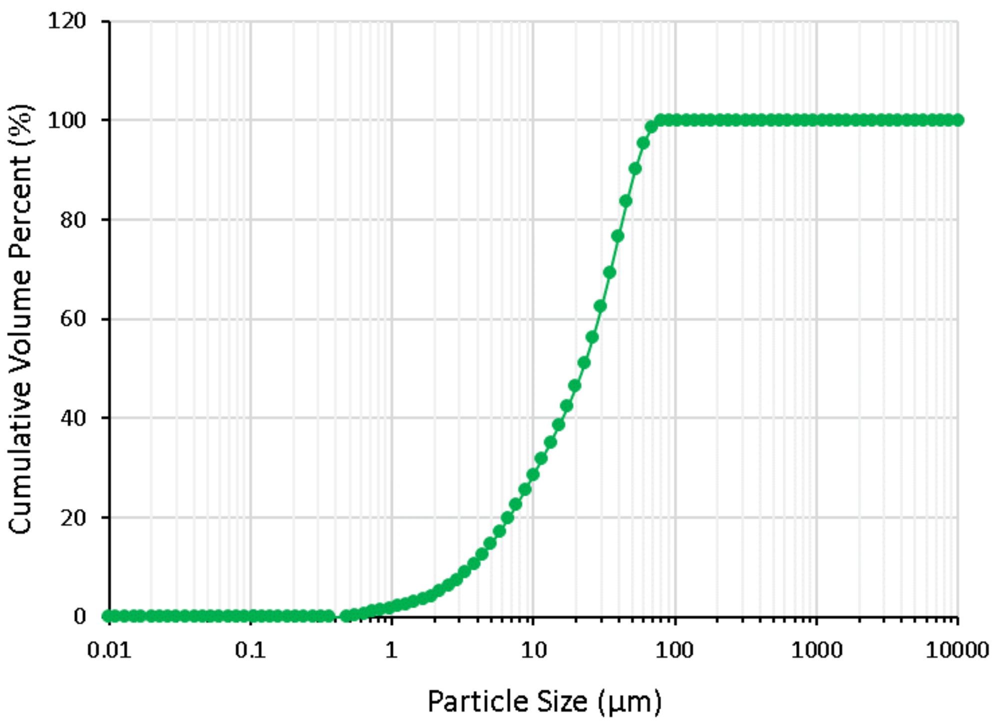

Figure A. 2: Cumulative volume percent versus to particle size for S sepiolite clay.

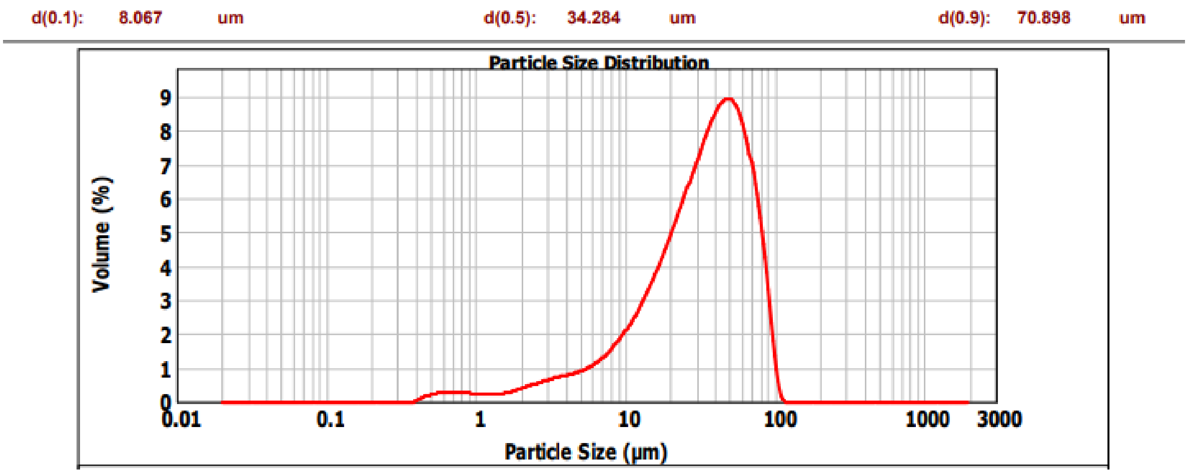

Figure A. 3: Volume percent versus to particle size for YDK sepiolite clay.

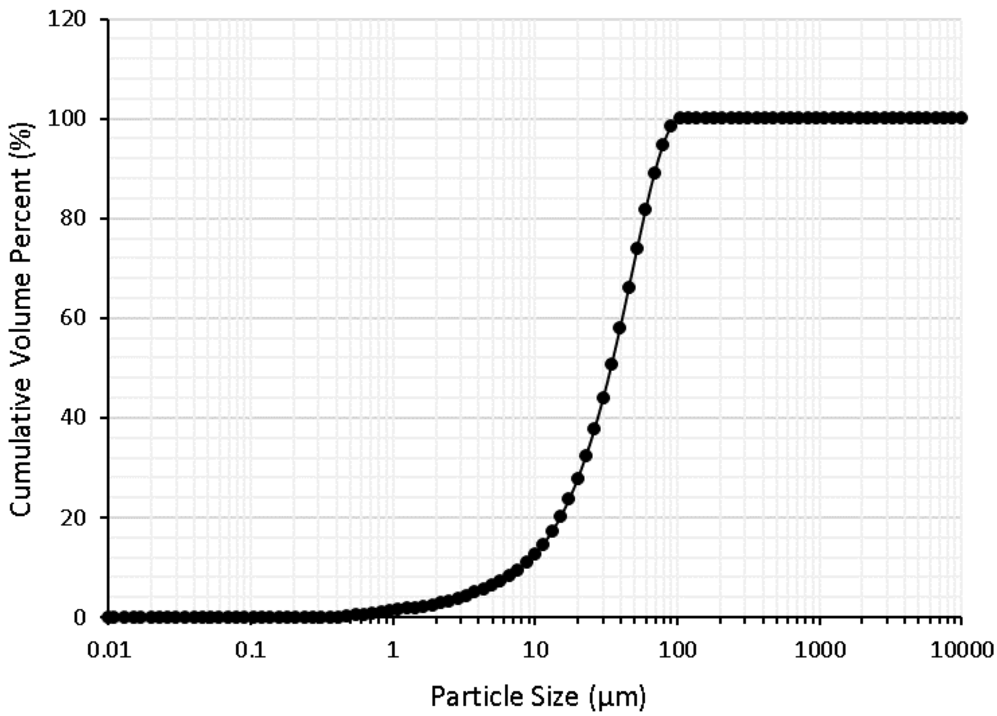

Figure A. 4: Cumulative volume percent versus to particle size for YDK sepiolite clay.

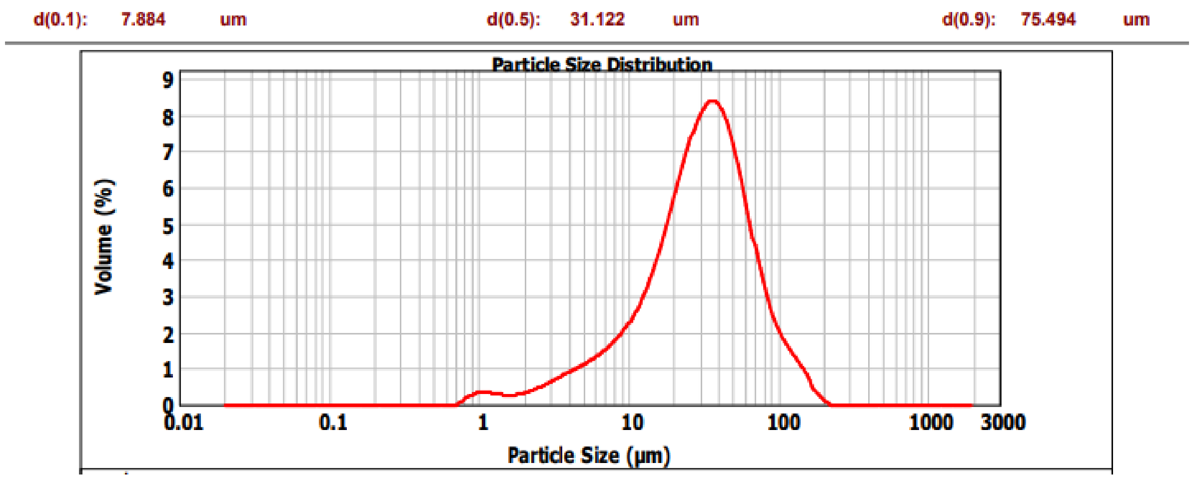

Figure A. 5: Volume percent versus to particle size for Kurtşeyh sepiolite clay.

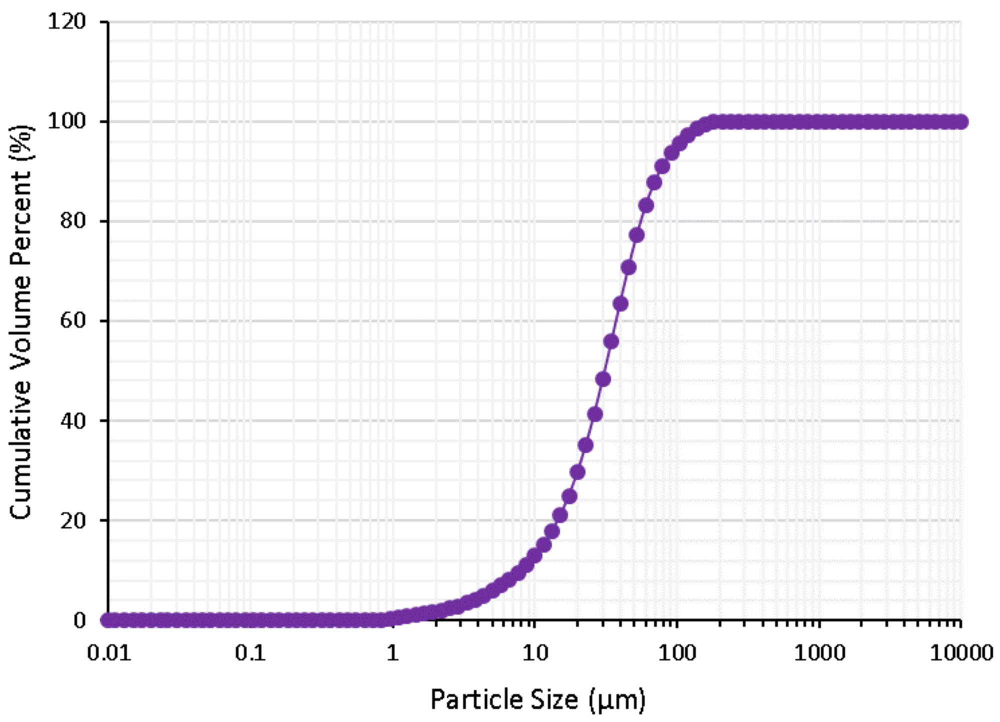

Figure A. 6: Cumulative volume percent versus to particle size for Kurtşeyh sepiolite clay.

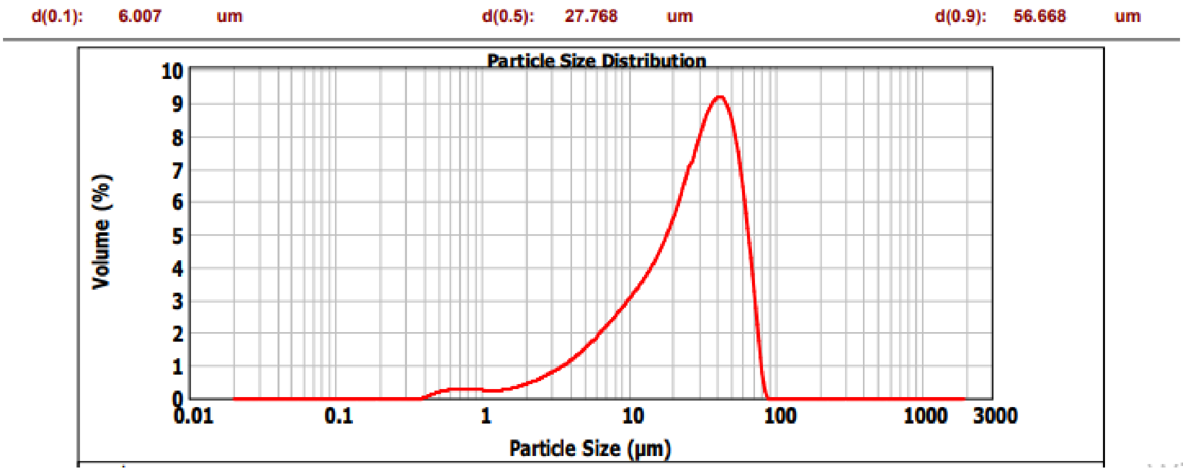

Figure A. 7: Volume percent versus to particle size for micro-sized TTB sepiolite clay.

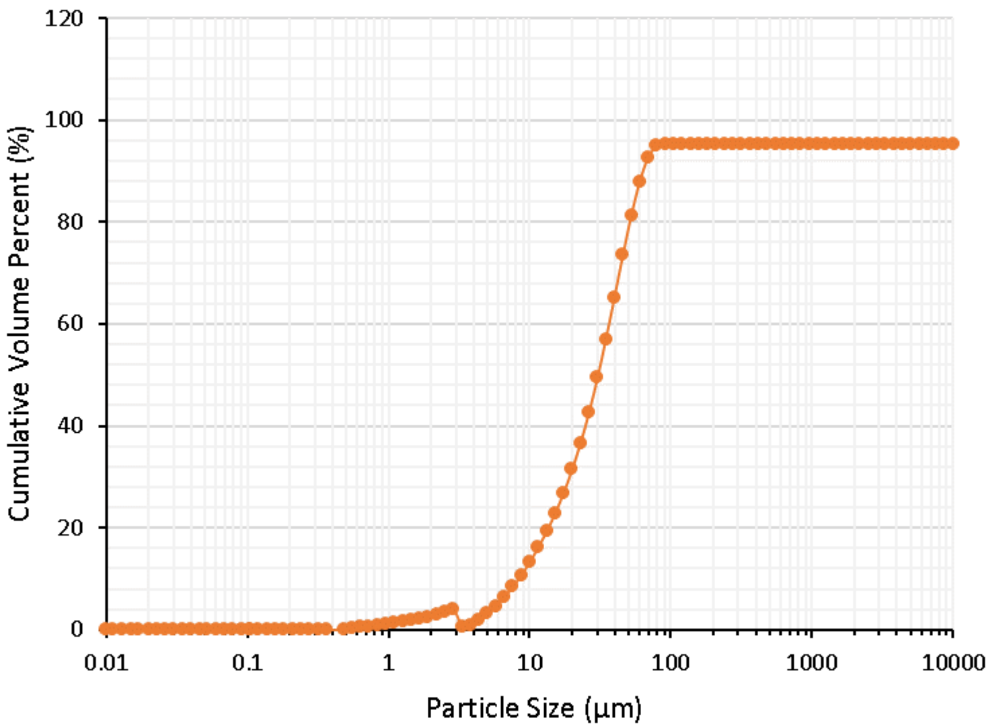

Figure A. 8: Cumulative volume percent versus to particle size for micro-sized TTB sepiolite clay.

APPENDIX B:

L-B Curves of All Suspensions

In this section, elastic and viscous Lissajous-Bowditch curves for five diffrent type sepiolite suspension and a bentonite suspension is given at four different frequency (0.25, 0.50, 0.75, 1.0 Hz) and at 25° C temperature.

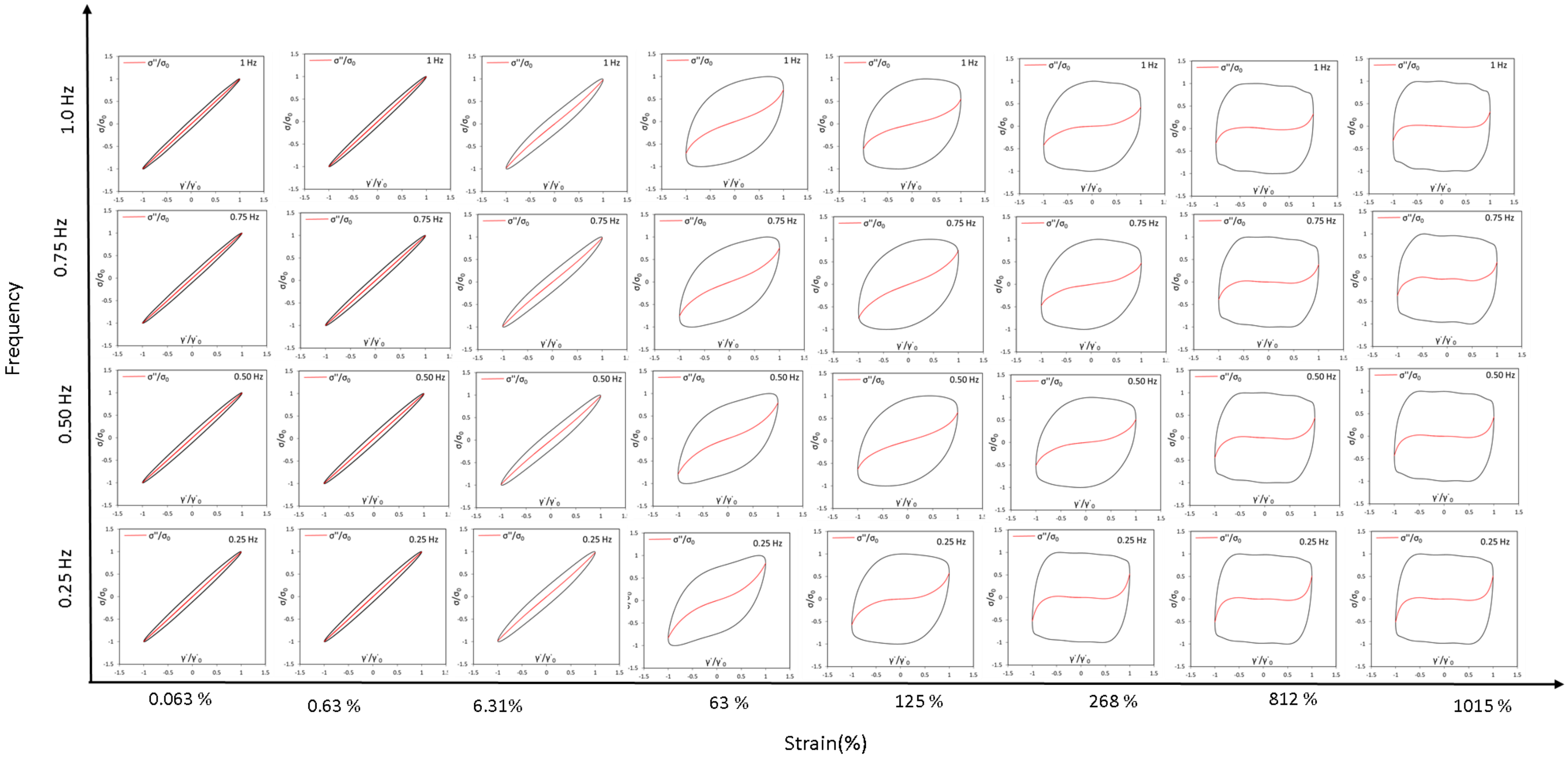

Figure B.9: Elastic Lissajous-Bowditch curves of YDK sepiolite suspensions at four different Frequency and at 25° C.

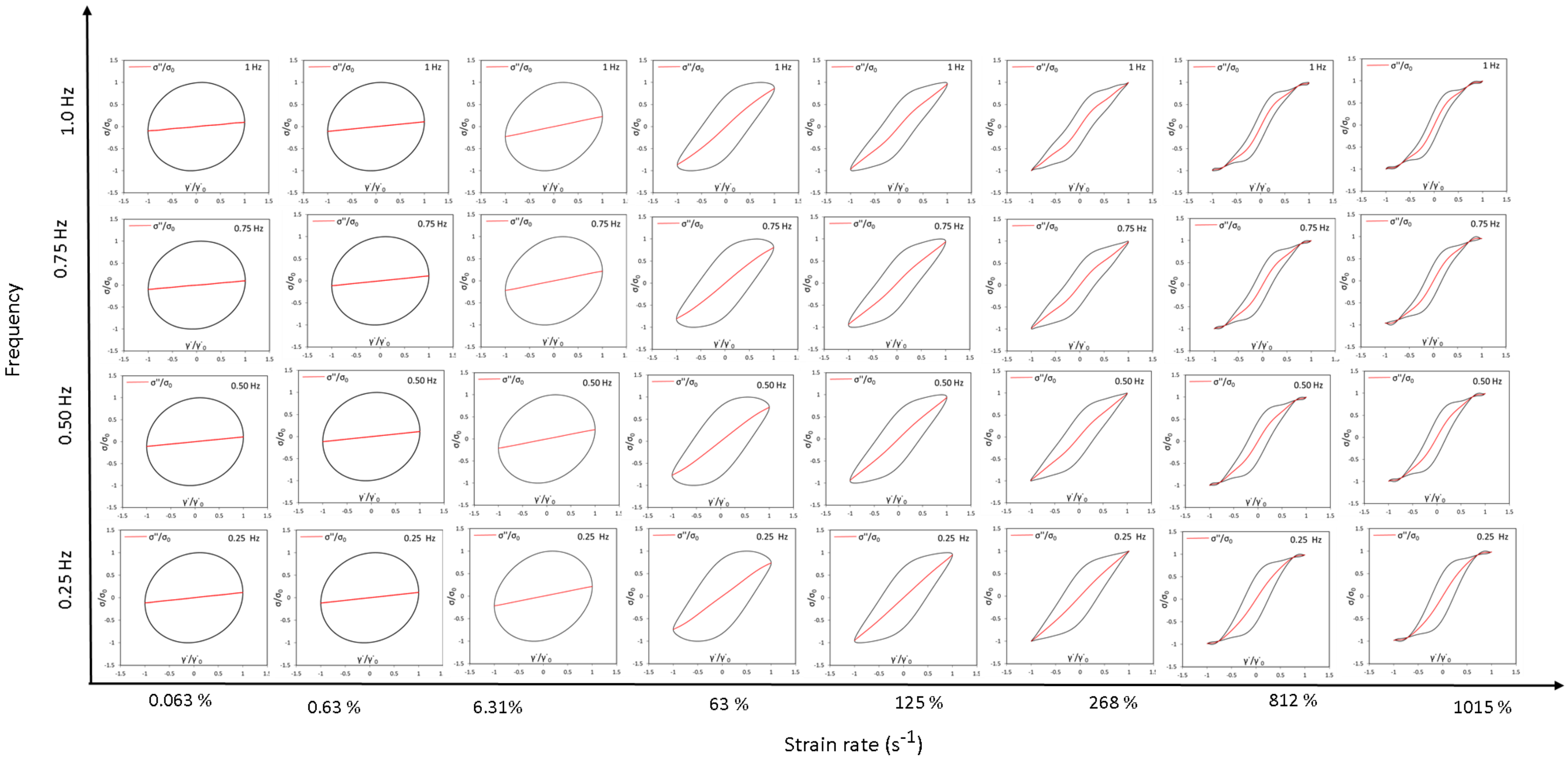

Figure B.10: Viscous Lissajous-Bowditch curves of YDK sepiolite suspensions at four different Frequency and at 25° C.

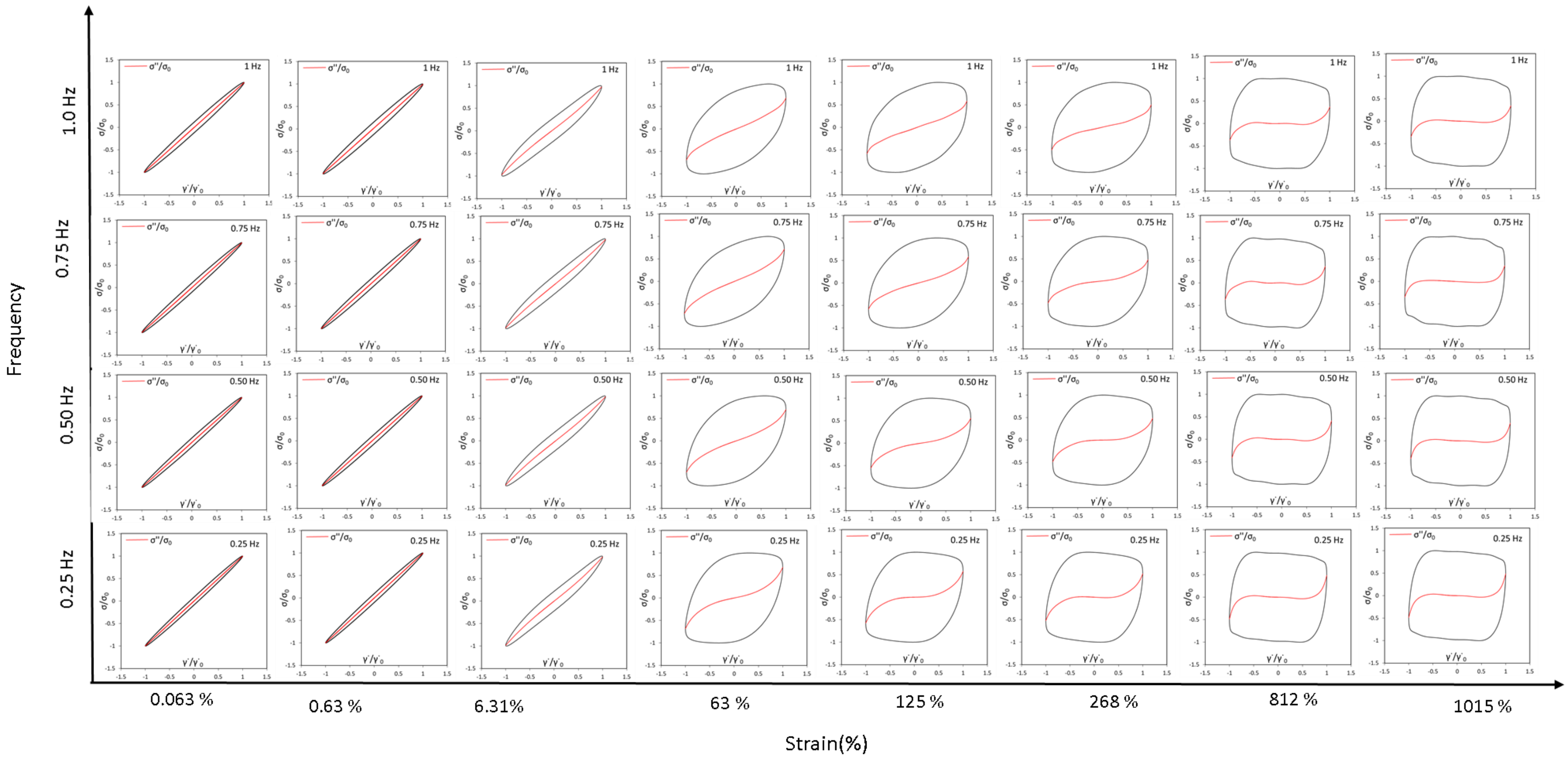

Figure B.11: Elastic Lissajous-Bowditch curves of Kurtşeyh sepiolite suspensions at four different Frequency and at 25° C.

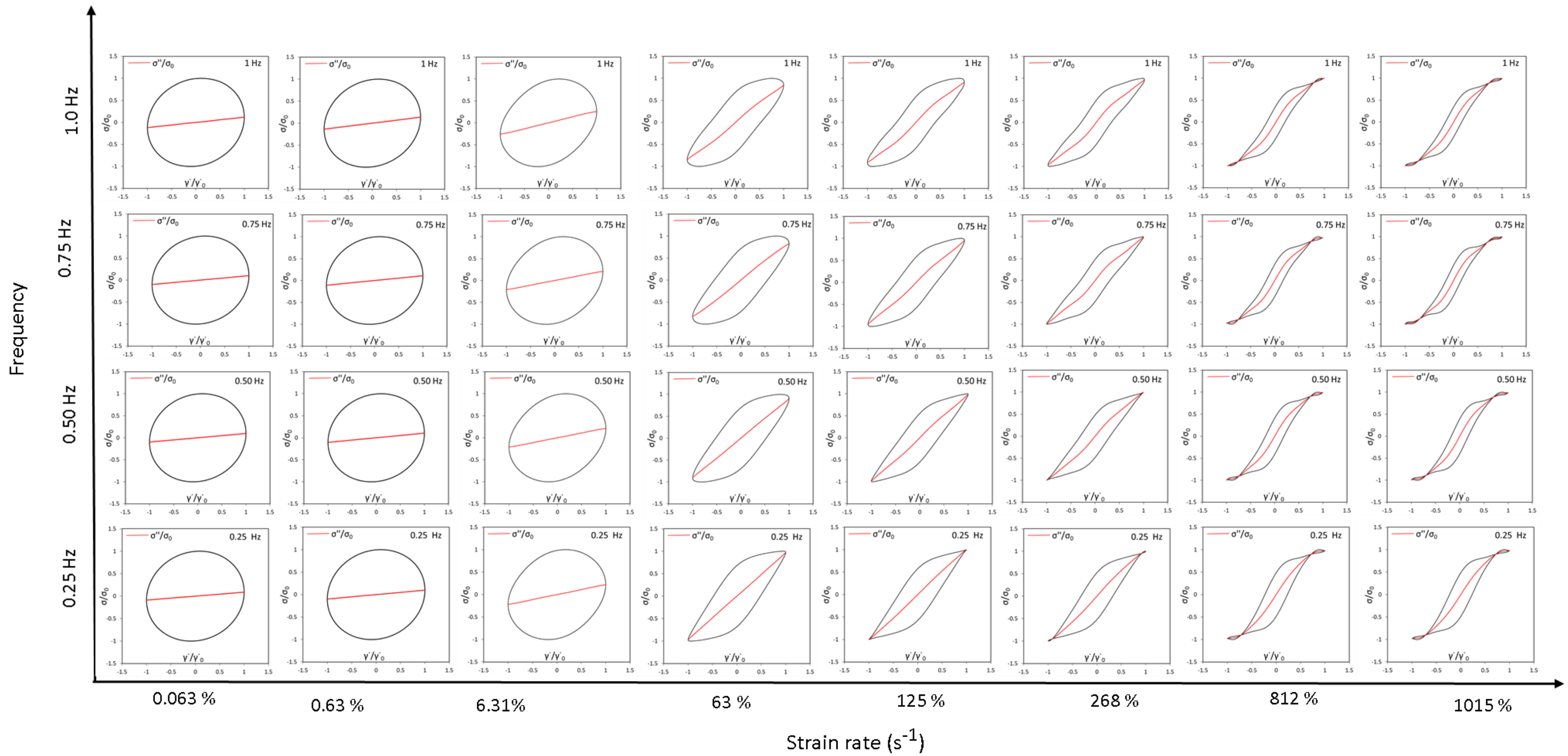

Figure B.12: Viscous Lissajous-Bowditch curves of Kurtşeyh sepiolite suspensions at four different Frequency and at 25° C.

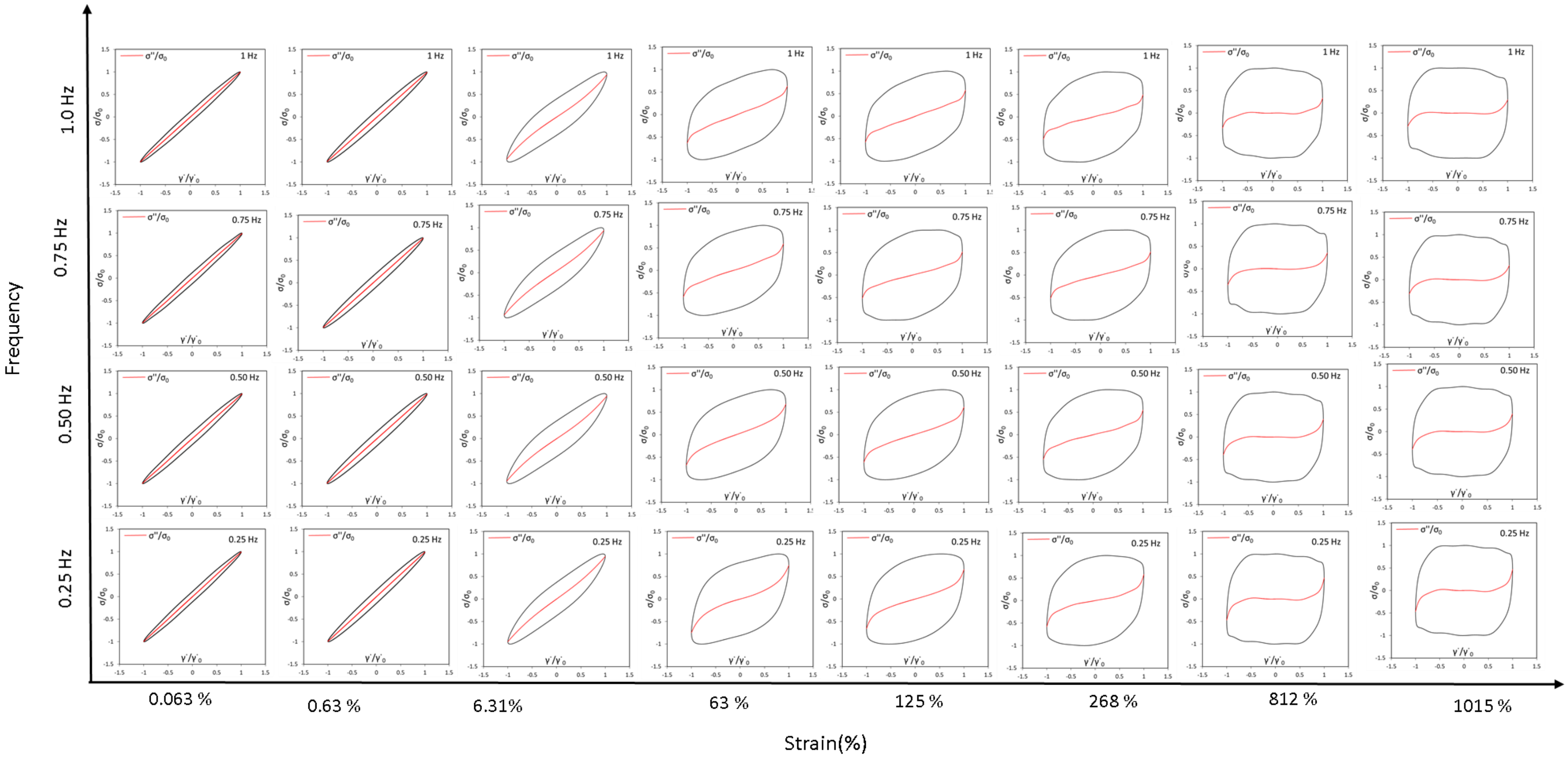

Figure B.13: Elastic Lissajous-Bowditch curves of S sepiolite suspensions at four different Frequency and at 25° C.

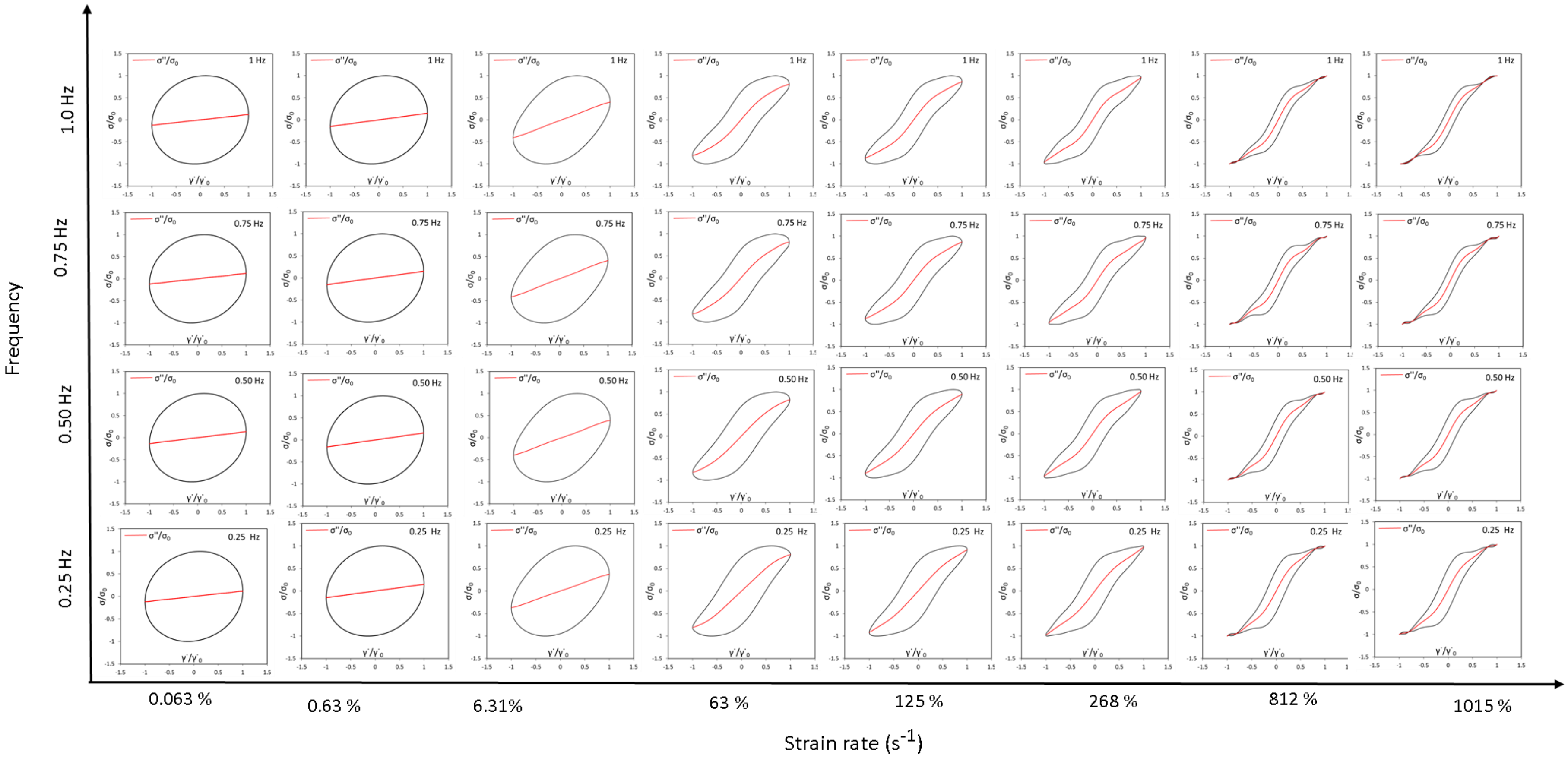

Figure B.14: Viscous Lissajous-Bowditch curves of S sepiolite suspensions at four different Frequency and at 25° C.

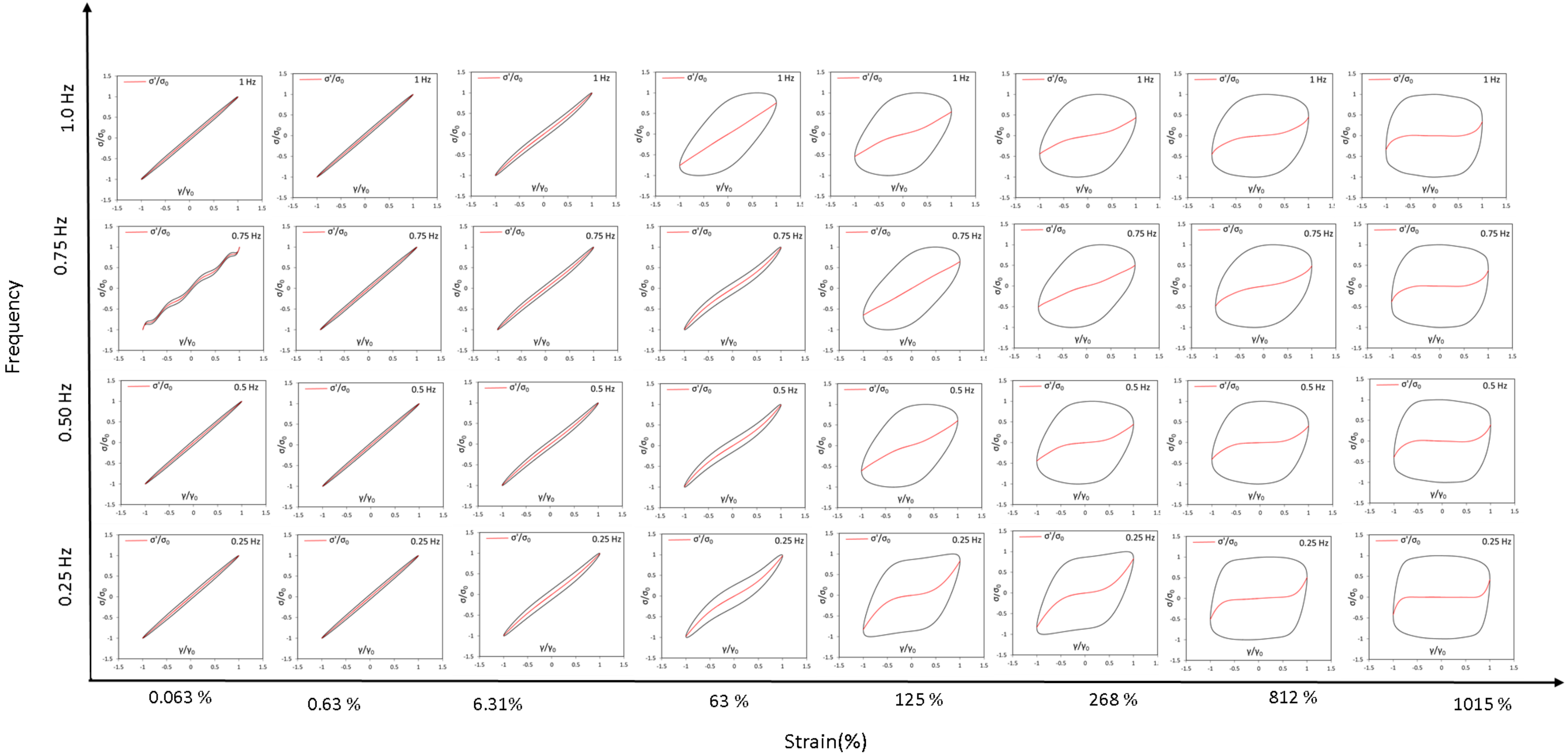

Figure B.15: Elastic Lissajous-Bowditch curves of Bentonite slurry suspensions at four different Frequency and at 25° C.

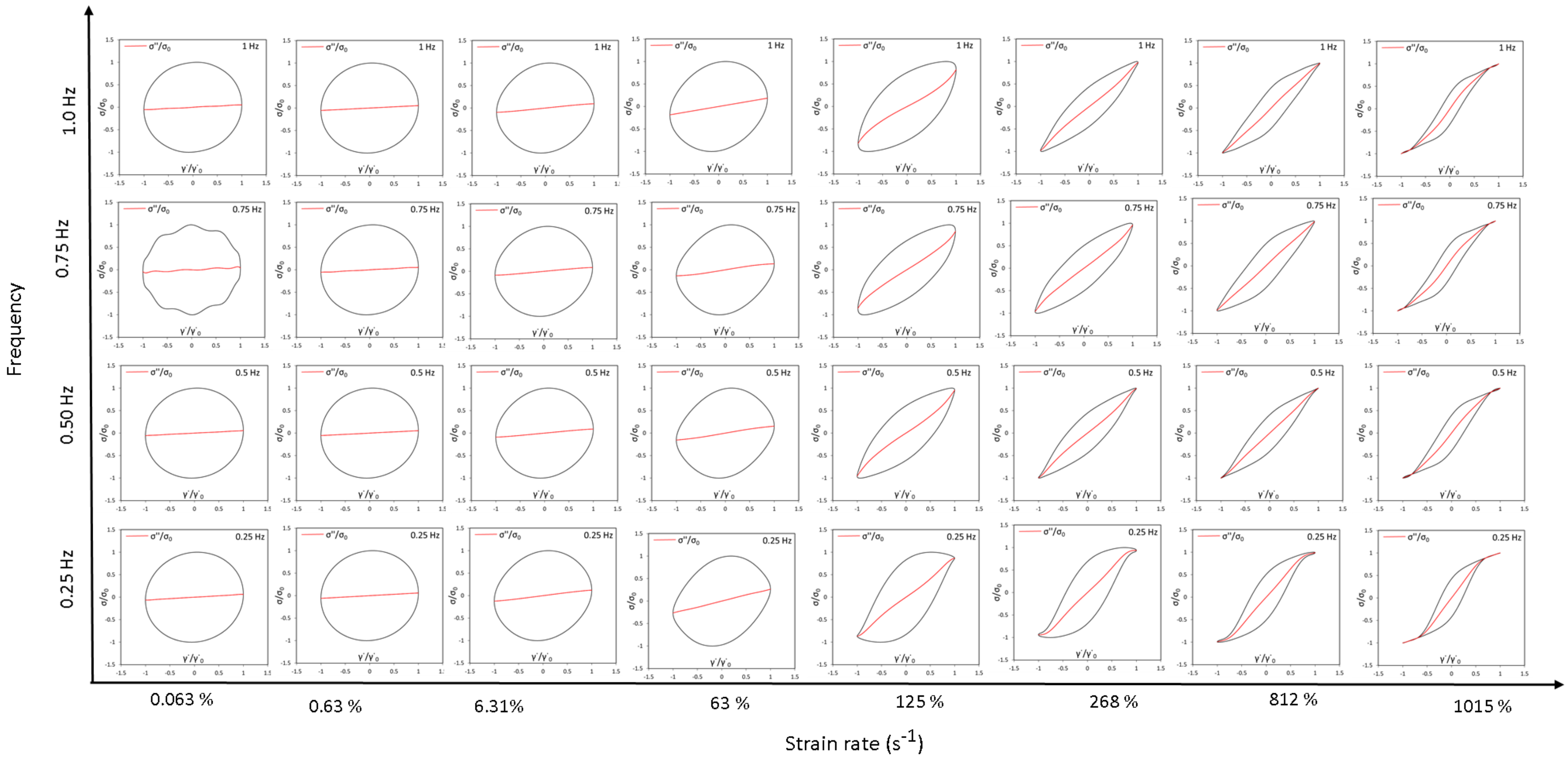

Figure B.16: Viscous Lissajous-Bowditch curves of Bentonite slurry suspensions at four different Frequency and at 25° C.

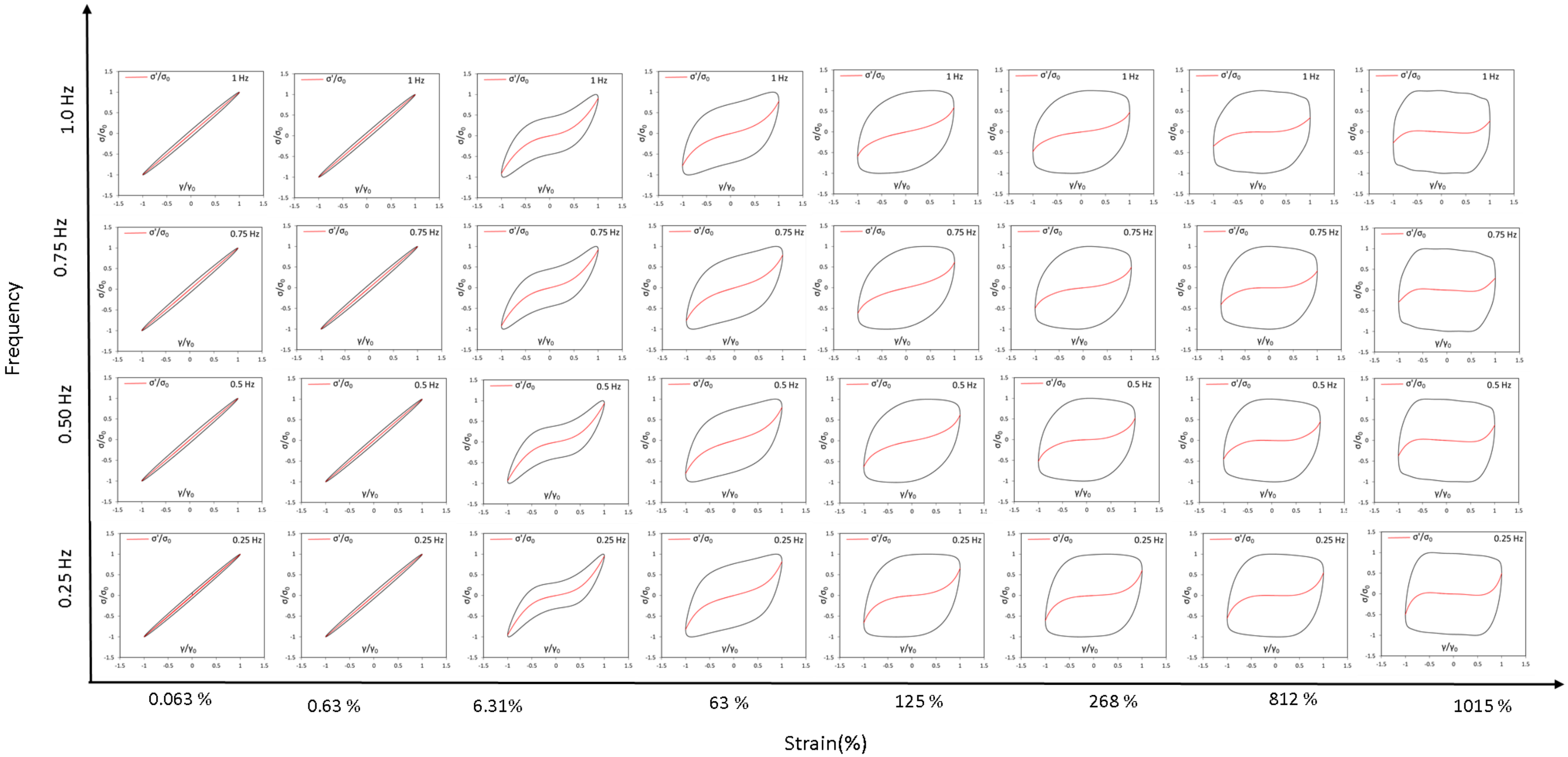

Figure B.17: Elastic Lissajous-Bowditch curves of TTB sepiolite suspensions at four different Frequency and at 25° C.

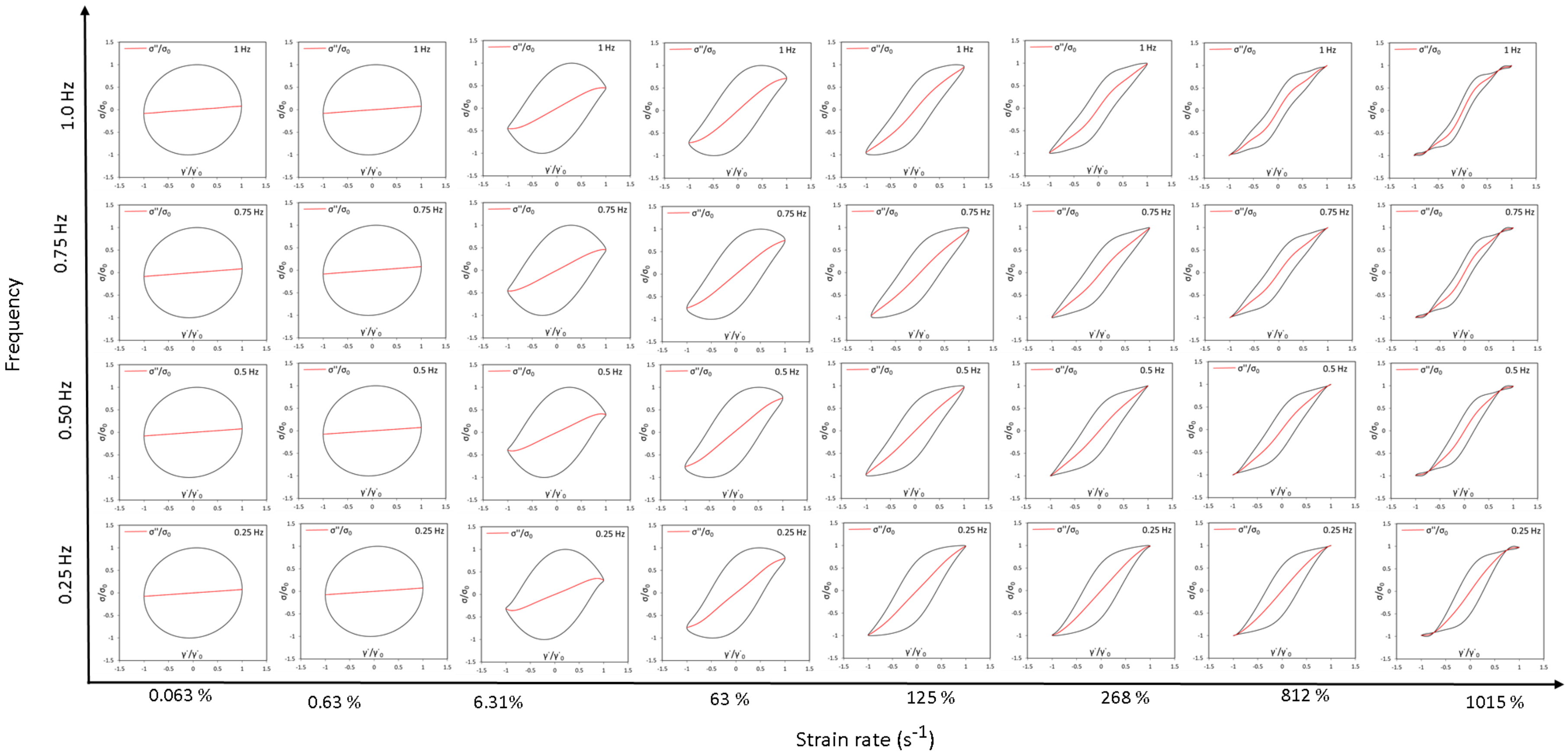

Figure B.18: Viscous Lissajous-Bowditch curves of TTB sepiolite suspensions at four different Frequency and at 25° C.

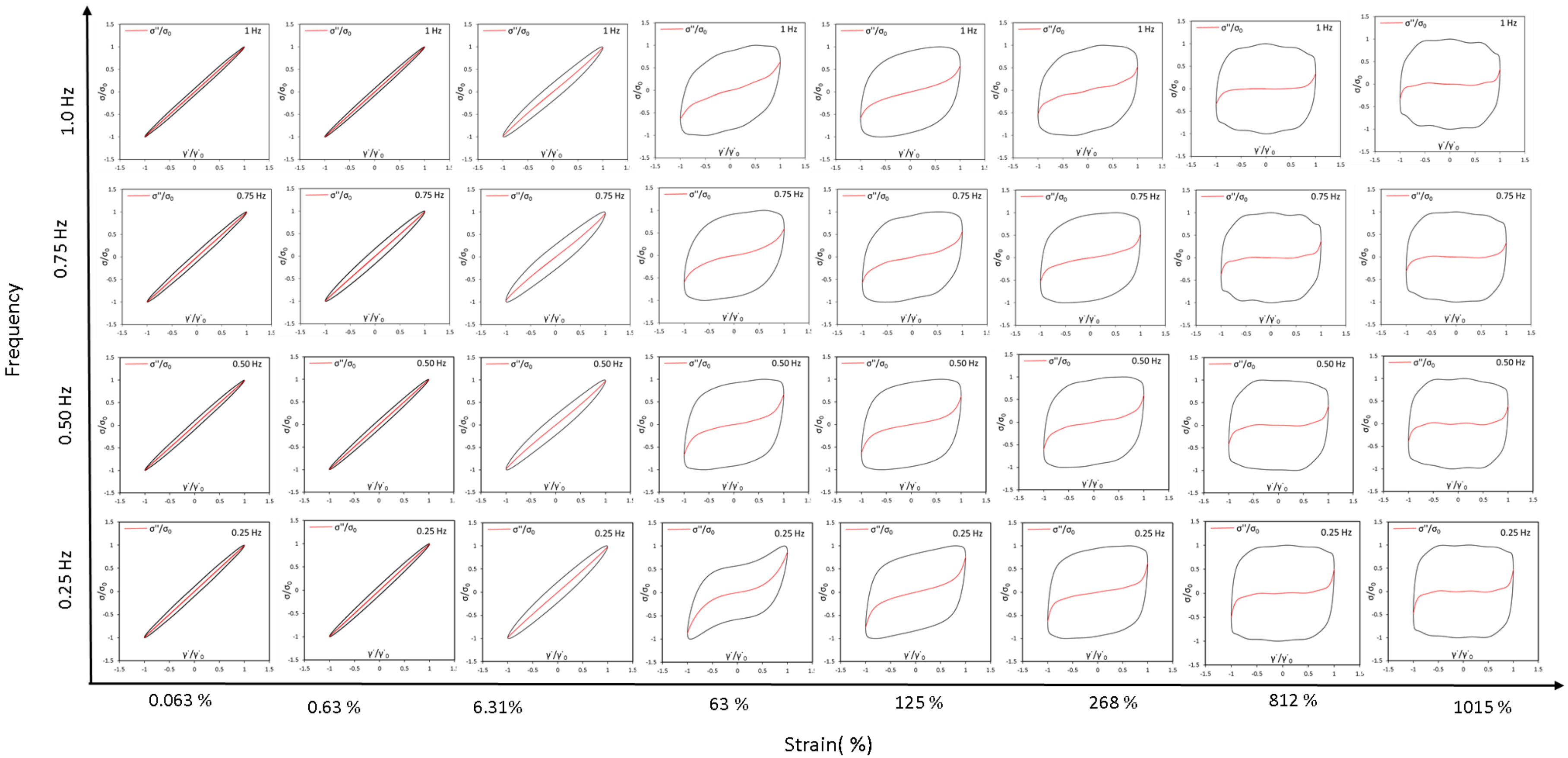

Figure B.19: Elastic Lissajous-Bowditch curves of nano-sized TTB sepiolite suspensions at four different Frequency and at 25° C.

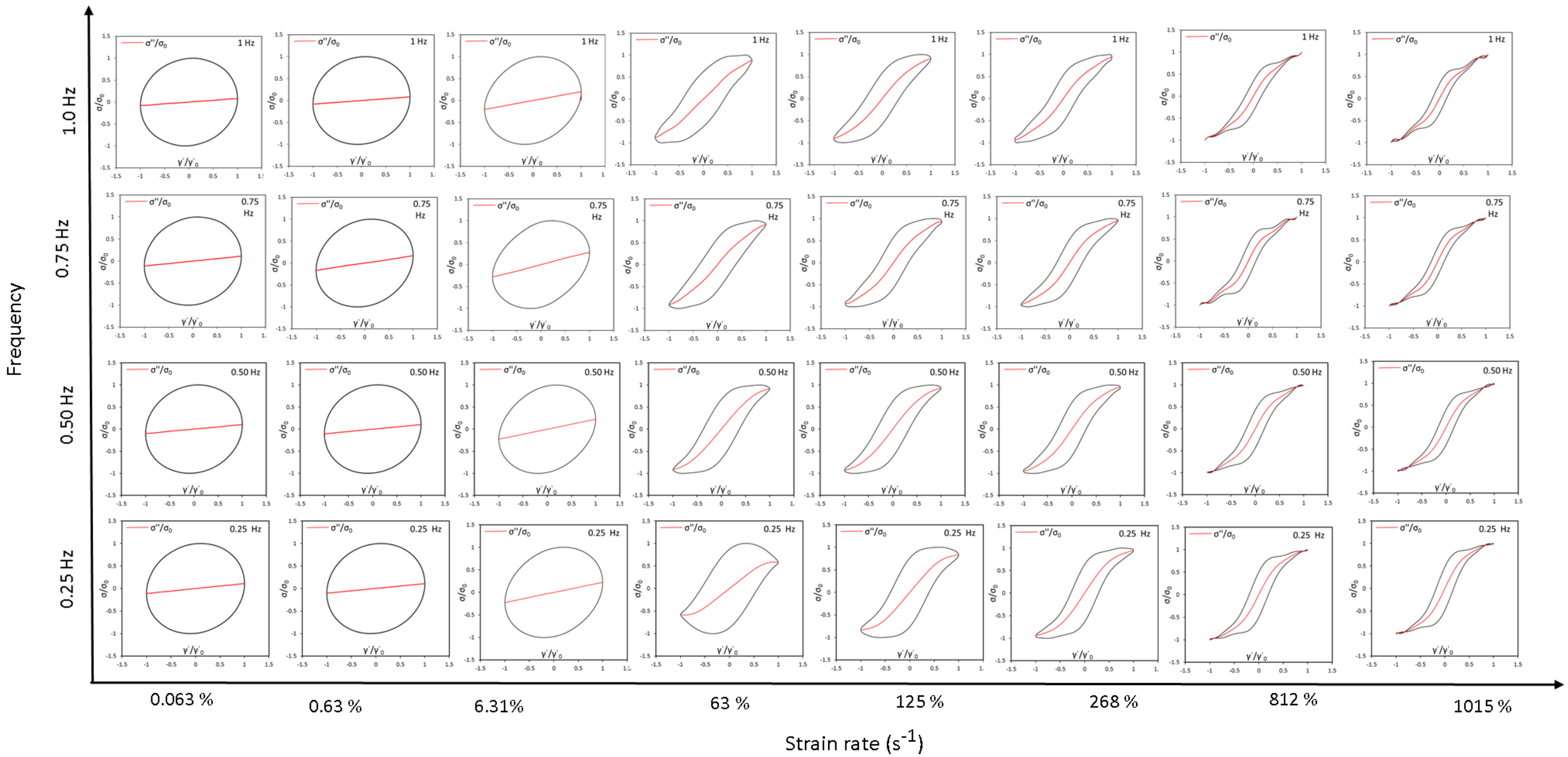

Figure B.20: Viscous Lissajous-Bowditch curves of nano-sized TTB sepiolite suspensions at four different Frequency and at 25° C.

APPENDIX C:

L-B Curves of Micro-Nano-Sized Sepiolite Suspensions

In this section, elastic and viscous Lissajous-Bowditch curves for micro and nano-sized sepiolite suspension at high (100, 150° C) and low (25, 50° C) temperatures at four different frequencies (0.25, 0.50, 0.75, 1.0 Hz).

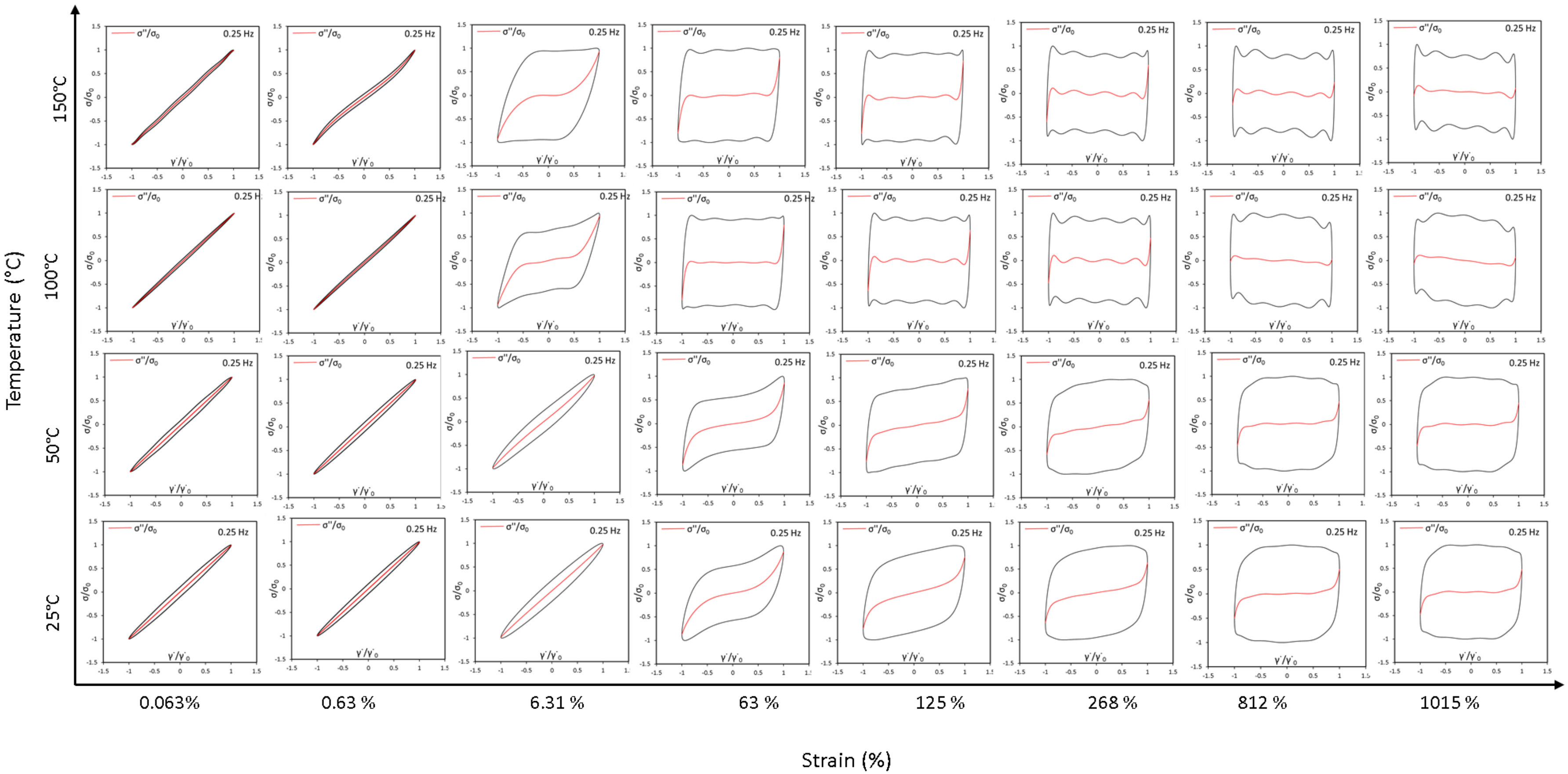

Figure C.1: Elastic Lissajous-Bowditch curves of nano-sized TTB sepiolite suspensions at four different temperature and at 0.25 Hz Frequency.

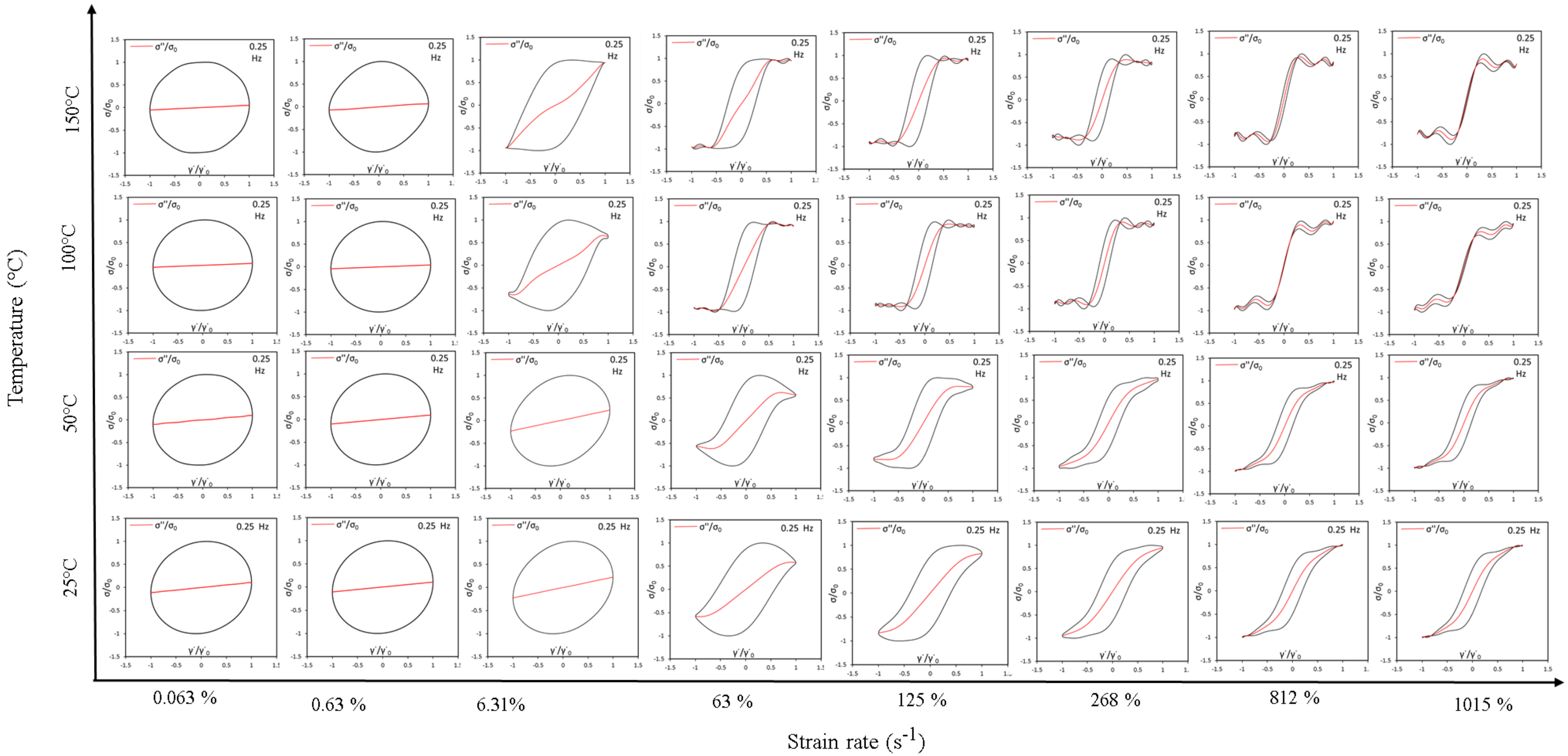

Figure C.2: Viscous Lissajous-Bowditch curves of nano-sized TTB sepiolite suspensions at four different temperature and at 0.25 Hz Frequency.

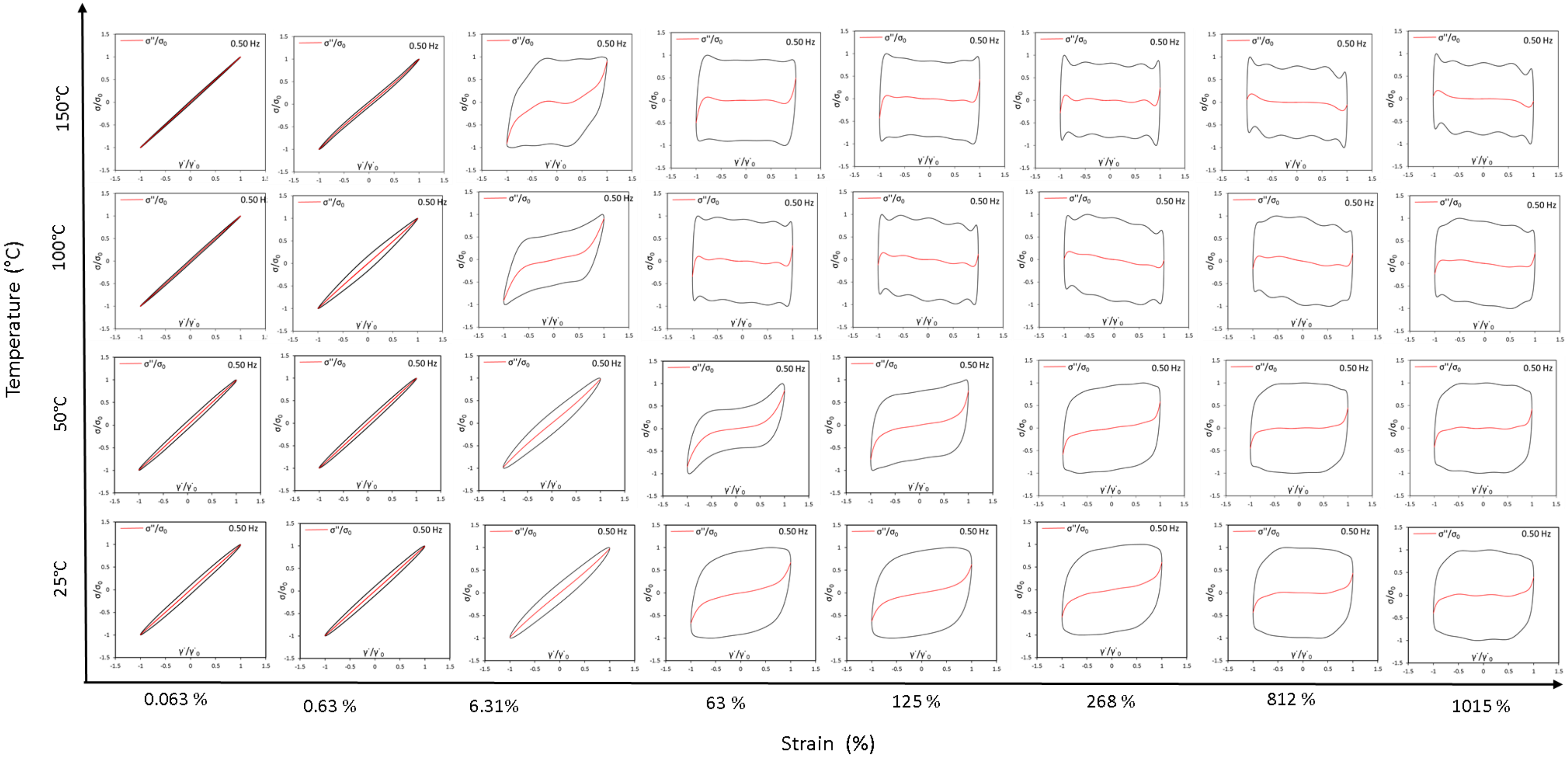

Figure C.3: Elastic Lissajous-Bowditch curves of nano-sized TTB sepiolite suspensions at four different temperature and at 0.50 Hz Frequency.

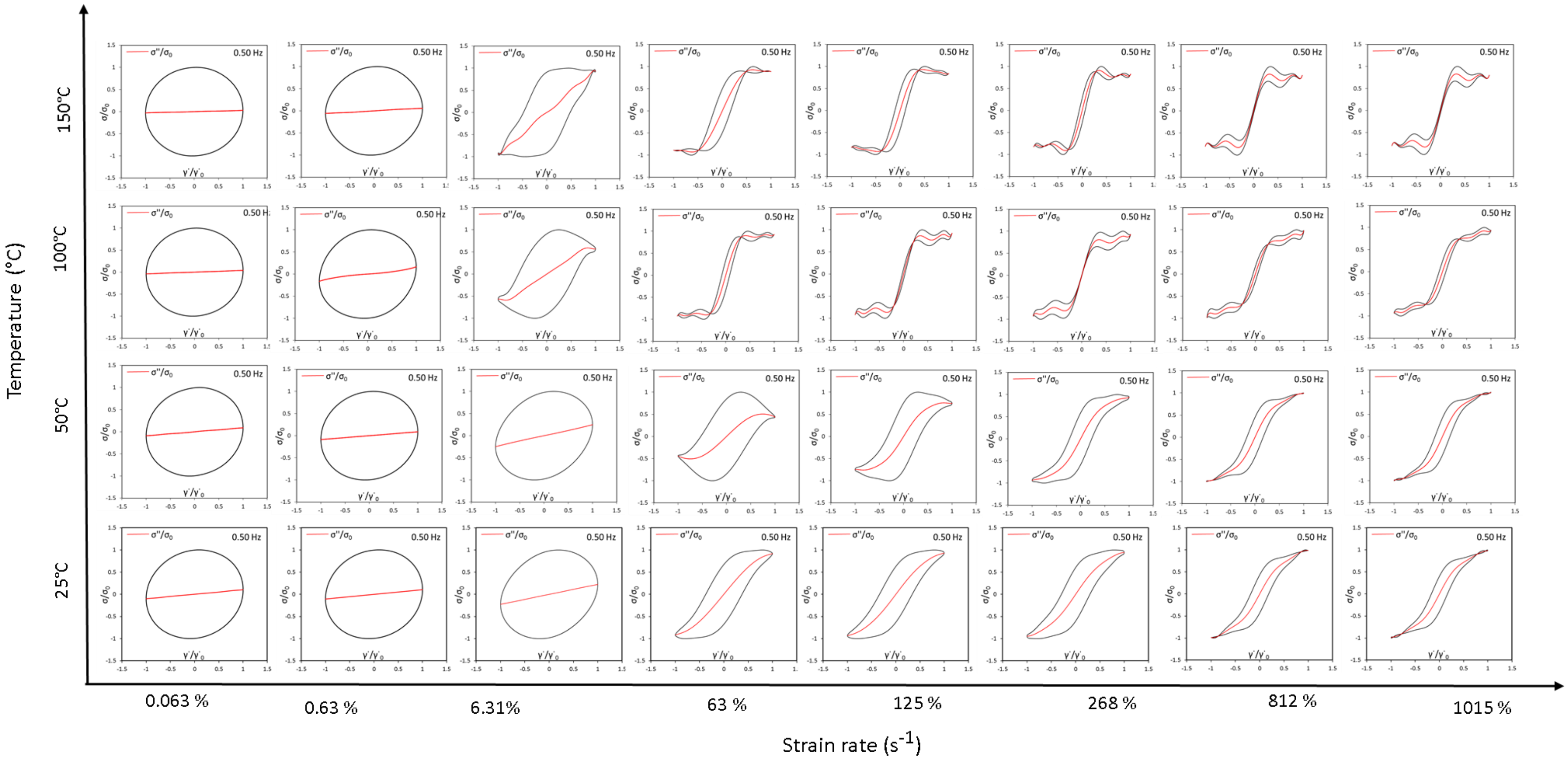

Figure C.4: Viscous Lissajous-Bowditch curves of nano-sized TTB sepiolite suspensions at four different temperature and at 0.50 Hz Frequency.

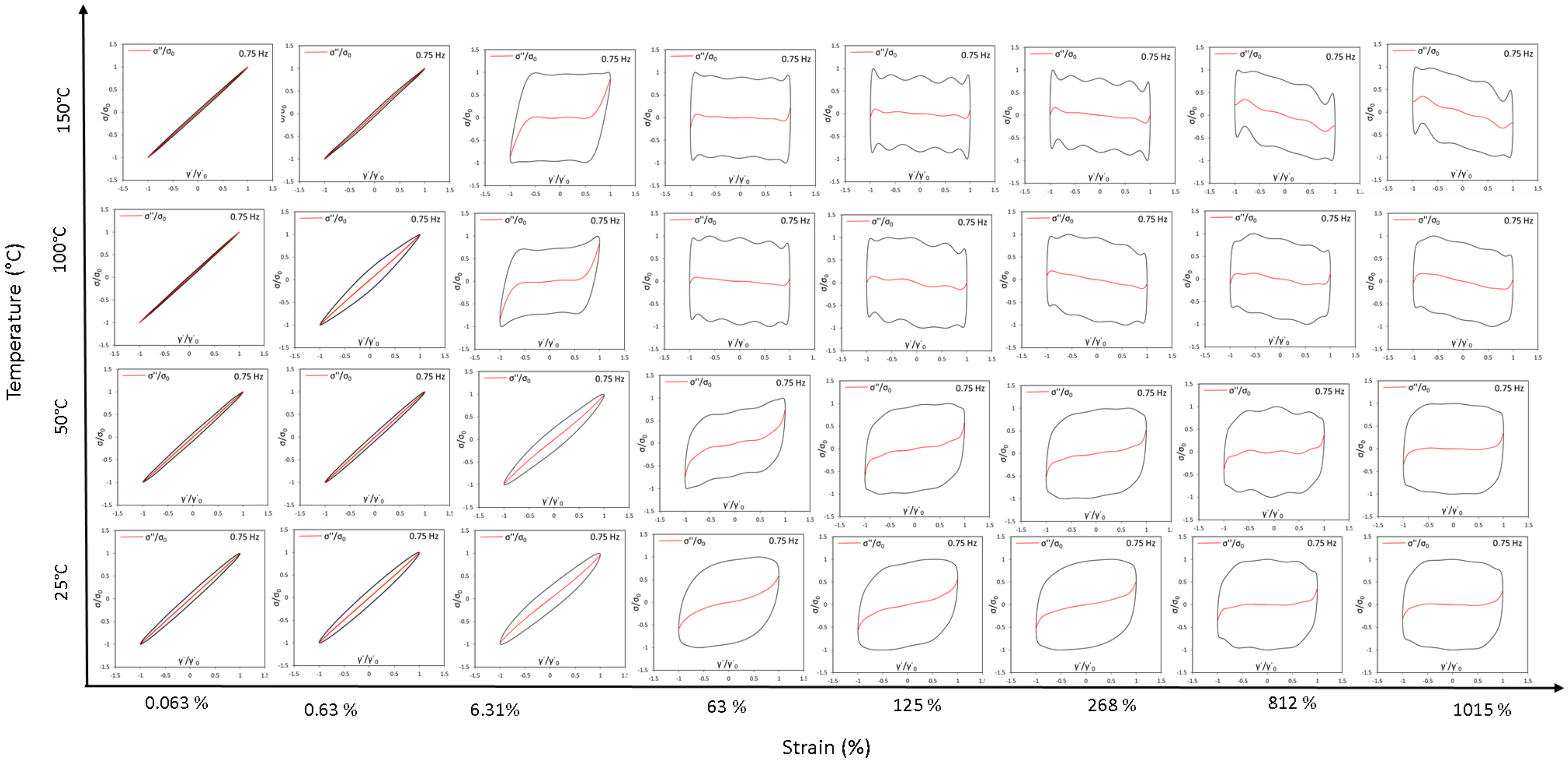

Figure C.5: Elastic Lissajous-Bowditch curves of nano-sized TTB sepiolite suspensions at four different temperature and at 0.75 Hz Frequency.

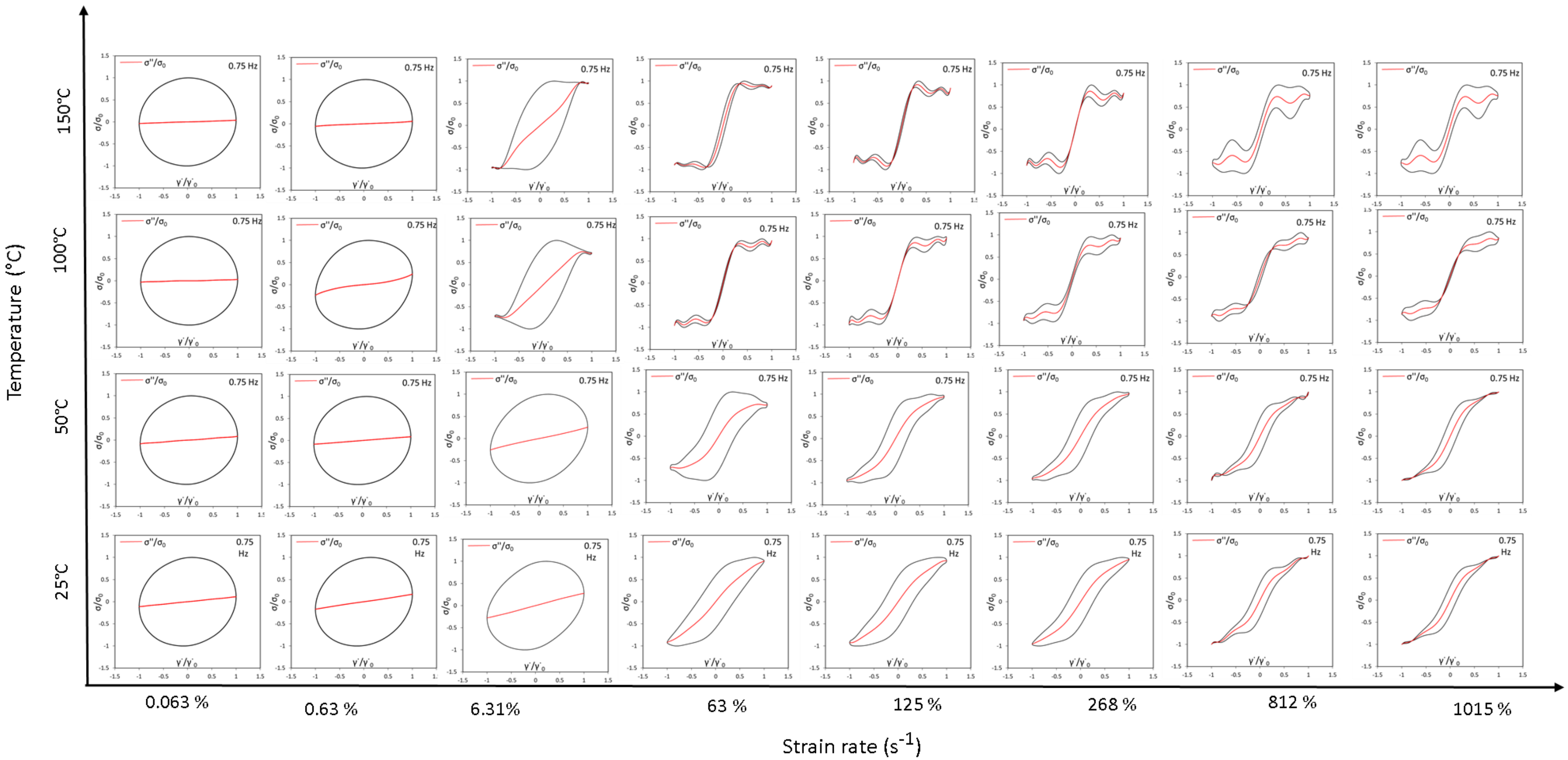

Figure C.6: Viscous Lissajous-Bowditch curves of nano-sized TTB sepiolite suspensions at four different temperature and at 0.75 Hz Frequency.

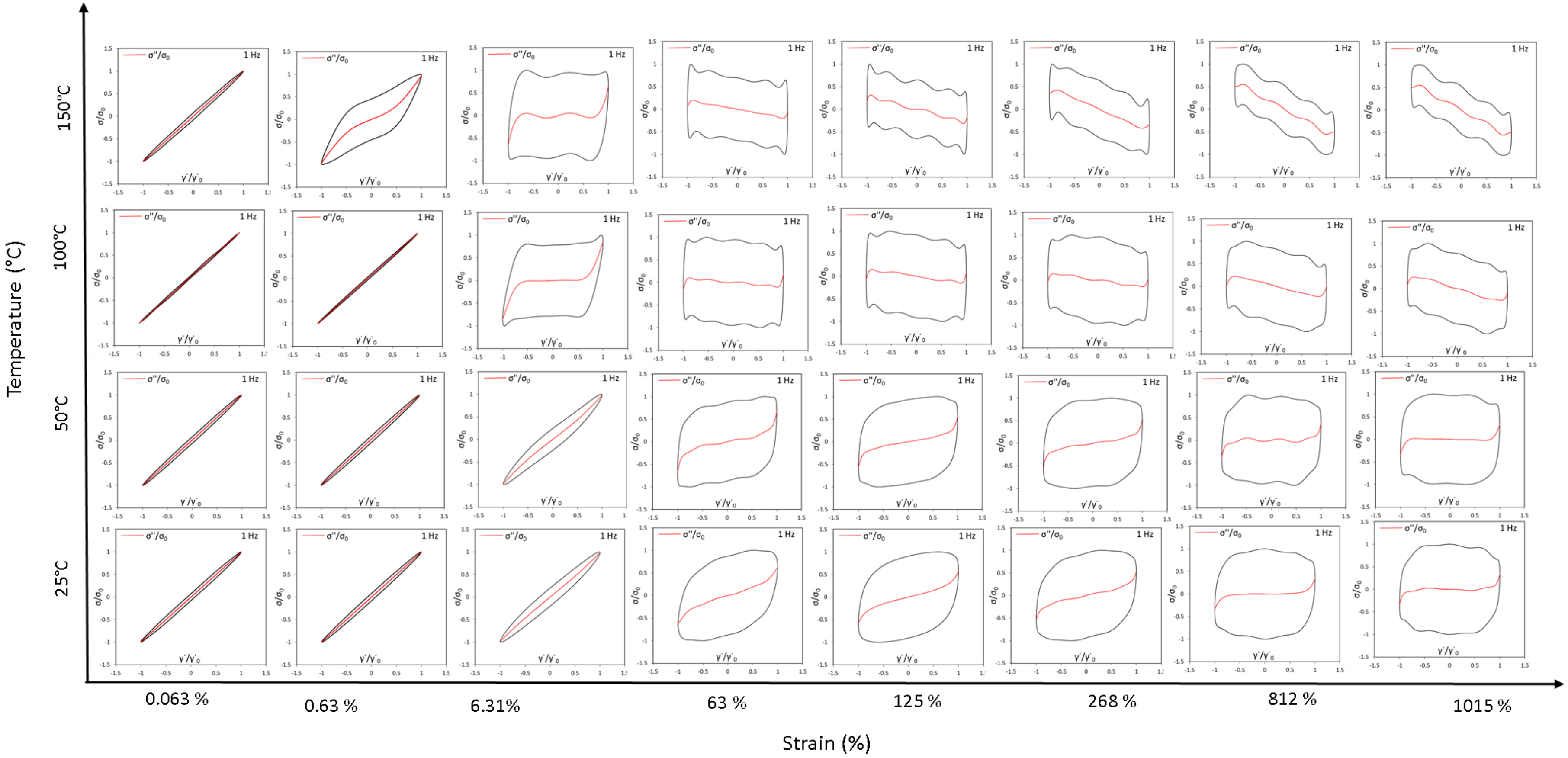

Figure C.7: Elastic Lissajous-Bowditch curves of nano-sized TTB sepiolite suspensions at four different temperature and at 1.0 Hz Frequency.

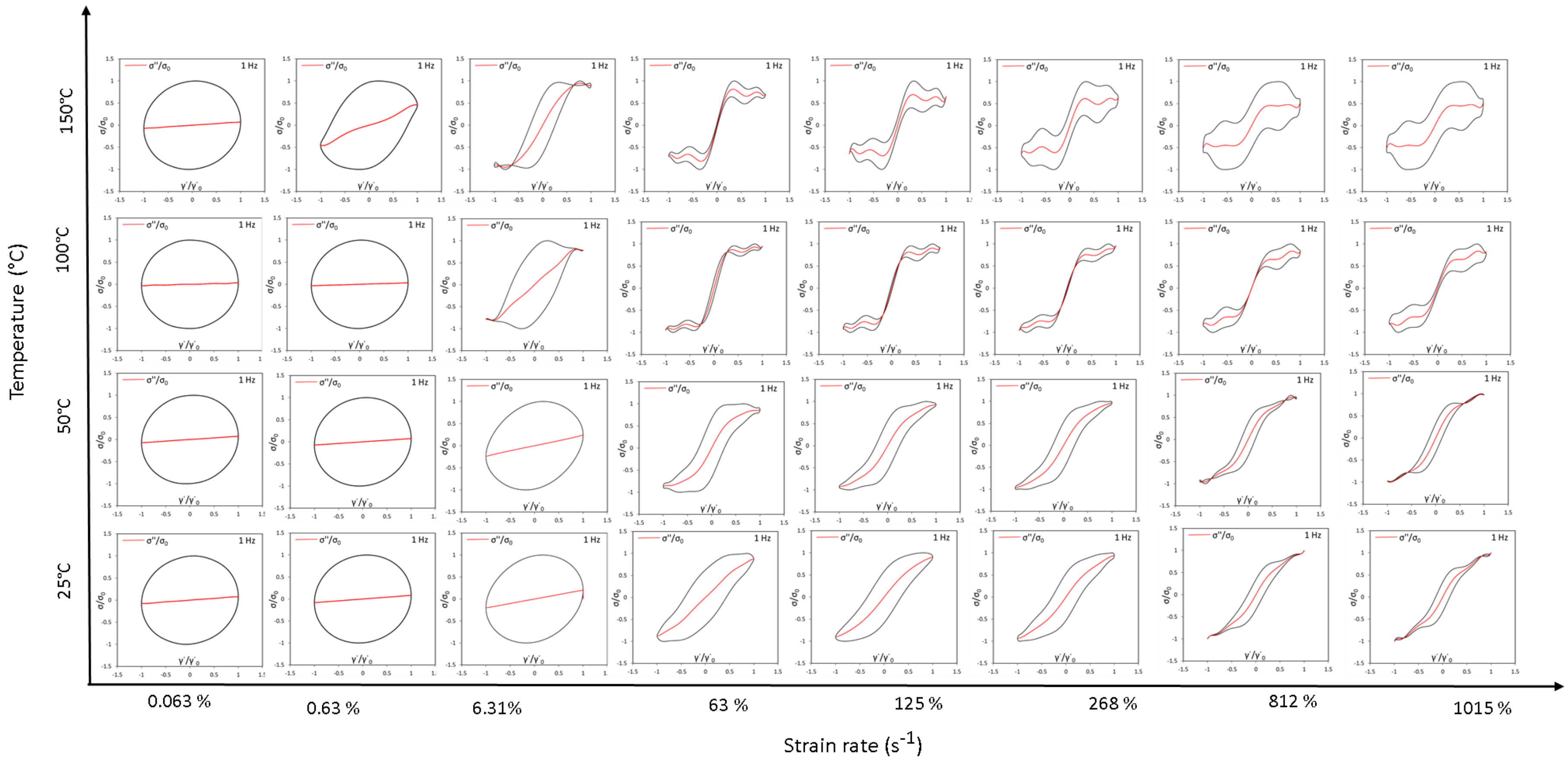

Figure C.8: Viscous Lissajous-Bowditch curves of nano-sized TTB sepiolite suspensions at four different temperature and at 1.0 Hz Frequency.

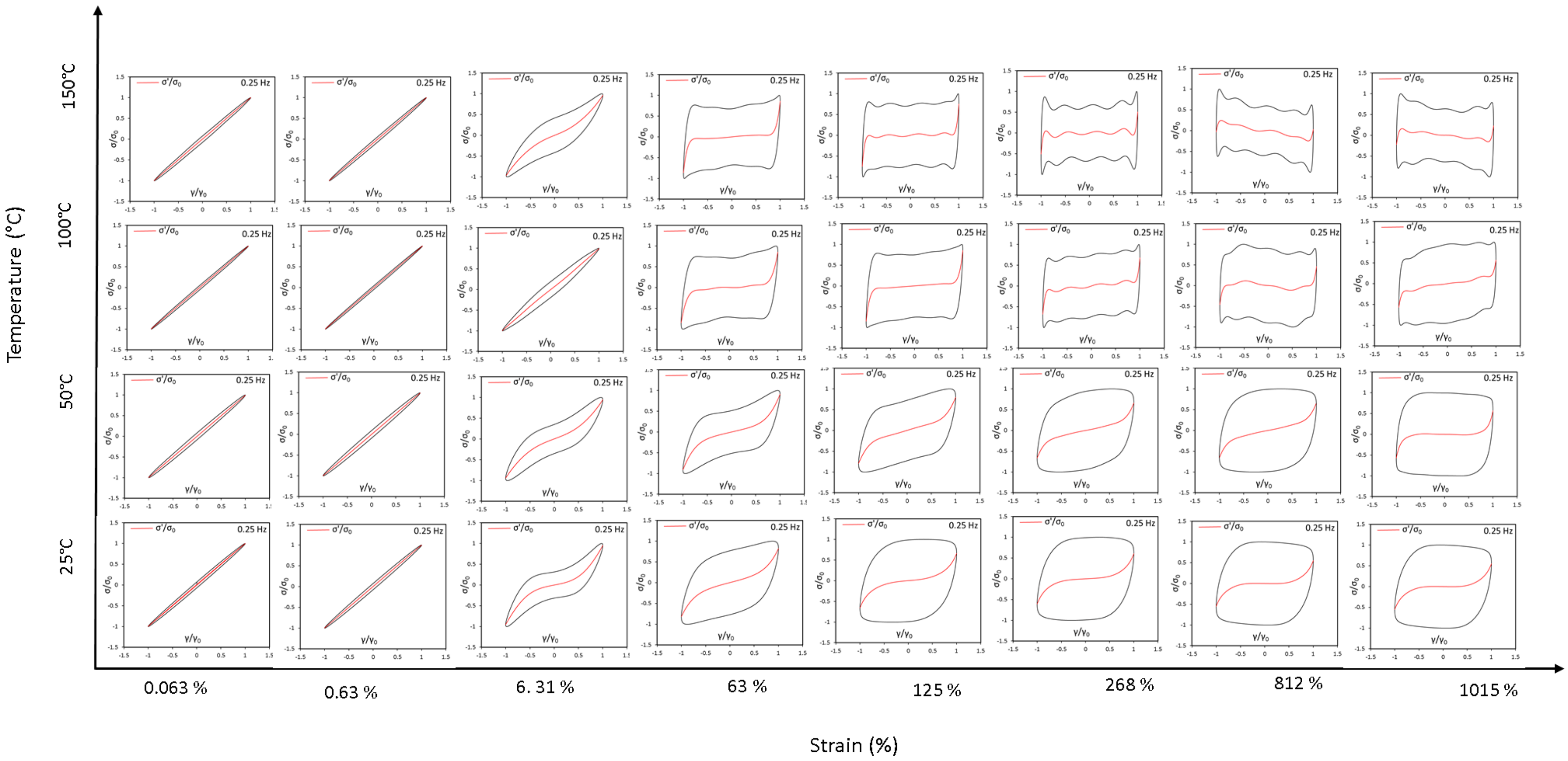

Figure C.9: Elastic Lissajous-Bowditch curves of micro-sized TTB sepiolite suspensions at four different temperature and at 0.25 Hz Frequency.

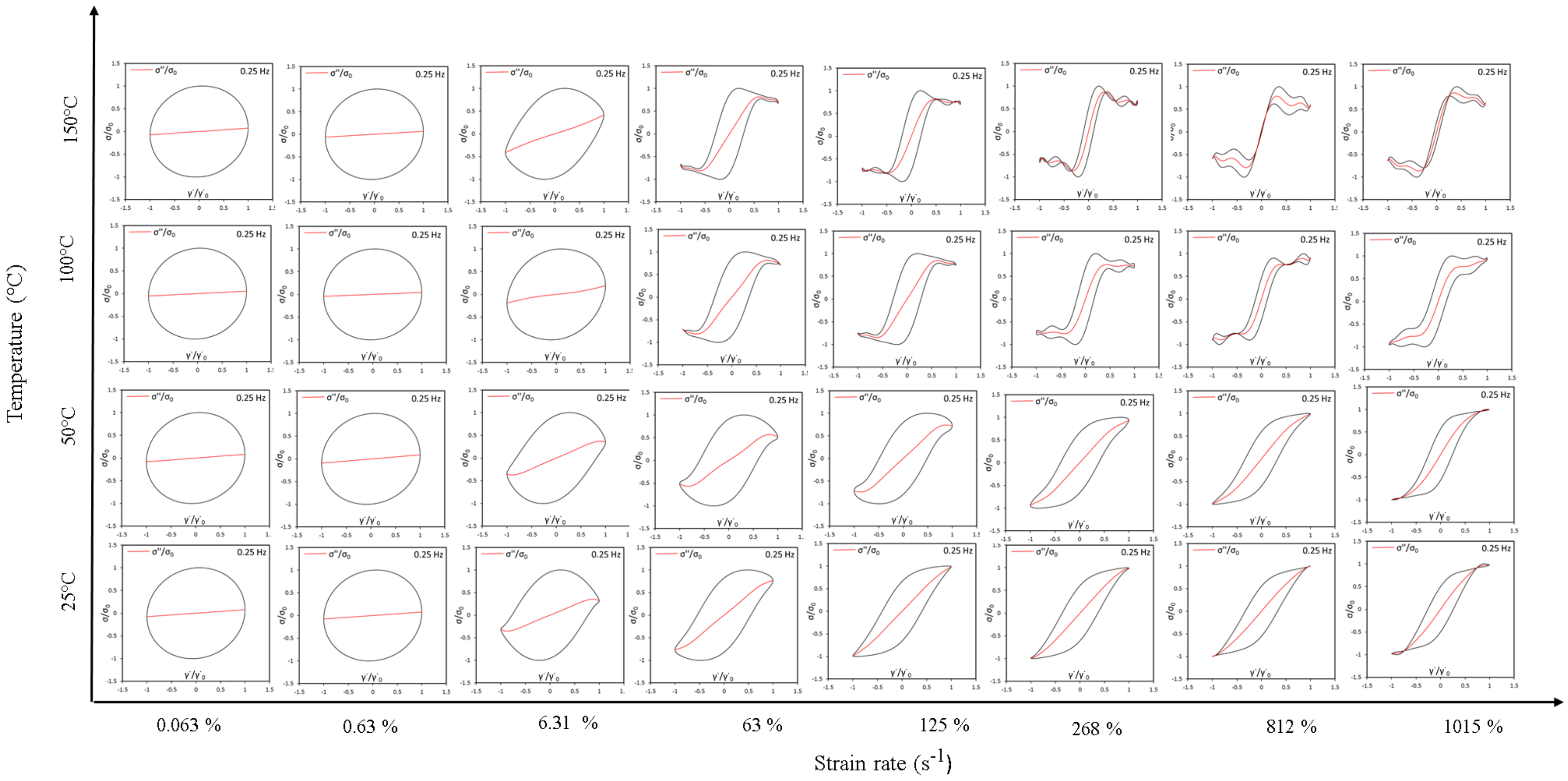

Figure C.10: Elastic Lissajous-Bowditch curves of micro-sized TTB sepiolite suspensions at four different temperature and at 0.25 Hz Frequency.

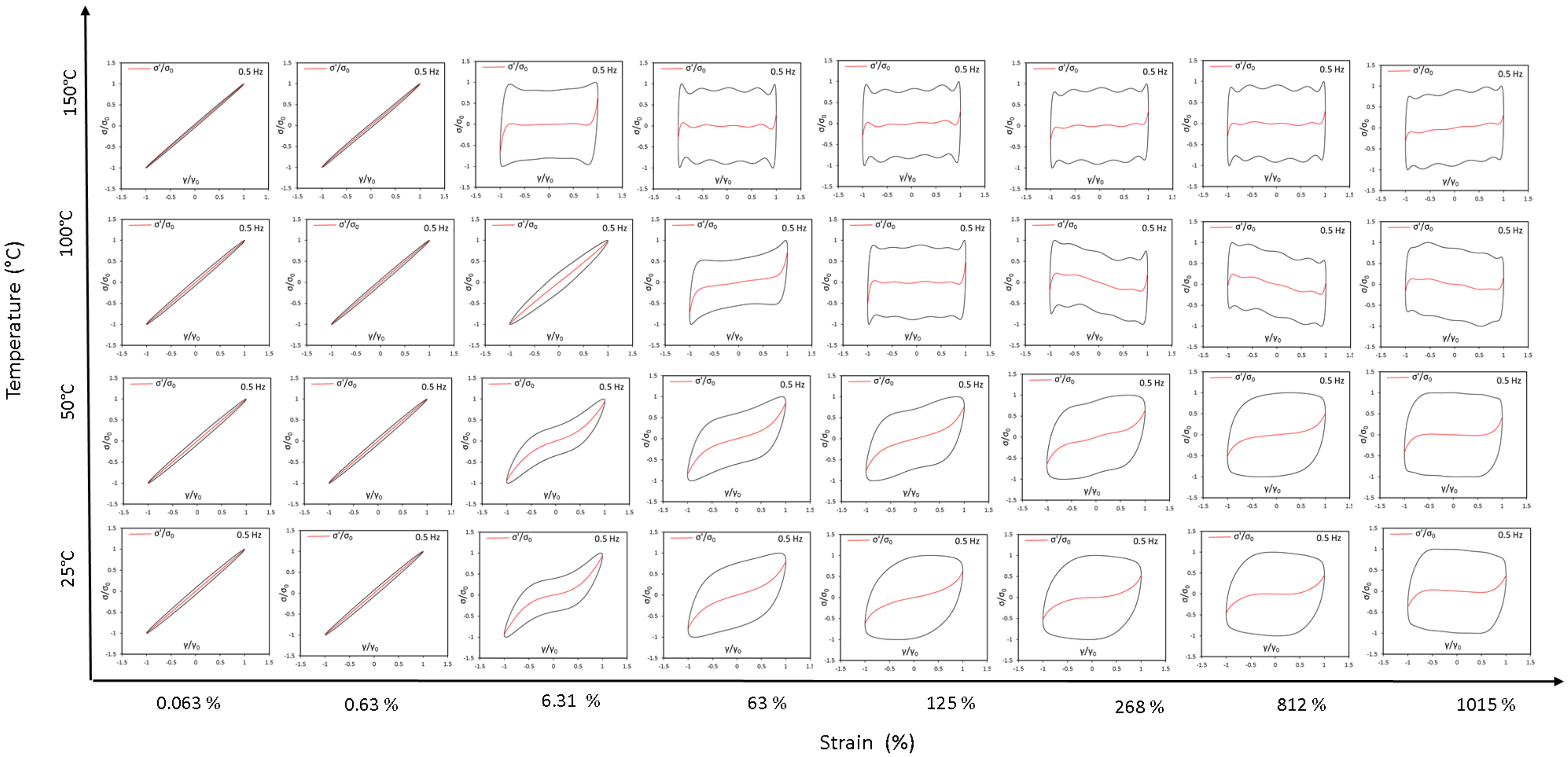

Figure C.11: Elastic Lissajous-Bowditch curves of micro-sized TTB sepiolite suspensions at four different temperature and at 0.50 Hz Frequency.

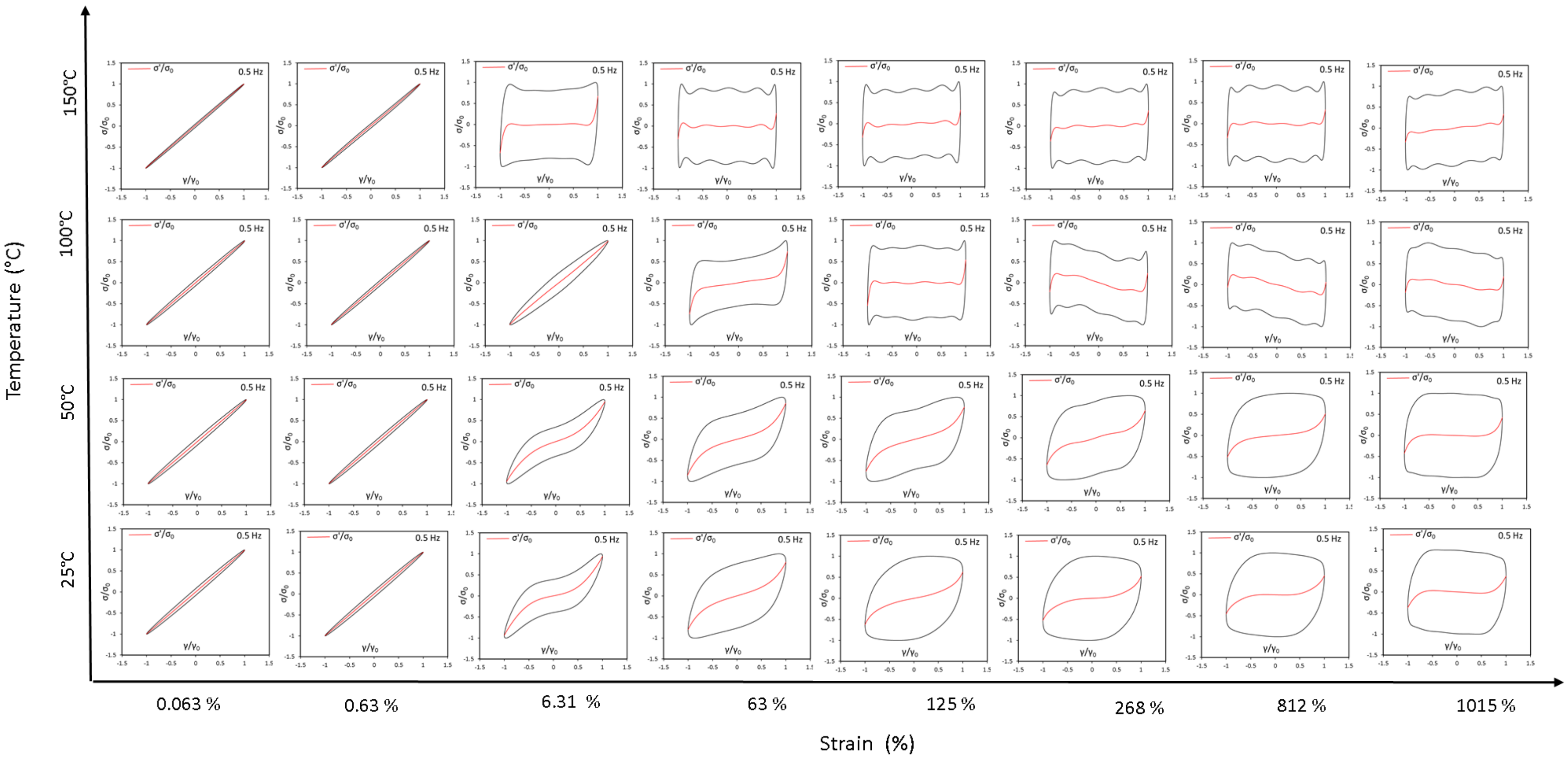

Figure C.12: Elastic Lissajous-Bowditch curves of micro-sized TTB sepiolite suspensions at four different temperature and at 0.50 Hz Frequency.

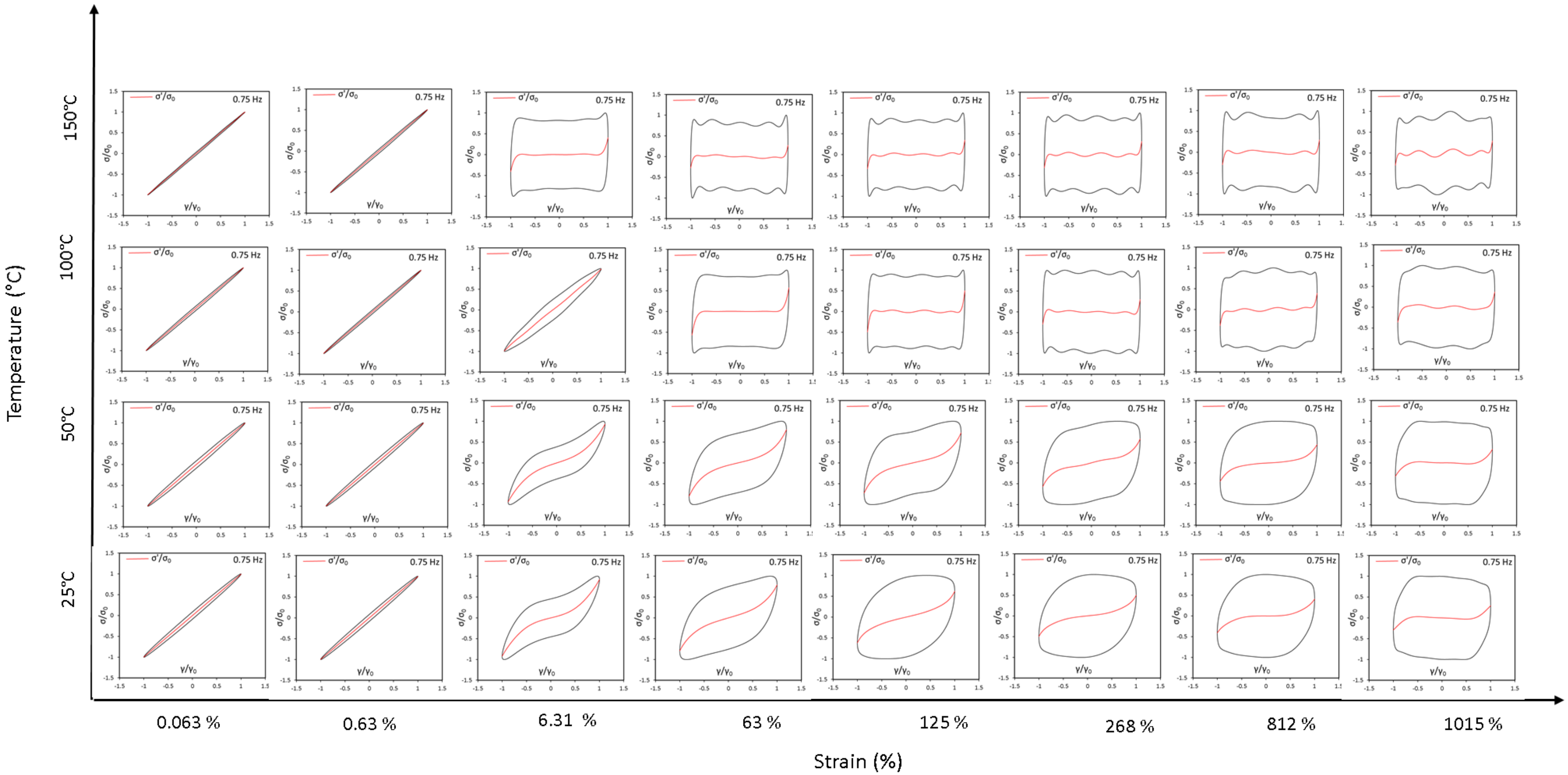

Figure C.13: Elastic Lissajous-Bowditch curves of micro-sized TTB sepiolite suspensions at four different temperature and at 0.75 Hz Frequency.

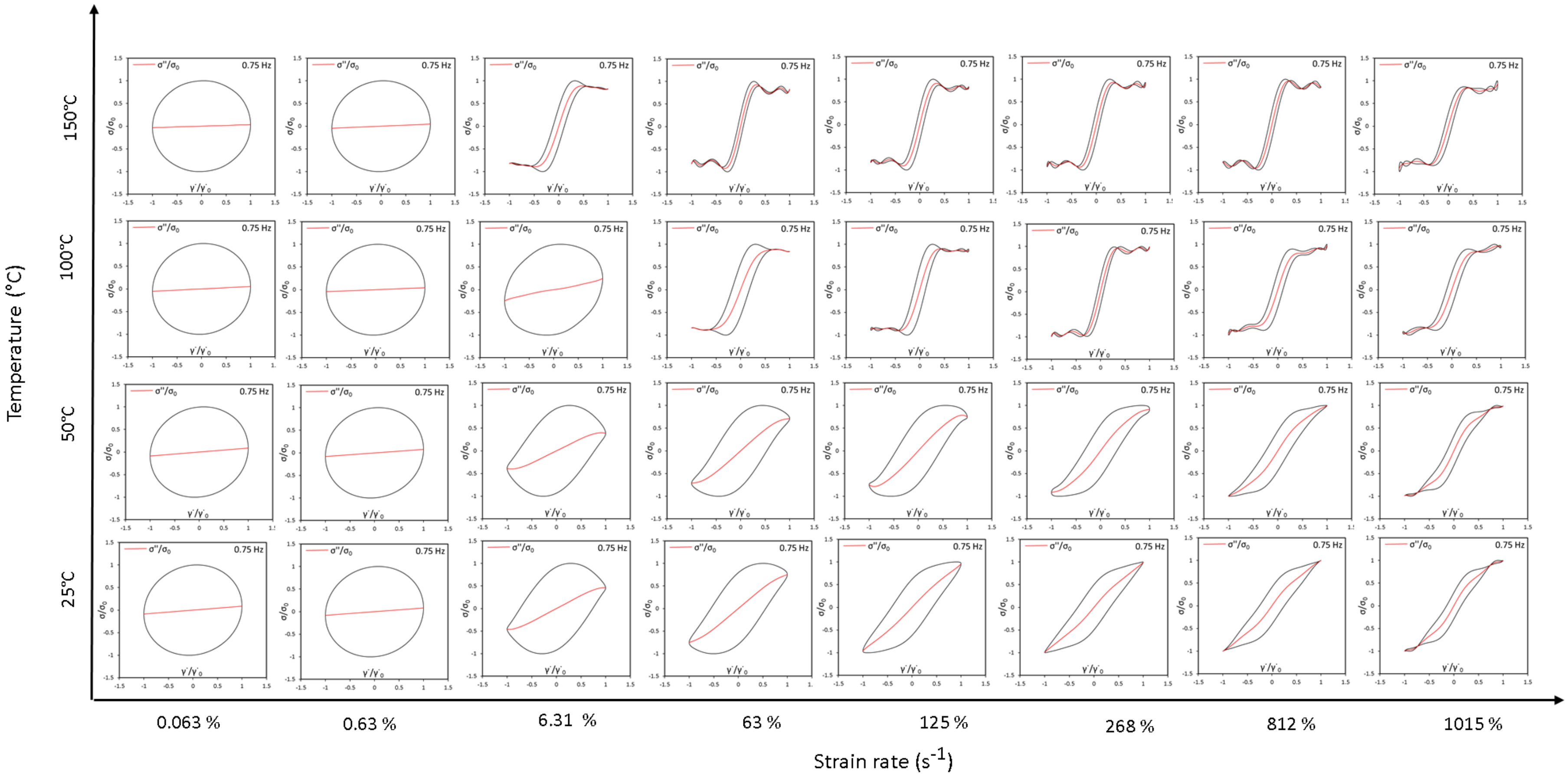

Figure C.14: Viscous Lissajous-Bowditch curves of micro-sized TTB sepiolite suspensions at four different temperature and at 0.75 Hz Frequency.

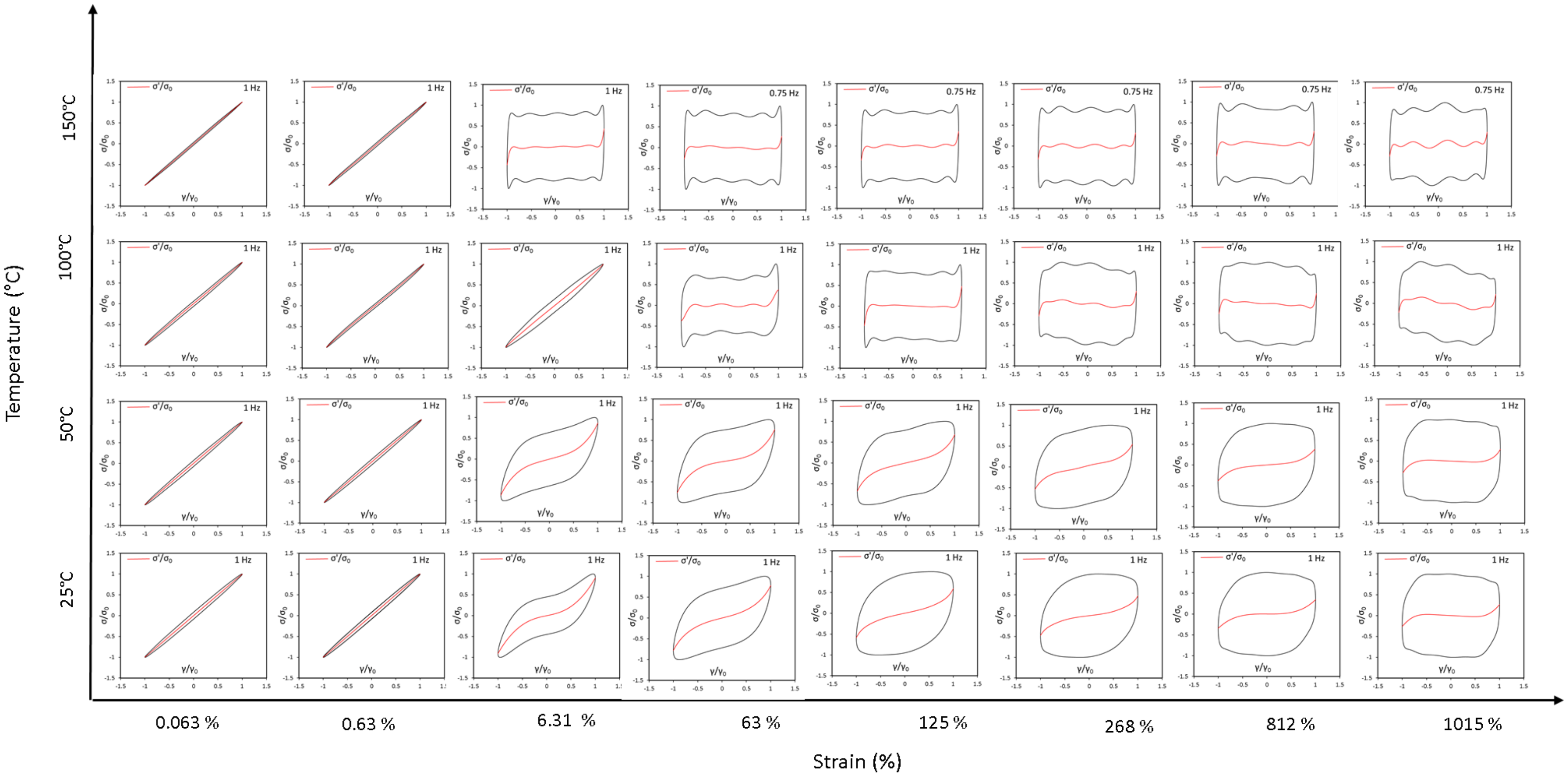

Figure C.15: Elastic Lissajous-Bowditch curves of micro-sized TTB sepiolite suspensions at four different temperature and at 1.0 Hz Frequency.

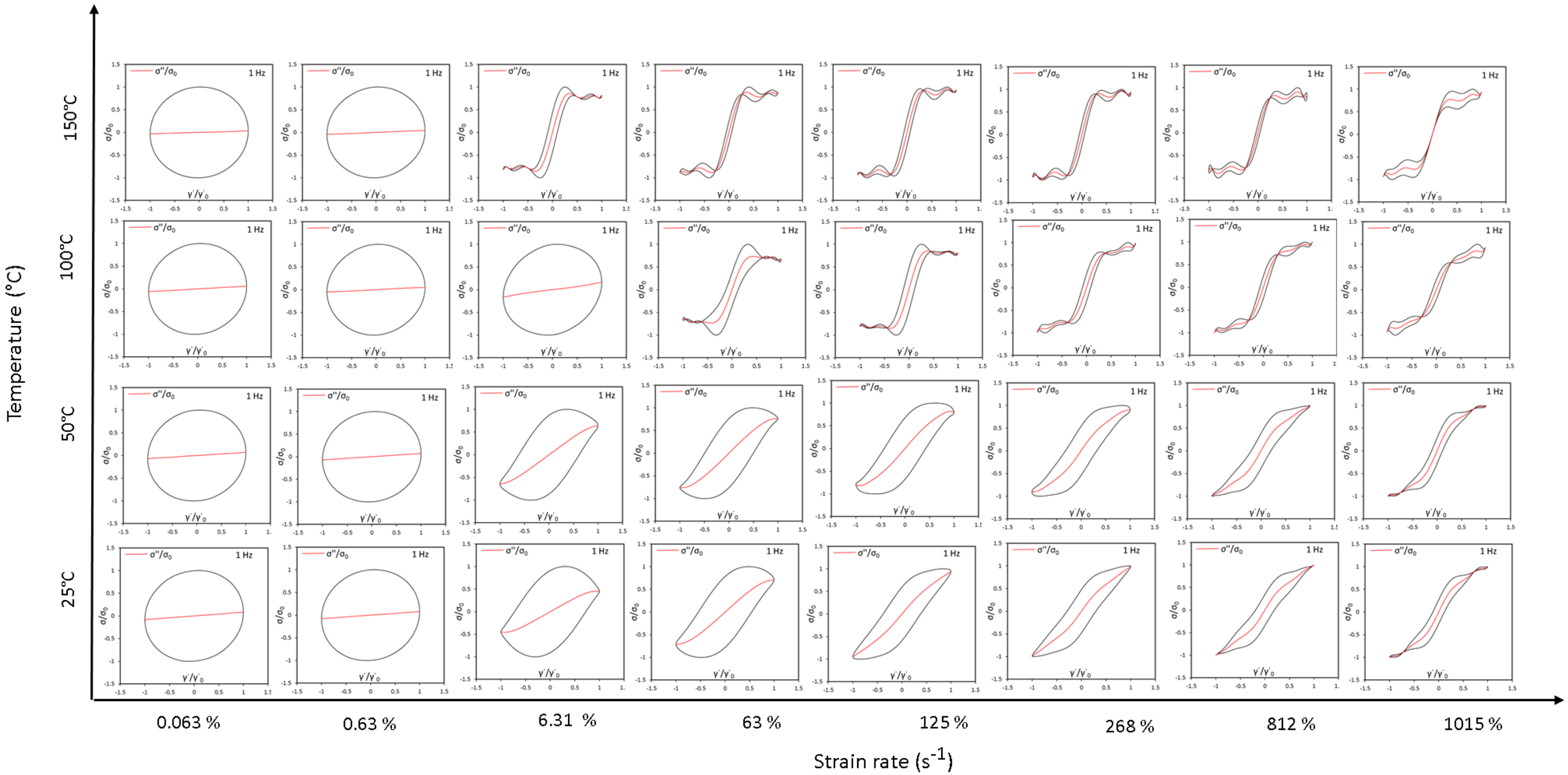

Figure C.16: Viscous Lissajous-Bowditch curves of micro-sized TTB sepiolite suspensions at four different temperature and at 1.0 Hz Frequency.

Republic of Turkey
İzmir Kâtip Çelebi University
Graduate School of Natural and Applied Sciences

Nonlinear Viscoelastic Properties of Nano and Micro Sized Clay Suspensions

Department of Nanoscience and Nanoechnology Engineering
Master's Thesis

Ceylan ÜLKER
ORCID 0000-0003-0793-7069

Thesis Advisor: Asst. Prof. Dr. Ali ETTEHADİ

February, 2022

ÜLKER   Nonlinear Viscoelastic Properties of Nano and Micro Sized Clay Suspensions

MASTER'S THESIS ;   2022

Curriculum Vitae

Name Surname : Ceylan ÜLKER
E-mail : cyln.ulkr@hotmail.com

Education:

2012–2018 İstanbul Technical University, Dept. of Petroleum and Natural Gas Eng.

2019–2022 İzmir Kâtip Çelebi University, Dept. of Nanoscience and Nanotechnology Eng.

Work Experience:

TUBITAK Project Researcher fellow;

2019-2022 Project Title: Observing of The Plugging Time For the Large Fractured Formation During Drilling Fluid Circulation

2019-2021 Project Title: Static Barite Sag Tendency and Rheological Properties of Drilling Fluid in Viscoelastic Range

Publications:

1. Nonlinear viscoelastic rheological behavior of bentonite and sepiolite drilling fluids under large amplitude oscillatory shear

A Ettehadi, C Ülker, G Altun - Journal of Petroleum Science and Engineering, 2021 - Elsevier

2. Nonlinearity in large amplitude oscillatory shear of drilling fluid: A comparative study on the oil and water base muds behavior

A Ettehadi, C Ülker, G Altun - Journal of Petroleum Science and Engineering, 2022 – Elsevier

3. Blockchain Teknolojisi: Enerji Verimliliği ve Ticaretine Etkisi

Ali Ettehadi, Melih Yalvaç ve Ceylan Ülker - Türkiye IV. Bilimsel ve Teknik Petrol Kongresi bildiriler kitabı, Petrol Mühendisleri Odası